Heat Transfers in Lake Memphremagog

© Sylvain de Margerie

Institute of Oceanography

Master of Science

Thesis submitted to the Faculty of Graduate Studies and Research

in partial fulfillment of the requirements

for the degree of Master of Science

Heat Transfers in Lake Memphremagog

Heat Transfers in Lake Memphremagog

Sylvain de Margerie
Institute of Oceanography
Master of Science

Thesis submitted to the Faculty of Graduate Studies and Research
in partial fulfillment of the requirements
for the degree of Master of Science

Thesis submitted to the Faculty of Graduate Studies and Research
in partial fulfillment of the requirements for the degree of
the degree of Master of Science

ABSTRACT

A description of the physical limnology of Lake Memphremagog is given, based on data obtained with recording instrumentation between 1975 and 1977. The marked changes in depth along the length of the basin are found to play a major role in hydrodynamic and thermodynamic processes in the lake. Surface seiching is found to generate internal waves over a topographic discontinuity in the same way barotropic tide generates internal tides at the continental shelf break in oceans. Upwelling from a deep to shallower portion of the lake is explained in terms of a modification to the solution for the wind response of a simple two-layer rectangular basin. Temperature differences between different parts of the lake in spring and fall is due to the more rapid heating and cooling of shallow regions. Heat storage in the sediment is also found to be an important factor in the heat budget of the shallow basins. In winter this is at least partly responsible for observed thermal convection under the ice. A numerical model was developed to simulate the vertical mixing induced by wind, the exchange of water between various parts of the lake, and heat fluxes through the surface and bottom of the lake. The model results agree qualitatively with observations.

RÉSUMÉ

Des données recueillies entre 1975 et 1977 dans le Lac Memphremagog sont utilisées pour décrire la limnologie physique de ce bassin. Des différences marquées de profondeurs, le long du lac, jouent un rôle capital dans le processus hydrodynamiques et thermodynamiques. Des ondes internes sont générées par la seiche de surface, à l'endroit d'une discontinuité topographique, de façon analogue à la génération d'onde interne due à la marée, à la jonction du plateau continental. La solution pour le mouvement, induit par le vent, dans un bassin rectangulaire à deux niveaux est modifiée afin d'expliquer la remontée d'eau venant de la partie profonde vers la partie de faible profondeur. Au printemps et à l'automne des différences de température observées sont dues au réchauffement et au refroidissement plus rapides des regions peu profondes. Dans ces dernières, les sédiments jouent un rôle important dans le budget calorifique local. En hiver, le dégagement de chaleur par les sédiments est un des facteurs provoquant une convection thermique sous la glace. Un modèle numérique fut développé pour simuler le mélange vertical dû au vent, l'échange d'eau entre différentes parties du lac et les transferts de chaleur par la surface et le fond du lac. Les résultats de cette simulation sont en accord qualitatif avec les observations.

PREFACE

The present paper is concerned with the physical processes affecting the waters of Lake Memphremagog in general and more specifically with its heat budget and stratification cycle. It follows work initiated in 1972 by R.G. Ingram in collaboration with J. Kalff. The earlier investigations were preliminary in nature. They provided a good description of the overall stratification cycle and some information on what hydrodynamic processes were at work in the lake.

The present study is based on data collected between 1975 and 1980. This information is used to complete the earlier data set on the seasonal stratification of the lake. A numerical model of the surface mixing, of the type originally proposed by Kraus and Turner (1967) and further refined by other authors (Niiler and Kraus, 1977), is used to explain the observations for the ice-free season. The principal difference between the model used herein and others is that variations in geometry along the axis of an elongated basin are taken into account, in effect, resulting in a two-dimensional rather than in a one-dimensional treatment of the problem. From a hydrodynamic point of view, observed surface seiches and upwelling events are explained along the general line of Heaps and Ramsbottom (1966). The theory of linear generation of internal waves by interaction of the surface tide with topography in oceans (Baines, 1982), finds application here, where the surface seiche plays the role of the tide, in generating internal waves. In the case of upwelling the solution for the wind response for a simple rectangular basin are modified for discontinuous bottom topography. This discontinuity is found conducive to the generation of internal surges travelling against the wind along the thermocline. In some cases these surges are found to degenerate into nonlinear undular bores similar to those observed in other lakes (Farmer, 1978).

This work is intended at least in part to support biological research in Lake Memphremagog. Apart from a simple description of the basic physical environment, biologists need knowledge of transport rates of nutrients either by advection or diffusion. Special attention has been given to provide some useful numbers, and to point the direction where the present work could be applied.

The author is indebted to R.G. Ingram who in addition to supervising this study, lent a strong hand in field work and helped in the analysis of the data. Acknowledgements are also due to J. Kalff, R. Flett and generally all the members of the Limnology Research Group, which provided research equipment, facilities and part of the funding for this work. My wife provided typind and proofreading skills in addition to indispensable moral support. Peter Chandler helped in proofreading and Martec Ltd provided the use of their word processor and drafting equipment.

TABLE OF CONTENTS

1. INTRODUCTION

The subject of the present paper is the physical limnology of Lake Memphremagog. Particular attention will be given to the stratification cycle and heat transport mechanisms in the lake. These two subjects are probably the most relevant for biologists interested in Lake Memphremagog. Stratification defines the basic physical environment in which biota evolves and also describes the medium in which baroclinic disturbances will propagate. Heat, on the other hand, offers a natural tracer to investigate mixing processes which will distribute dissolved and suspended matter in the water.

The environment of the lake will be presented first. By environment is meant all factors outside of the lake water itself, which have an influence on the physical processes within it. This included the shape of the basin, the surrounding topography, river runoff and weather conditions above the water. The most distinguishing feature of the environment of the lake is the abrupt changes in depth which occur along the length of the lake.

In chapter 3 we will present observations and explain the physical processes occuring in the lake. Among the phenomena to be discussed are surface seiching, internal waves, upwelling, steady state circulation and convection under ice. It will be found that in each case the peculiar morphometry of Lake Memphremagog plays a crucial role.

Finally, in chapter 4, a stratification model for Lake Memphremagog will be presented. In a first step, existing work on numerical stratification modeling will be reviewed. Then, Lake Memphremagog will be considered in particular. Because of the disparity in shape of different parts of the lake, it is divided into three regions each with a characteristic morphometry. In the simulation the three basins are allowed to exchange water at a fixed rate, but the surface fluxes of mixing energy and heat are considered individually. In effect this model takes into account both horizontal and vertical mixing.

2. LAKE ENVIRONMENT

2.1 Geographical Location

Lake Memphremagog is a long, narrow basin stretching across the Canada-United States border between Quebec and Vermont. Approaching from the west it is just past the Sutton Mountains which is the first of a series of ridges forming the Appalachian Range. Lying in a north-south axis, the lake is set into steep banks. The shores are steepest on the western side with a mean grade of 20% and Owl's Head Mountain rises to 500 m above the water level just 1 km from the shore.

As seen in figure 2.1 there are two small towns at the extremities of the lake, Magog at the northern and Newport at the southern end. Montreal, about 100 km to the west, is the largest nearby city, followed by Sherbrooke, 40 km to the north-east. Most of the land in this part of the Eastern Townships is forested although small cleared areas are used for cattle grazing and crop growing. The immediate shores of the lake are used mostly for recreational purposes, tourists from Montreal providing a major source of income to local communities.

2.2 Morphometry

Lake Memphremagog is 40 km long and on the average 2.4 km wide. Because of its shape and bathymetry it lends itself to division into three

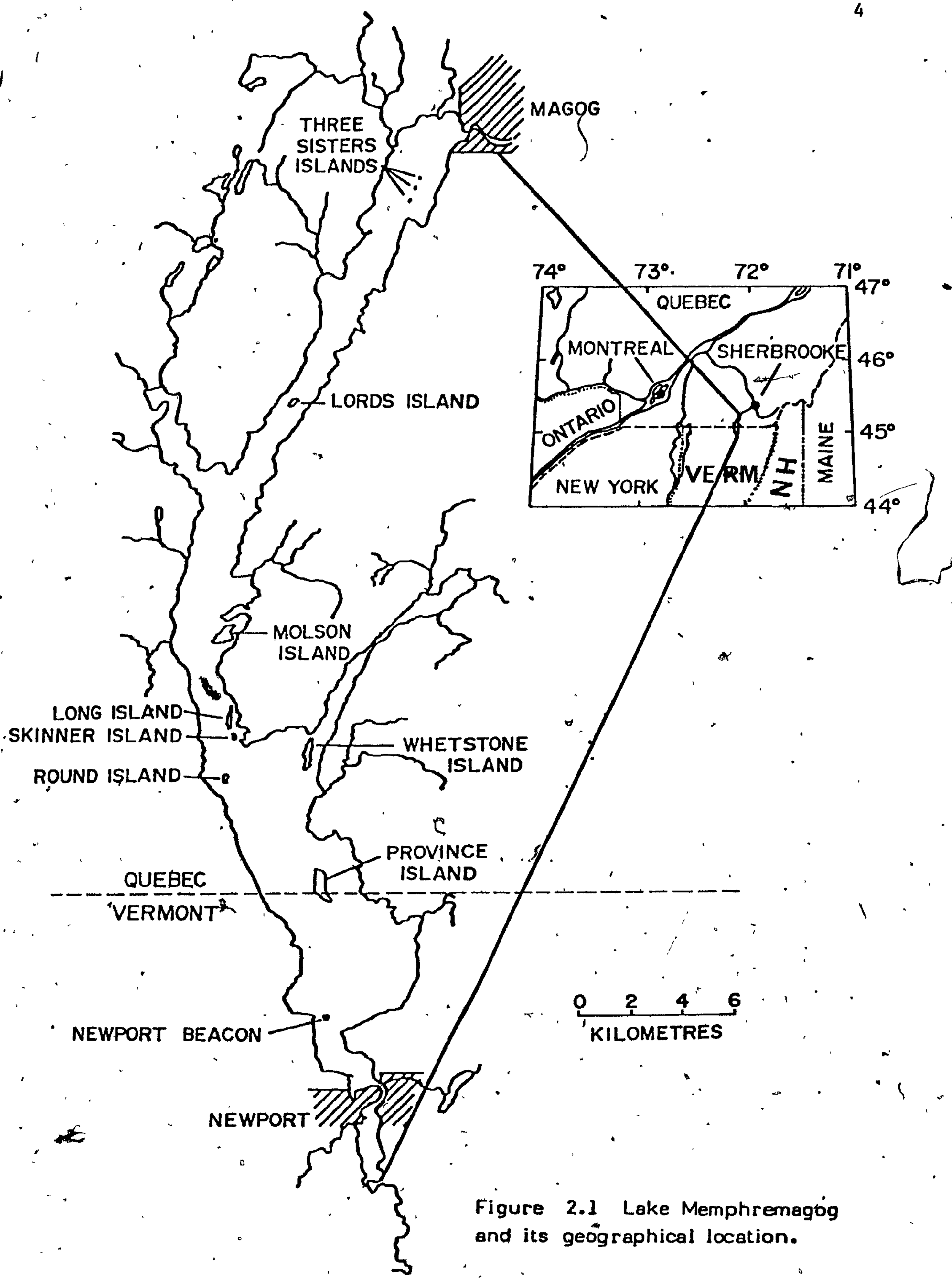

Figure 2.1 Lake Memphremagog and its geographical location.

major basins, separated by constricted areas. These are referred to according to their relative position as North, Central and South Basins (see figure 2.2a). Other subdivisions such as Sargent's Bay and Fitch Bay may be identified but are of lesser importance.

The glacial origin of all but South Basin is evident in the long narrow shape and steep-sided cross section of the lake. In this, Lake Memphremagog resembles the Finger Lakes in nearby New York State. According to McDonald (1967), Lake Memphremagog was formed as a result of glacial erosion, overdeepening existing valleys and regions of weaker material. Supporting this, surficial geology charts (Clark, 1967), show that North and Central Basins lie in a syncline at the junction of two different rock formations, while Fitch Bay is on a fault line. The shallow depth and generally different shape of South Basin may be explained by the presence of a granitic outcrop which is considerably harder to erode than surrounding materials. The sills separating the various basins may be remnants of harder rock formations or morain deposits or both. The presence of several morainic systems in the region and the unconsolidated nature of material on Lord's Island suggest that glacial deposits are at least partly responsible for the division of the lake.

In order to obtain systematic information on lake morphometry, the soundings from the bathymetric chart no. 1361 of the Canadian Hydrographic Service were coded and entered into McGill University's computer system. This consisted of entering a set of three numbers for each sounding shown on the map. These were depth and two horizontal

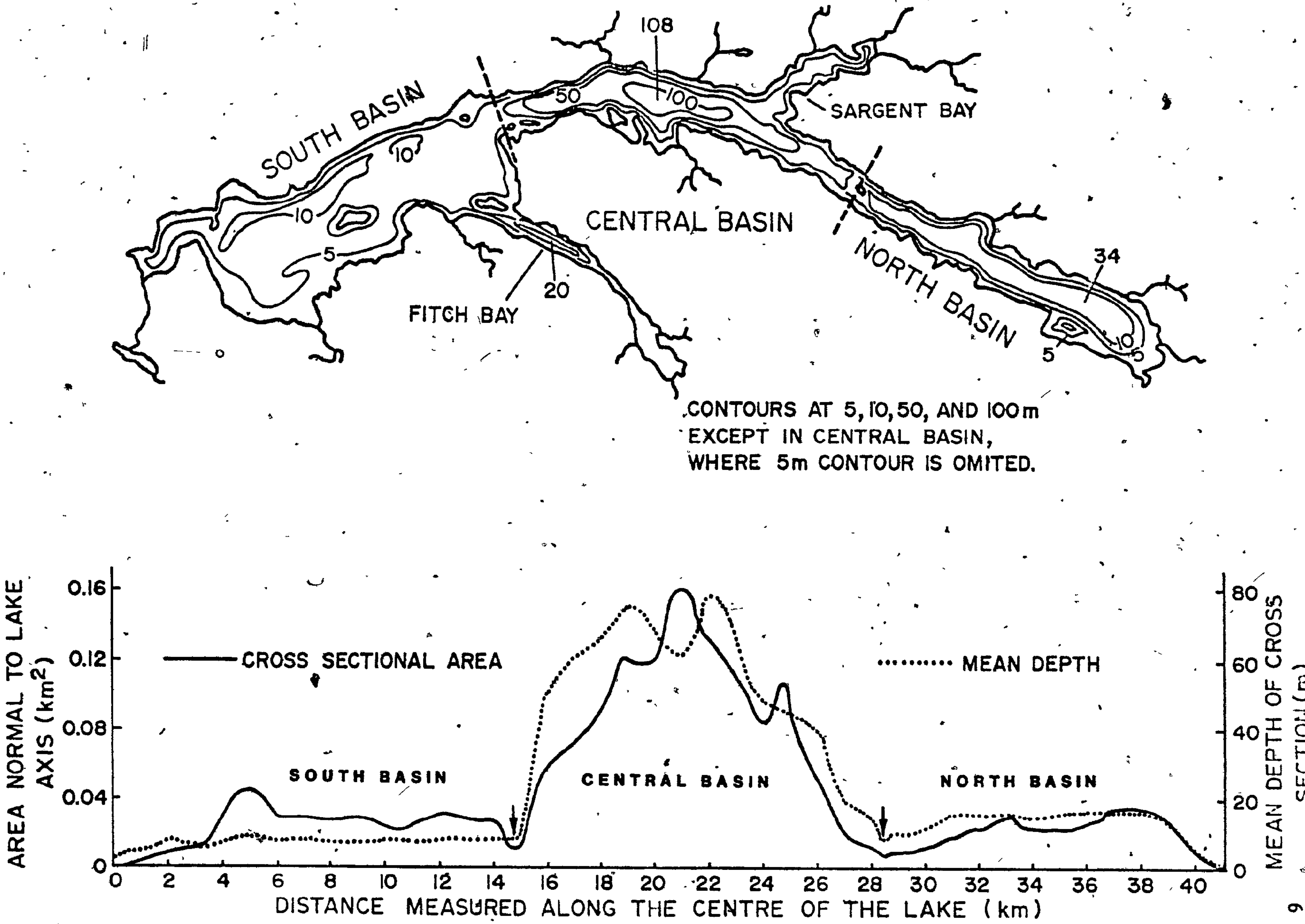

Figure 2.2a) Bathymetry of Lake Memphremagog

values were interpolated on a rectangular grid, at 100 m intervals. This regular data set may then easily be manipulated to provide any morphometric information. Based on the accuracy of the soundings and positioning, volumes may be estimated to within 3%, areas to 2% and depth to 1%.

Figure 2.2a shows a bathymetric contour map and a cross sectional area plot which were generated using the computerized information. The cross sectional area shows how well the three basins are separated. Not only is the lake narrower at the junction between the basins but shoaling occurs there also.

Volume development curves are illustrated in figure 2.2b, showing the striking morphometric differences between the basins. South Basin, a wide shallow basin, accounts for 52% of the lake surface area but only 18% of the volume. Central Basin with 67% of the water volume occupies only 26% of the area. North Basin is intermediate with a more proportional surface and volume of 22% and 15% respectively. The lake as a whole contains 1.53 km^3 of water, covering 92 km^2.

Although the interconnecting channels are clearly too wide to consider Lake Memphremagog as a system of individual river-linked lakes, it is clear that the divisions and assymetries between basins have to be taken into account in a physical limnology study.

2.3 Drainage and Discharges

Lake Memphremagog is situated in the St. Lawrence River drainage

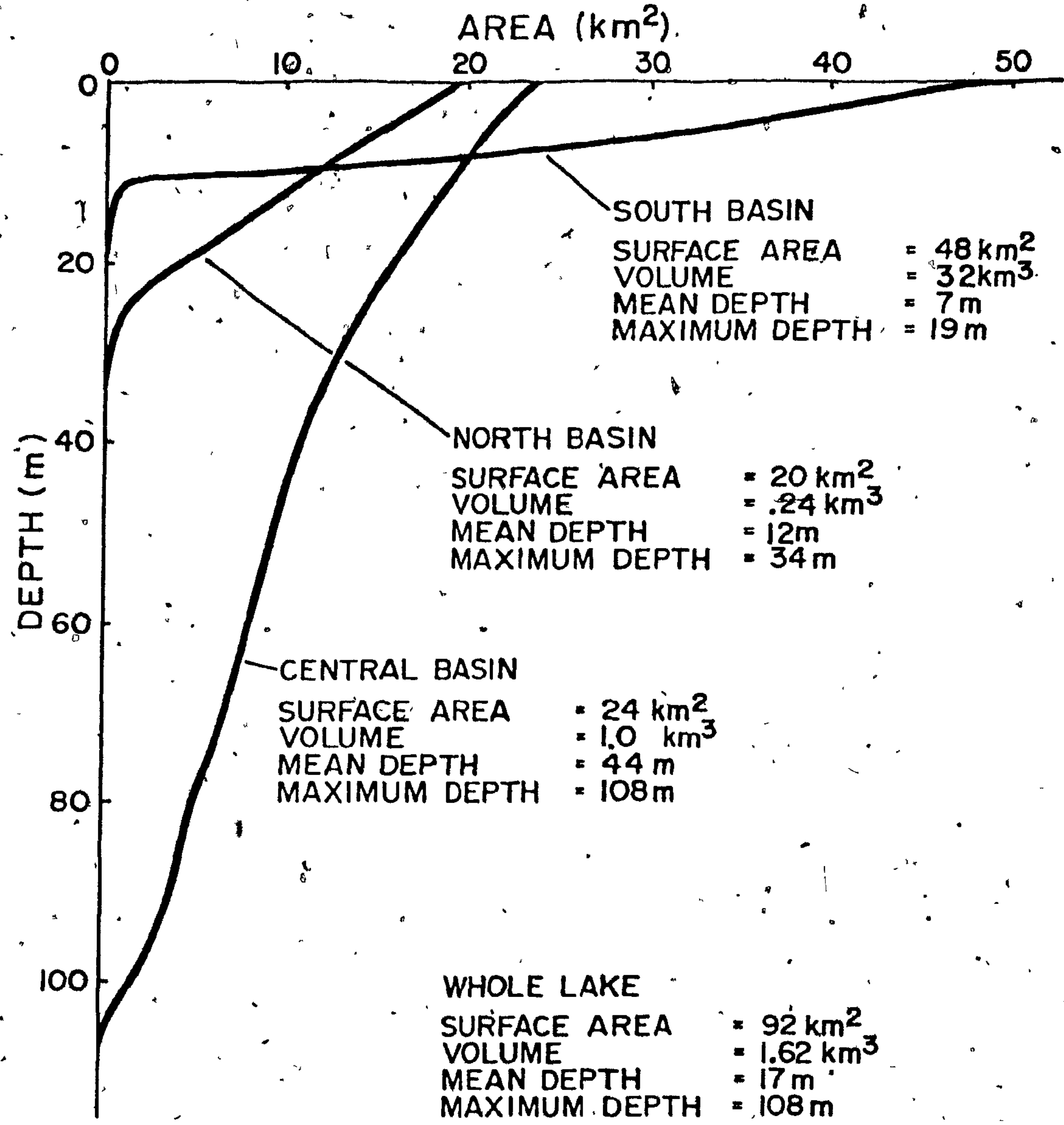

Figure 2.2b) Volume development curves for Lake Memphremagog's three basins.

basin. Its total watershed area is 1678 km^2, 70% of which is drained by three rivers, the Black, the Barton and the Clyde, entering the lake at its very southern extremity. Of the remaining area, 5.5% is the lake surface itself, while the rest is drained by numerous minor streams, distributed around the lake. The discharge is at the northern end of the lake into the Magog River, which joins the St. Francois River in Sherbrooke 35 km to the north-east. The St. Francois is a major tributary of the St. Lawrence River.

The present drainage system of Quebec's Eastern Townships is relatively recent. According to Gadd, McDonald and Shilts (1971), only 15000 years ago this region was entirely covered by the Pleistocene ice cap. As the glacier retreated, melt water collected between the glacier front and the Appalachian highlands, forming Glacial Lake Memphremagog. Because the ice completely obstructed the flow to the north, the water level adjusted itself to whatever pass was available as a spillway in the mountains to the south. The glacial lake first drained directly to the south into the Connecticut River Valley. As the ice receded, successively lower spillways were uncovered and around 14300 years ago (Prest, 1969) the drainage shifted westward into Lake Champlain and the Hudson River watershed. During these early periods, the lake level was up to 100 m above the present and the Glacial Lake Memphremagog flooded all of the area which is now the valleys of the St. Francois and its tributaries until about 12500 years ago. At this time the glacial front started a rapid recession and by 12000 B.P. (before present) the ocean entered the St.

Lawrence lowlands to form the Champlain Sea. This is when Lake Memphremagog must have adopted a level and drainage pattern approaching the present day situation, although the lake outline has been slightly modified by the hydrostatic adjustment of the earth crust which has caused a differential tilting of the land at a rate of 0.72 m per kilometer. The lake level is presently 208 m above mean sea level.

Two of the major tributaries to the lake, the Black and the Clyde rivers, draining 43% of the watershed, are gauged by the U.S. Department of the Interior's Geological Survey. The Magog River is also monitored at the lake discharge. The total inflow into the lake can be estimated from the discharge rates of the two gauged rivers, by assuming that runoff is proportional to watershed area. This assumption is supported by a correlation coefficient of 0.99 between mean yearly discharge and watershed area obtained from six nearby Vermont rivers (Kalff et al, 1976). The mean yearly inflow into the lake is thus calculated to be 1.00 km^3, which compares well with measured lake discharge. Based on precipitation data from nearby Sherbrooke airport this inflow represents 55% of the total yearly precipitation on the lake catchment area. This corresponds to a typical runoff coefficient for this type of rural area, the balance of the water being accounted mostly by evapotranspiration losses (Gray, 1970). Comparing the mean yearly flow rate to the lake volume we obtain a mean flushing period of 18 months.

Figures 2.3 illustrates the temporal variability in the flow rates, computed by using the assumption just described. It should be borne in

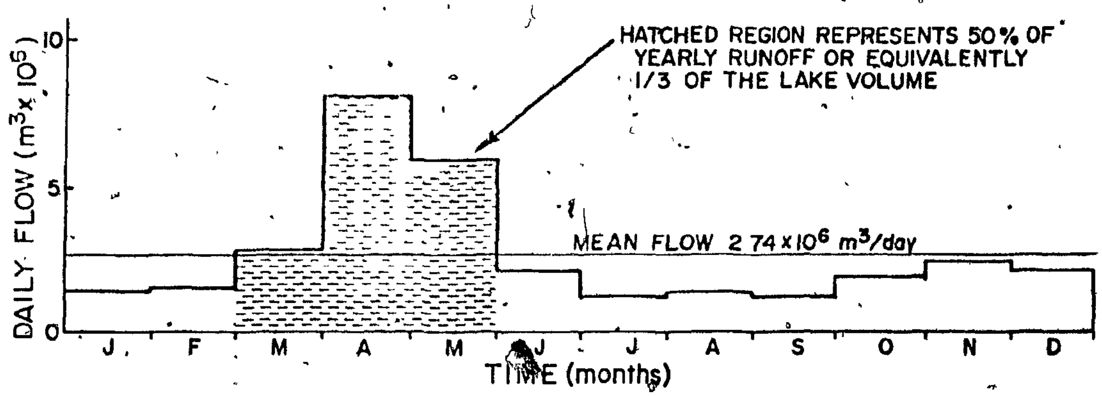

Mean monthly inflows for a 10 year period

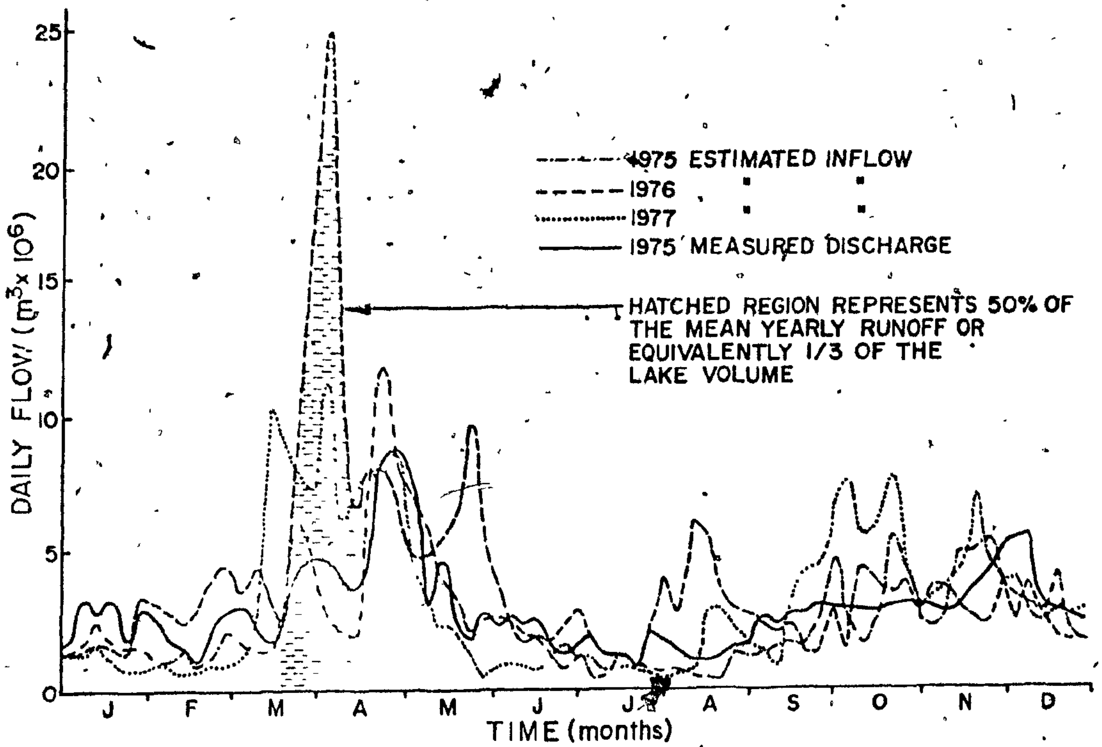

Figure 2.3 Short term variations in flow. Graphs are based on 5 day averages so as not to clutter the curves with high frequency signals.

mind that although the assumption of watershed proportionality for discharge estimates is adequate for long periods of time, it will become less accurate as the time scale is shortened, especially since one of the monitored rivers is artificially regulated. This will cause estimated fluctuation in flow to be smoother and to lag actual inflow. Seasonal variability estimates using this method should therefore be conservative. As can be seen in figure 2.3 the yearly runoff cycle is dominated by the spring freshet. During the months of March, April and May the mean flow is 5.7×10^6 m^3/day, representing 50% of the annual runoff. During the rest of the year flows are well below the yearly mean; October, November and December averaging 2.2×10^6 m^3/day while the rest of the year averages 1.4×10^6 m^3/day.

Figure 2.3 also shows the year to year variability of flow. It can be seen that spring runoff is not evenly spread over a three-month period but rather is composed of a few shorter events of rapid snow melt. In 1976 which was a year of exceptional snow accumulation followed by a warm spring, 33% of the lake volume was flushed in a period of only 30 days. Also shown in this figure is the Magog River discharge for 1975, measured at a small hydroelectric dam using the lake as a reservoir. Due to flow regulation there is less variation in discharge than there is in inflow. This results in lake level fluctuations with a maximum seasonal amplitude of 1.3 m as measured at the power plant.

In summary Lake Memphremagog is characterized by a low through flow except during the spring melting season when one third of the lake volume may be replaced in the time of a month or two. During summer and winter flushing rates are about 2.5% per month while in fall a secondary runoff peak due to precipitation increases flushing rates to 5% per month. Flow regulation limits seasonal lake volume fluctuations to less than 8%.

2.4 Climatology and Weather from Remote Stations

Since net flow through Lake Memphremagog has been found to be small, we can expect that interaction with the atmosphere will be the prime source of heat and momentum to the lake waters. Therefore it is of capital importance to determine the atmospheric conditions over the lake. Several attempts have been made to record meteorological variables at the lake, however we were left with short intermittent time series, with the exception of short wave radiation which was recorded almost continuously. Our principal source of information is therefore data from nearby A.E.S. (Atmospheric Environment Service) weather stations. The bulk of the daily data is from Sherbrooke airport which is 30 km north-east of the lake discharge and about 40 km from the center of the lake, at an altitude of 238 m above MSL or 30 m higher than the lake. Insolation which is not recorded at Sherbrooke will be taken from nearbyLennoxville which is about the same distance from the lake.

First we will examine the mean seasonal variations of temperatures, wind speed and insolation, and look at their variability. A simple analysis on a small data set is used, and the results are subject to all the limitations associated with this, but will be easy to interpret and adequate for our purpose. The information presented is all derived from the Monthly Meteorological Summaries for 1976, the year of most intensive measurement at the lake. Three sets of curves are shown in figures 2.4a to 2.4c. The full lines represent the normal seasonal values of each variable. The dashed lines are the standard deviations of daily values from the norm and give an indication of day to day variability. The dotted lines show the standard deviation of monthly mean values from the normal, for the decade preceding 1976, giving a measure of how much we may expect a given month to depart from the norm.

As shown in figure 2.4a the seasonal cycle dominates the temperature climate, with a range of 29 °C, the peak occuring in July and the lowest value in January. Normal daily minimums and maximums have also been plotted to give an indication of typical diurnal fluctuations. These are seen to have an amplitude of about 13° throughout the year. It is interesting to note that the standard deviations of daily and monthly values exhibit a marked seasonal trend with deviations from the norm being almost three times smaller in summer than in winter. This means that temperatures are generally more uniform in summer.

Wind depicted in figure 2.4b shows much less seasonal variation, with a minimum mean speed of 9.8 km/hr in August and a maximum of 13.3 km/hr in March. Day to day fluctuations are more important than seasonal trends, with a standard deviation averaging 5.2 km/hr. Monthly

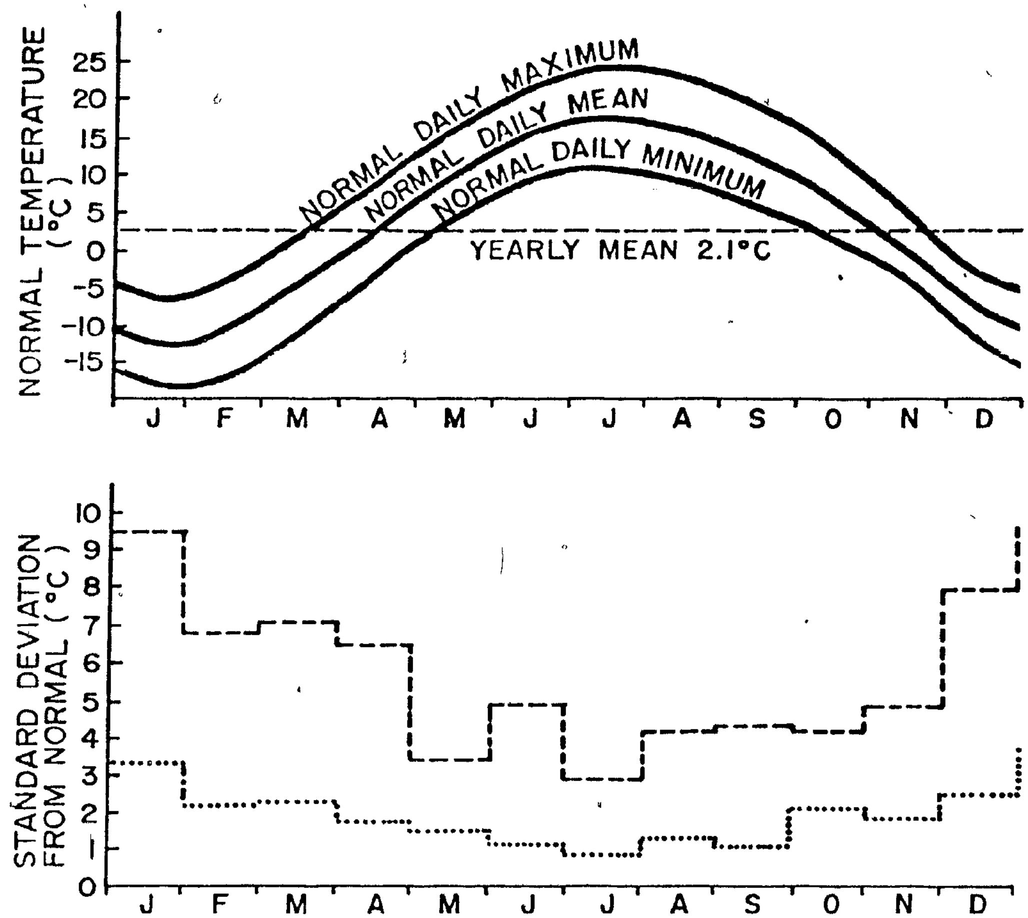

Figure 2.4a) Observed air temperature at Sherbrooke. The upper graph shows the normal daily temperatures. In the lower graph the dashed and dotted lines represent the standard deviations from the norm of daily and monthly means respectively.

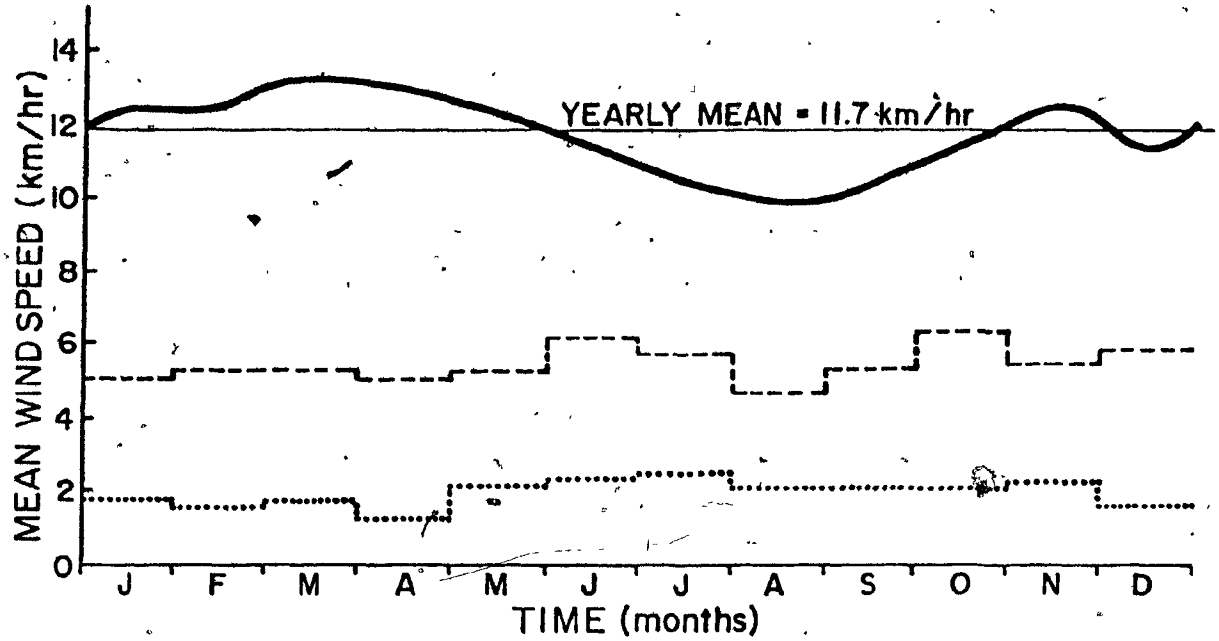

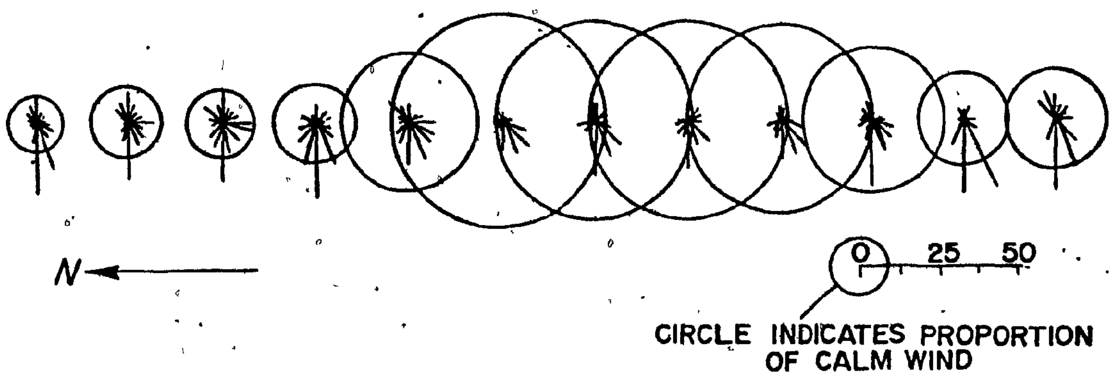

Figure 2.4b) Observed wind speeds and directions at Sherbrooke. In the upper graph the heavy curve is the normal (mean seasonal wind speed), while the dashed and dotted lines are the standard deviations from the norm of daily and monthly means respectively.

deviations are of the same size as seasonal fluctuation. The prevailing wind direction is either west or south-west for each month. The bottom of the figure shows wind roses generated from hourly observations in 1976. These clearly show the general wind direction. About 50% of the time the wind blows in the south to west quadrant, and for a large part of the remaining times (~ 25%) there is no wind.

In figure 2.4c the maximum possible number of sunny hours per day (or duration of daylight) has been calculated by astronomical geometry, and is plotted with the other curves. As may be expected all curves follow the same seasonal cycle. It may be more instructive to examine the relative amplitude of each curve rather than their absolute value. In summer the observed duration of sunshine accounts for 60% of the maximum while in winter the sun shines only 24% of the time; the solar disk is therefore obscured by clouds a much larger fraction of the time in winter. The standard deviations are quite proportionate to the duration of daylight. In winter the daily standard deviations are of the same size as the mean number of hours of sunshine. We can therefore expect days with no sunshine to be a common occurence (no sunshine does not imply no radiation, as some light does pass through clouds).

Table 2.4 is meant to compare the variance of daily and monthly means. The values tabulated are the sample variance based on daily standard deviations and the values of the variance among groups based on monthly standard deviations. According to the central limit theorem of statistics these should be two independent estimates of the population

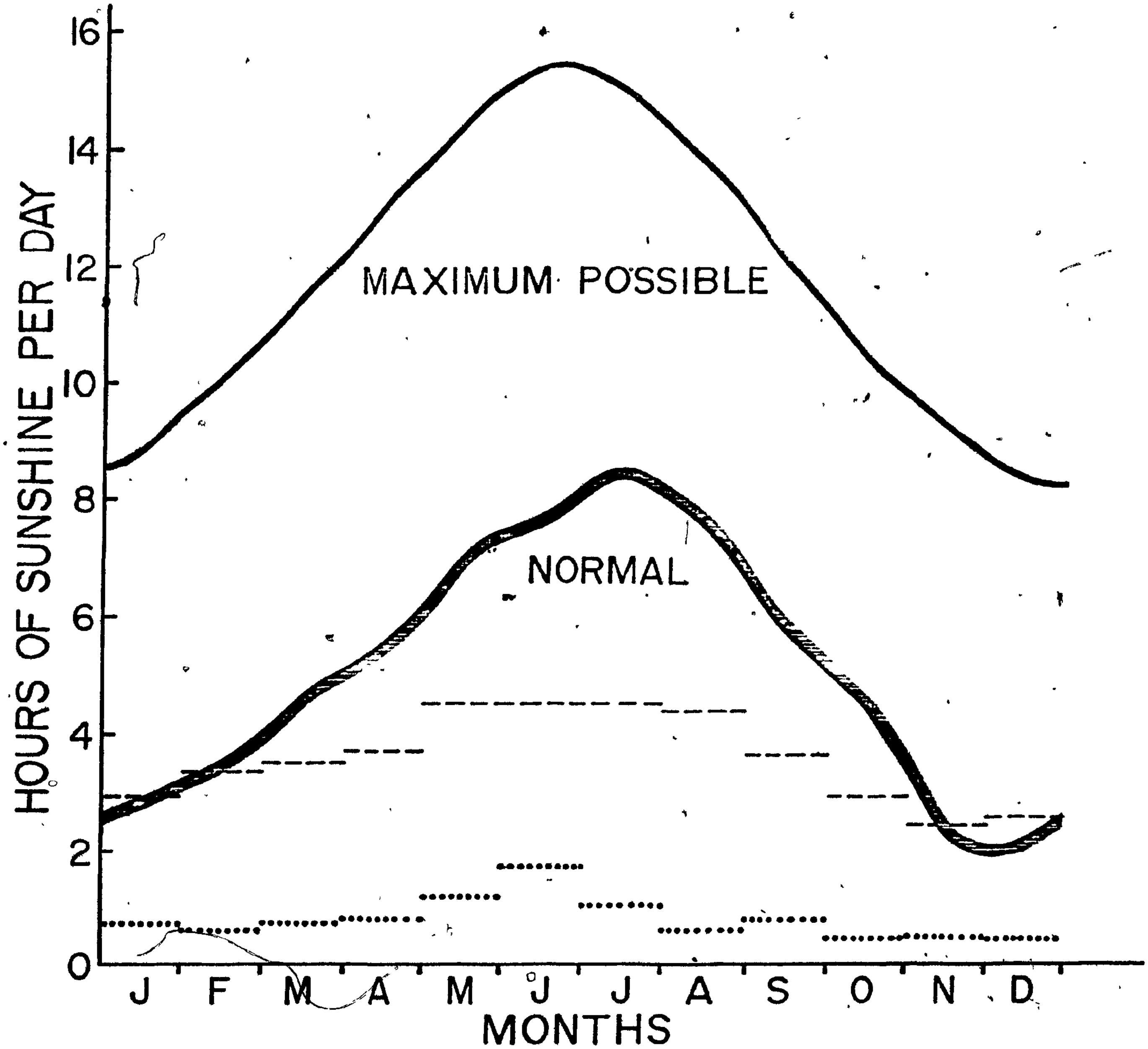

Figure 2.4c) Observed daily duration of sunshine at Lennoxville compared to the maximum possible daily duration of sunshine. The heavy curve represents the normal while the dashed and dotted lines represent the standard deviations from the norm of daily and monthly means respectively.

TABLE 2.4

COMPARISON OF DAILY AND MONTHLY VARIANCES

	n	Temperature S_d^2 (°C^2)	Temperature nS_m^2 (°C^2)	Wind S_d^2 (km^2/hr^2)	Wind $n S_m^2$ (km^2/hr^2)	Insolation S_d^2 (hr^2)	Insolation $n S_m^2$ (hr^2)
January	31	90	358	25	103	9	16
February	28	45	135	26	70	11	10
March	31	50	164	26	104	12	17
April	30	42	108	25	48	13	21
May	31	12	79	26	143	21	47
June	30	23	36	38	164	20	92
July	31	8	31	32	185	20	35
August	31	17	52	19	119	20	12
September	30	18	36	26	118	14	19
October	31	18	137	40	115	9	8
November	30	23	108	28	131	6	8
December	31	62	194	35	71	7	9

Meaning of the Symbols

n is the number of days in each month and also the sample size.

S_d is the standard deviation of daily values for each month and its square is the sample variance for that month.

S_m is the standard deviation of monthly mean values for 10 years and its square times n is the variance among groups of daily values. In principle $n S_m^2$ should be an independent estimate of S_d^2.

variance, if the samples are random subsets of the same population. As can be seen the variance among groups is always too large and random daily fluctuations are not sufficient to account for the monthly variations. The reason for this behaviour is that our samples are not random but rather clumped. In other words any weather condition is likely to last more than a day and in that sense today's weather is not independent of yesterday's. This clumped behaviour is to be expected in any time series where considerable energy is present at frequencies lower than the sampling frequency. A good example of the effect of low frequency components is the 1976 monthly wind speed which were consistently 30% lower than normal throughout the summer season. This is seen in the wind roses (figure 2.4b), where the large percentage of calm weather in the summer should be interpreted as a particularity of that year rather than a seasonal trend.

Temperature and duration of sunlight exhibit the strongest seasonal cycle and we can expect that they will be the prime factors affecting the annual stratification of the lake. Because the meteorological variables are found sometimes to vary systematically from year to year we may also expect to find marked variations in the lake's thermal cycle.

2.5 Comparison with Meteorological Observations over the Lake

Let us now compare observations at the lake with data from Sherbrooke and Lennoxville. For this purpose the Monthly Summaries, giving daily values, again form the main information source, except for the comparison of wind vectors which were based on hourly readings obtained from A.E.S. Apart from the continuous recording of incident short wave radiation, all of the successful meteorological data recording at the lake was done in a period from July 17th to November 15th, 1977. The recording instrument package was installed 7 m above the water level on a beacon near Newport at the southern extremity of the lake (see figure 2.5). Air temperature, vapour pressure and wind speed were successfully recorded for 98 days, while only 37 days of good quality direction information were obtained. The short wave radiation measurements were done at shore-based stations near the center of the lake. The information used spanned the years from 1974 to 1977. All suspect data were removed and of the remaining, 730 days are included here.

Table 2.5 summarizes the results of comparison. Air temperatures over the lake average 2 °C above those of Sherbrooke; 0.3 °C of the difference may be accounted for by the adiabatic lapse rate between the levels of observation. Because the measurements were done in late summer and fall when the lake is warmer than the air above it, this difference may represent a seasonal bias. In order to remove this, the difference between air temperature at the lake or at Sherbrooke and the water surface temperature, were examined and compared. As seen in the second column of the table this is at the cost of a lower correlation coefficient, but it is felt that this comparison makes more sense because heat exchanges between the air and the water are bound to influence the

TABLE 2.5

COMPARISON OF OBSERVATIONS ON LAKE MEMPHREMAGOG
WITH NEARBY AES WEATHER STATIONS

	Air Temperature	Temperature Difference Between Air and Water Surface	Wind Speed: Absolute Value	Wind Speed: North Component	Wind Speed: East Component	Insolation
Lake						
Mean value	15.0	-2.3	13.0	-11.0	-1.0	0.567*
Standard deviation	16.0	4.2	14.0	7.9	6.8	0.230*
Sherbrooke						
Mean value	13.0	-4.2	6.50	-2.55	-1.41	0.473*
Standard deviation	14.0	5.7	7.40	2.90	2.50	0.300**
Correlation coefficient	0.99	0.94	0.68	0.49	0.43	0.93
	Based on 98 Daily Means			Based on 890 Hourly Observations		Based on Two Years of Daily Observations

* These numbers are for the ratio of observed to clear sky incident short wave radiation.

** These numbers are for the ratio of observed to maximum possible daily duration of sunshine.

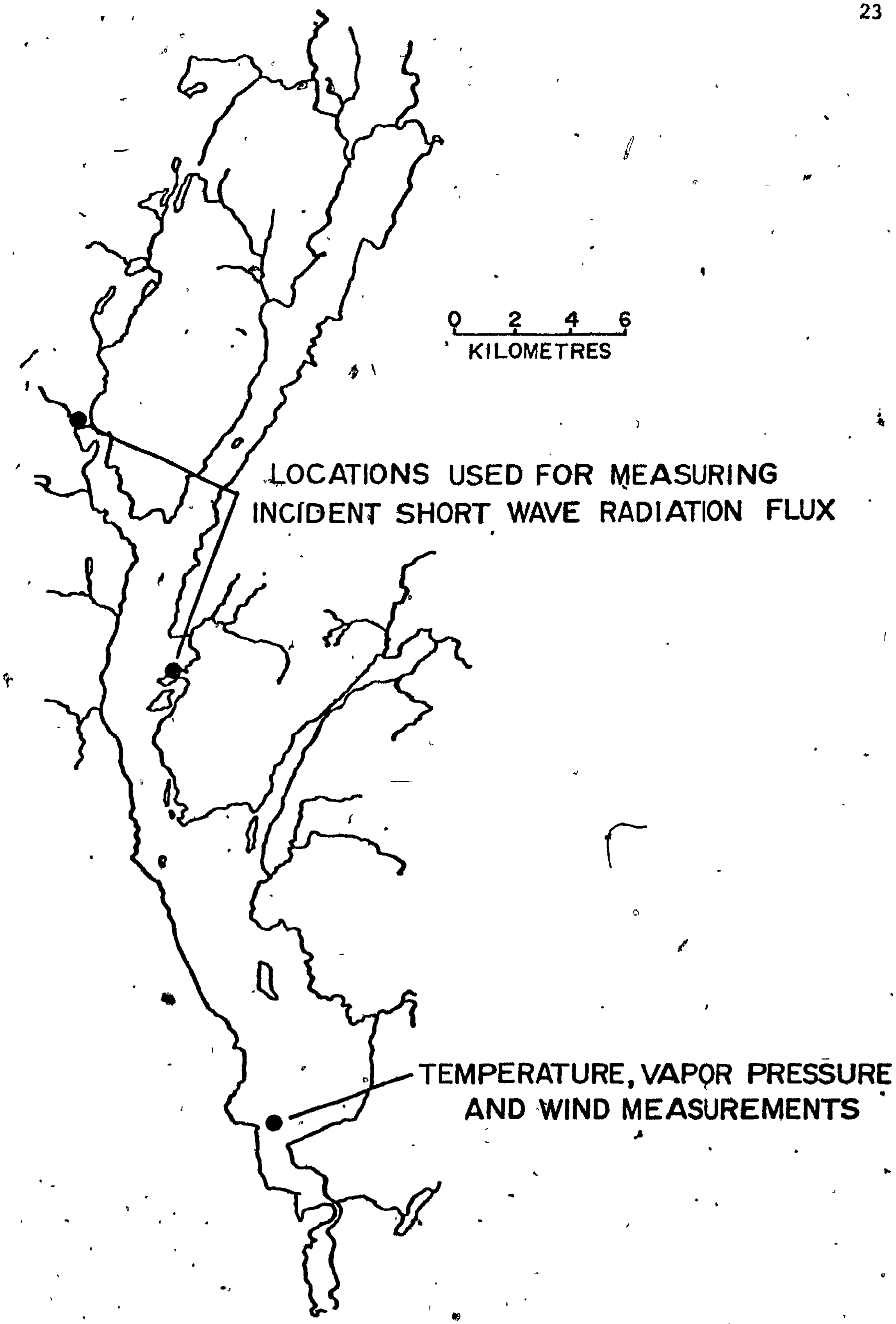

Figure 2.5 Location of weather recording instrumentation.

measurements.

From column three we see that the observed wind speeds (absolute values) are not very well correlated, with observed mean speeds at the lake being twice those at Sherbrooke. Another correlation analysis using 5 day averages yielded a coefficient of 0.82, suggesting that over a longer time scale the winds are better related. The next two columns in the table show a comparison of the wind as vectors. This is one of several analyses (including cross correlation of north and east components) undertaken in an attempt to relate wind direction at the two locations, correlation coefficients were however even lower and we are forced to accept the fact that there is no simple relationship between wind at the two locations. The ratio of the magnitude of the vector mean velocity to the mean scalar velocity is sometimes used to compute a coefficient of directionality in oceanography. Applying this we obtain 0.85 and 0.45 for the lake and for Sherbrooke respectively, indicating that wind directions are steadier at the lake. These results suggest the importance local topography may have, which in turn raises the question of how representative measurements at the Newport beacon are of conditions over the lake in general, since the low landscape in the sourthern part of the lake contrasts with the mountainous shores elsewhere. Although a few instantaneous observations were taken sporadically while installing other instrumentation in the lake, there is much too little data to answer these questions, and at best we may consider our wind measurements applicable to South Basin only.

The number of hours of sunshine were not recorded as such at the lake. Instead a more relevant parameter to heat budget of the water, incident short wave radiation flux, was measured almost continuously. This quantity is formed almost entirely by the visible light spectrum and according to Gray (1970) the ratio of observed incident shortwave radiation to maximum clear sky shortwave radiation can be linearly related to the ratio of actual number of sunny hours to the maximum daily duration of sunshine. These quantities for the lake and for Lennoxville respectively are tabulated under "insolation" in table 2.5, and show a high degree of correlation. Not included in the table is the result of correlation based on weekly averages of these quantities. This resulted in an even higher correlation of 0.98 suggesting that these two quantities may be used equivalently over a long time scale.

In summary we can say that all meteorological observations at the lake and at Sherbrooke or Lennoxville are well correlated, with the exception of wind direction. Temperatures 7 m over the lake are about halfway between water surface temperatures and air temperatures at Sherbrooke. Absolute wind speed over the lake is also about twice what it is at Sherbrooke, winds blowing along the axis of the lake, however, are enhanced by a factor of 1.2, suggesting that the relationship is strongly influenced by local topography and therefore varies over the lake. The above analysis is valid only for the ice-free season as the fluxes of heat, radiation and momentum will change over the solid ice and snow boundary. Vapour pressure and long wave radiation were not considered here.

However, they are controlled mostly by temperature and discussion will be left for later, in the context of the lake thermal budget.

3. LAKE PHYSICS

The investigation of physical processes in Lake Memphremagog was initiated in 1972. Before 1975, measurements by R.G. Ingram and P. Ross consisted of taking temperature and velocity profiles, and undertaking a series of drifter tracking experiments, at numerous stations (unpublished data and reports).

The temperature observations showed that the thermal cycle of the lake is typical of dimictic basins. Throughout the year the stratification is predominantly stable with warm water overlying cool water in summer, and the reverse in winter. There are two short transition periods in the year, in spring and fall when the surface water approaches the temperature of maximum density (3.98 °C). At these times convective overturn vertically mixes the whole water column. Figure 3.0a shows the thermal cycle observed in North Basin during the 1972-73 season. The region of sharp temperature gradient, called the thermocline, is the prevalent feature of the summer stratification of both Central and North Basins. In mid-July the central depth of the thermocline in all basins approaches the mean depth of South Basin and from this time until fall turnover stratification is observed intermittently in this basin. The presence of marked tilting of the isotherms (see figure 3.0b) suggests that this may be due to the exchange of deep waters, through the action of long internal waves.

The velocity and drift experiments revealed complex circulation patterns. In some instances the flows seemed to follow recognizable

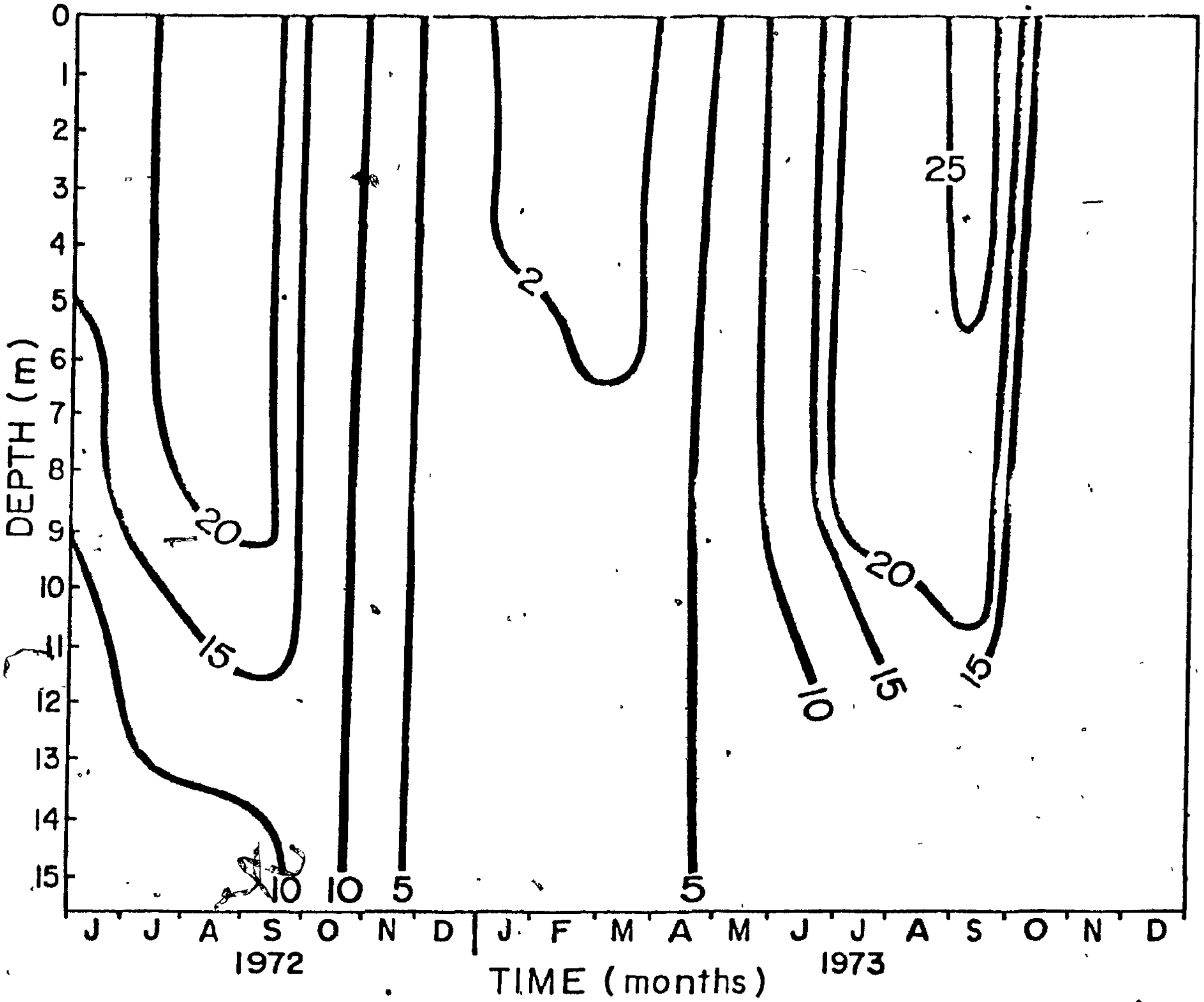

Figure 3.0a) Seasonal temperature structure of North Basin during 1972-73 (from unpublished data, R.G. Ingram)

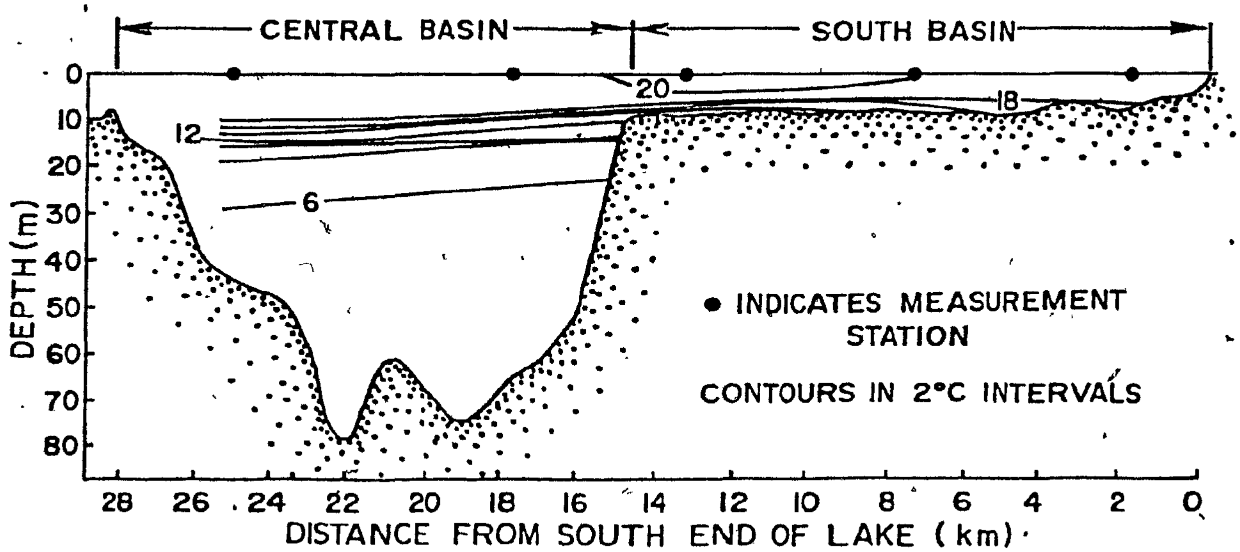

Figure 3.0b) Observations of isotherm tilt on July 31, 1974 (from unpublished data, R.G. Ingram)

patterns with a surface current forced by the wind, separated from a bottom counter current by a shear zone sometimes located across the thermocline. Generally, however, the data showed widely varying flow directions with velocities typically in the 5 to 15 cm/sec range. Notwithstanding the fact that some of the variability may be due to boat motion while taking a profile at anchor, the degree of current variability measured is typical of lake measurements (Bengtsson, 1978).

These early observations provided valuable information on the general properties of Lake Memphremagog, but it became evident that continuous measurements of temperature and velocity would be necessary to elucidate some of the observed behaviour. In the fall of 1975 several recording current meters and a recording thermistor chain consisting of 11 sensors at 5 m intervals became available for moorings over extended periods of time. During the first year of the mooring program, attention was focussed on determining prevailing conditions in each part of the lake. Mooring sites were thus selected near the middle of the three basins. Preliminary results confirmed the importance of inter-basin exchanges and for the second year of the study instruments were installed primarily near the junction of South and Central Basins. Figure 3.10c shows the location of mooring stations while table 3A gives the mooring schedule. Only the moorings for which data were successfully recovered are included in the schedule. For example, due to instrument failures no data were collected at station St 7.

The present chapter will be devoted to the analysis of data

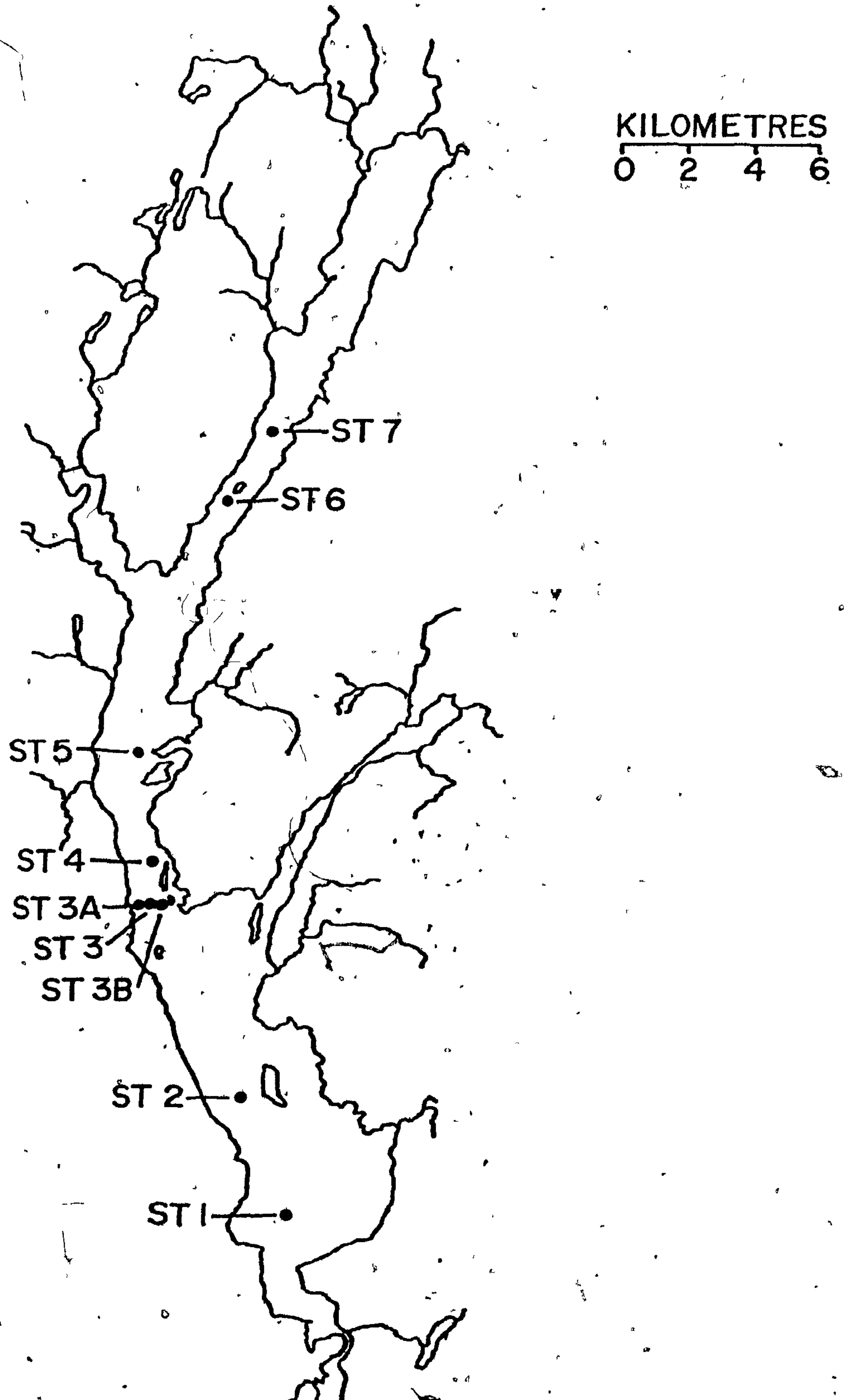

Figure 3.0c) Location of instrumented moorings.

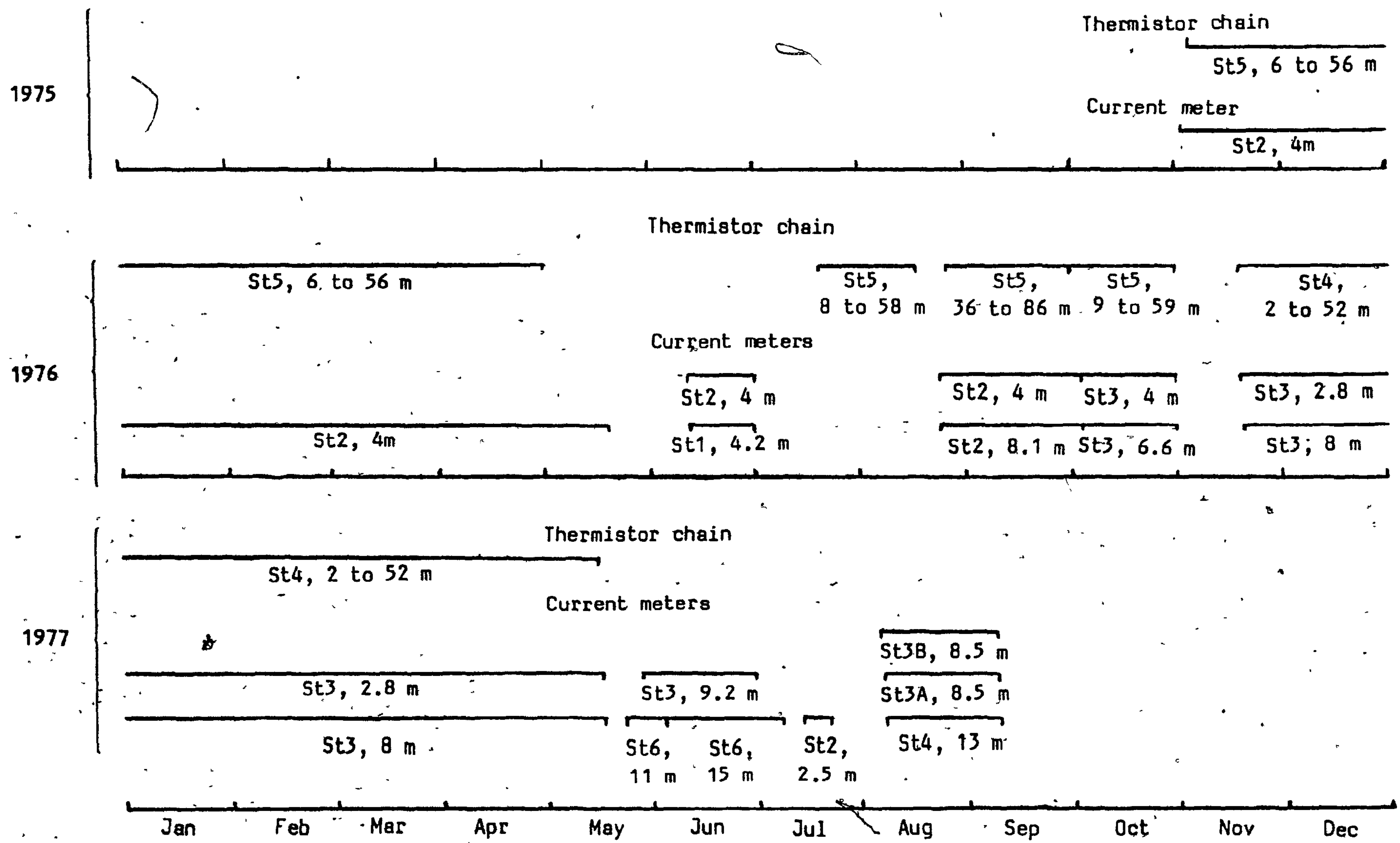

Table 3A. Mooring schedule for thermistor chain and current meters. Each line represents a period of measurement at a given location. Below the lines, the station number and depth of measurement are indicated.

obtained during those two years, and to some theoretical explanation of observations. Although the chapter is divided into two sections entitled Hydrodynamics and Thermodynamics, both topics are strongly interrelated and in many instances it is difficult to put a phenomenon into one category. During the course of the study it has become apparent that the flow velocities in the lake were often below the threshold of detection of the current meters (1.5 cm/sec). Temperature measurements are therefore of critical importance and most of the processes to be discussed deal with heat transport in some way.

3.1 Hydrodynamics

In this section we will discuss motions within Lake Memphremagog which are primarily driven by atmospheric forces. These include the familiar surface and internal seiches but also the occurence of non-periodic motions. As mentioned earlier no wind information is available that relates well to conditions over the lake, therefore we can only speculate as to the atmospheric coupling of these motions.

Because of the large number of moorings involved we will not consider each data record individually. The first step in the analysis is the examination of the general features of the current measurements, as they are the most direct indicators of hydrodynamic properties. Then several observed hydrodynamic phenomena will be discussed in turn with both current and temperature data being used to support the text.

General Character of Current Observations

Table 3.1A presents the overall properties of current observations for various locations and seasons. It can be seen that currents often fall below the limit of detection of our instruments (1.5 cm/sec), and in any case are not much greater than the instrument accuracy claimed by the manufacturer (± 1 cm/sec). This makes it very difficult to obtain meaningful statistics of flow patterns in the lake. Measurements in laboratory of the bearing friction and the estimated drag force on the large vane (0.5 m^2) which serves to orient the instrument into the current lead us to believe that at least the direction information is reliable even for flows down to a fraction of a centimeter per second. In the table, two values are given for the mean speed; the lower one is based on the assumption that all current speeds are zero when undetected by the instrument, while the higher value is for the current set to the stall speed of the sensor (1.5 cm/sec), whenever no flow is recorded. These values give a measure of the range in which the real mean is expected to lie. No vector averaging was done as the results fall far below the measurement error.

The lowest overall currents were observed at stations St1 and St6. At both locations water displacements are limited by shores in three directions. The effect of this containment is supported at station St6 by the fact that currents very seldom flow in a northerly direction, while at all other stations the flow is predominantly in a north-south direction.

	St1	St2	St3	St4	St6
Summer (June to August)	V_{max} = 5 cm/sec 15% < 1.5 cm/sec no direction measurements V_{mean} = 0.4 - 1.7 20 days	V_{max} = 14 cm/sec 60% < 1.5 cm/sec 31% N, 18% E, 31% S, 20% W V_{mean} = 3.0 - 3.6 26 days	V_{max} = 22 cm/sec 77% < 1.5 cm/sec 39% N, 10% E, 42% S, 9% W V_{mean} = 3.8 - 4.2 54 days	V_{max} = 12 cm/sec 10% <1.5 cm/sec 40% N, 15% E, 28% S, 17% W V_{mean} = 0.3 - 1.6 26 days	V_{max} = 10 cm/sec 4% < 1.5 cm/sec 18% N, 40% E, 1% S, 41% W V_{mean} = 0.1 - 1.6 35 days
Fall (September & October)		V_{max} = 14 cm/sec 45% < 1.5 cm/sec 28% N, 16% E, 38% S, 18% W V_{mean} = 1.4 - 2.6 60 days	V_{max} = 15 cm/sec 67% < 1.5 cm/sec 43% N, 11% E, 33% S, 13% W V_{mean} = 2.3 - 2.8 50 days	V_{max} = 12 cm/sec 3% < 1.5 cm/sec 49% N, 22% E, 8% S, 21% W V_{mean} = 0.1 - 1.6 9 days	
Winter (ice-covered season)		V_{max} = 3 cm/sec 0.5% < 1.5 cm/sec 28% N, 71% E, 1% S, 0% W V_{mean} = 0.0 - 1.5 120 days	V_{max} = 4 cm/sec 3% < 1.5 cm/sec 71% N, 6% E, 20% S, 3% W V_{mean} = 0.0 - 1.5 140 days		
Spring (before June)		V_{max} = 9 cm/sec 66% < 1.5 cm/sec 32% N, 17% E, 29% S, 22% W V_{mean} = 2.6 - 3.1 30 days	V_{max} = 12 cm/sec 55% < 1.5 cm/sec 30% N, 16% E, 38% S, 16% W V_{mean} = 2.2 - 3.0 24 days		V_{max} = 7 cm/sec 35% < 1.5 cm/sec 8% N, 9% E, 50% S, 23% W V_{mean} = 1.4 - 2.4 13 days

Entries follow this format:

V_{max} = maximum speed
% of the time with velocities < 1.5 cm/sec
% of the time with flow to north, east, south and west
V_{mean} = range of mean speeds
duration of sampling

N.B. Station St5 was used for temperature measures only

Table 3.1A General current statistics in Lake Memphremagog.

The maximum velocities were recorded at St3 where the flows were also the most strongly polarized along the axis of the lake. These are not much greater than observed currents at St2, indicating that the effect of the constriction at Skinner's Island, which by continuity should yield larger flows, is of the the same order as the effect of increased wind fetch over South Basin. At St4 neither constriction nor fetch can enhance the flow and observations show generally low currents.

The most obvious seasonal feature is the almost total cessation of detectable circulation as soon as ice covers the water column. Direct observations and the scrutiny of satellite photographs revealed that the freeze-up of Central Basin lags that of the rest of the lake by up to a month. This seems to have very little effect over currents in South Basin, which stop as soon as there is a local ice cover. During the winter only a few small spikes of current associated with runoff, lasting no more than half a day, were detected. These, however, are about twice as large as what would have been expected from our estimates of peak discharge in section 2.2, pointing to the inadequacy of the method used, when dealing with short rapid events.

For the rest of the year, differences between 1976 and 1977 are of the same size as seasonal variations and no definite seasonal trend can be identified.

In the upcoming discussion a closer look will be given to the time series of both current and temperature measurements. Unfortunately the clipping of the velocity signal each time it falls below the threshold of the instrument acts to confuse the results of spectral analysis and we will have to rely primarily on visual interpretation of the current record. Temperature measurements, however, are easily subjected to standard time series analysis and the temperature profile measurements in Central Basin will supply important information on baroclinic motions of the lake. The author is indebted to R.G. Ingram who undertook most of the spectral analysis of the data.

Motion at the Frequency of the Surface Seiche

Visual inspection and spectral analysis of all current meter measurements at station St3 during ice-free seasons reveal a strong oscillation at a period of 2.1 hours. To determine if this could be due to surface seiching Defant's method (Neumann and Pierson, 1966) was used to determine the period of the first resonant barotropic mode. This involves solving numerically the one-dimensional equations of momentum and mass conservation, for a long wave propagating along the axis of the lake. The lowest eigenvalue for which velocities at the extremities of the basin are zero, correspond to the fundamental resonant mode. Higher eigenvalues can be used to give the higher order harmonic resonances. Because the expected resonant period is much shorter than the inertial period for the latitude of the lake (17 hours), coriolis acceleration can be neglected. Similarly, viscous dissipation is neglected because the damping time constant of observed oscillations is about five times the resonant period. By analogy to damped harmonic oscillators (Hamblin, 1976), this will yield a shift in period of only 0.05%. From the bathymetric information presented earlier, the solution depicted in figure 3.1a and a period of 2.0 hours were found for the fundamental seiche. The small difference between computed and observed resonance period may be attributed to the idealization of lake geometry. Specifically, in order to retain one-dimensionality, Sargent's Bay and Fitch Bay were neglected, as was the lateral shift in lake center-line which occurs at the two extremities of South Basin.

From figure 3.1a we see that the maximum velocities occur at the junction of South and Central Basins. It is not surprising then that seiching oscillations were detected only at St3. The reason for the velocity maximum is twofold: first, this is the location of the central node of the oscillation, and second, it is the narrowest point along the lake. Another slightly less important velocity maximum exists near Lord's Island between Central and North Basins. Unfortunately, all the moorings in this region were at station St6, in the lee of Lord's Island rather than in the adjoining channels, and no seiching was recorded.

Three portions of the October 1976 record at 4.0 m and 6.6 m, where seiching is predominant, are plotted in figure 3.1b. Periods of stratification, which are marked by a large temperature difference between the instruments, are noted. These are the results of upwelling events which will be investigated later. As can be seen, the oscillatory motion is not always in phase and of the same magnitude, as would be expected for a simple barotropic wave. Particularly on October 9th, both seiching and

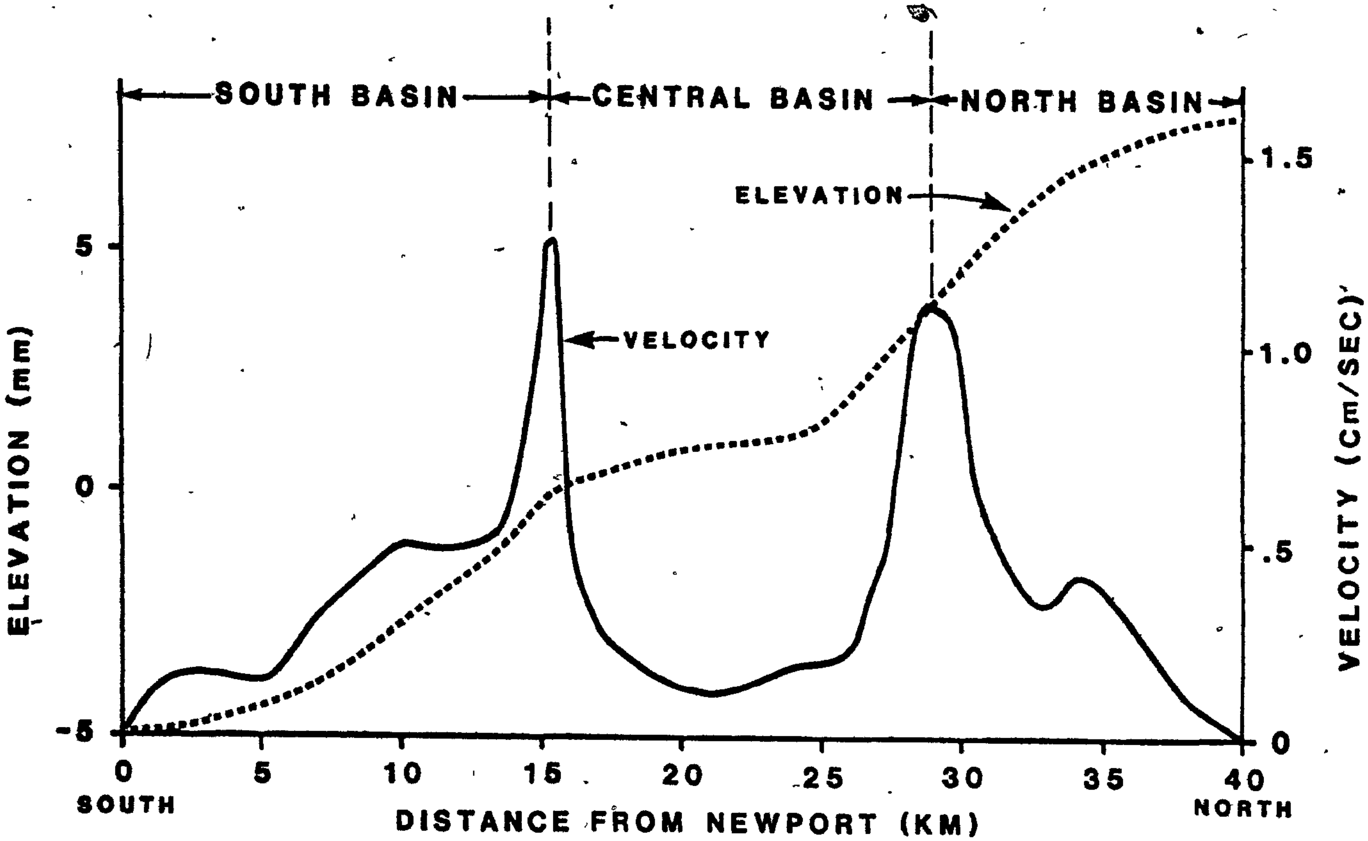

Figure 3.1a Solution to the first barotropic resonant mode for Lake Memphremagog. The amplitude of 5 mm at Newport is arbitrarily chosen, all other values are proportional to this.

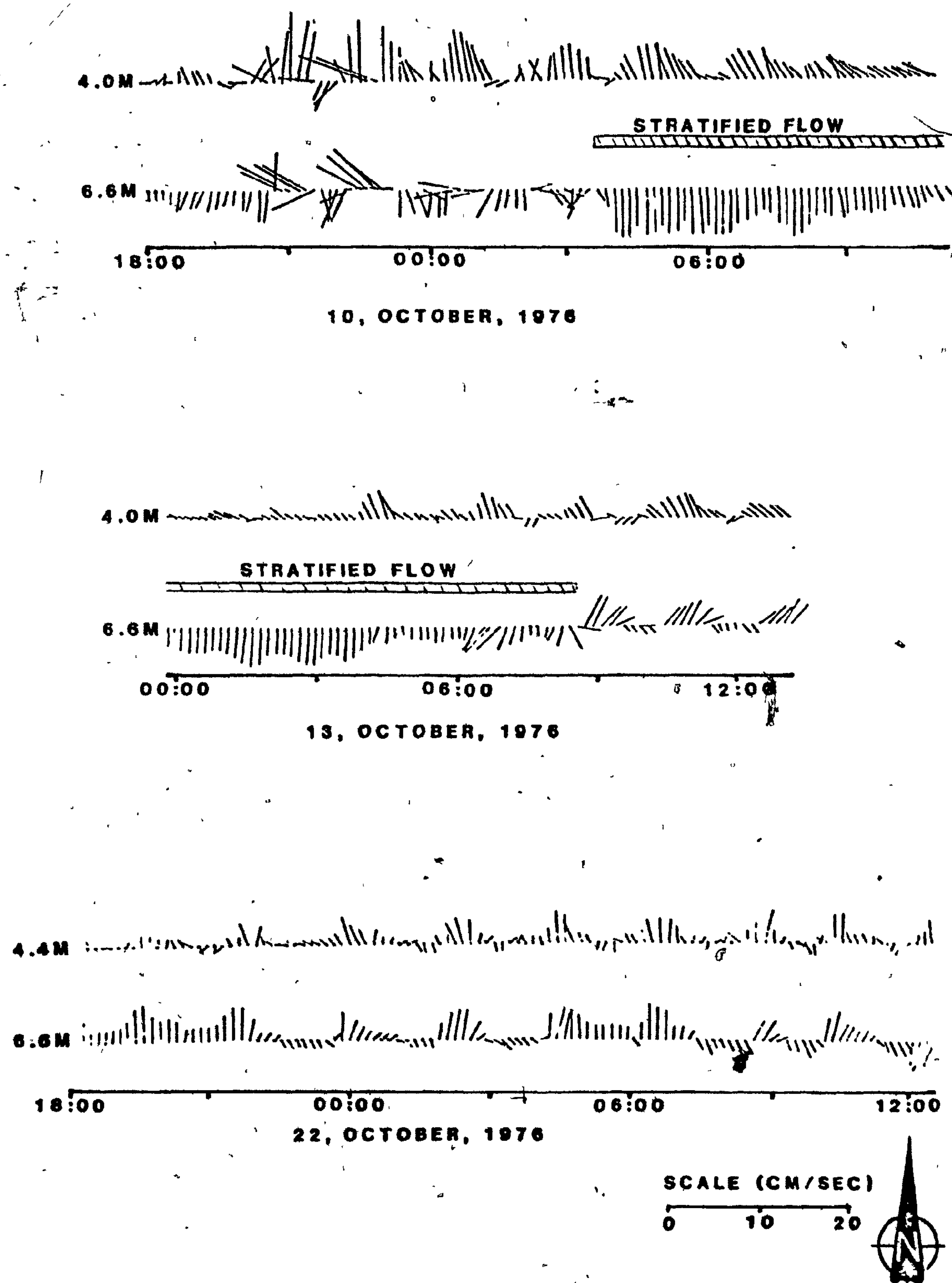

Figure 3.1b. Data records at St3 showing strong surface seiching.

steady motion are strongly sheared. Surprisingly, the oscillations at 6.6 m are from side to side of the basin. Three processes come to mind which may induce shear: bottom friction, nonlinear interaction between the sheared steady flow and oscillatory flow and finally, baroclinic motion. We will now examine each of these and assess their potential for causing the observed behaviour.

Both Smith (1977) and Grant and Madsen (1979) have investigated theoretically the interacting bottom boundary layers of steady and oscillating flow. Although primarily concerned with the case of wind waves superimposed on a background current, some aspects of their analysis are applicable here. They give the thickness of the oscillatory flow boundary layer as:

$$\delta = 2\kappa \quad U_{*}\mathrm{max} / \omega$$

where $\kappa = 0.4$ is the Von Karman constant

ω is the angular frequency of the oscillation

and $U_{*}\mathrm{max}$ is the friction velocity corresponding to the maximum instantaneous shear stress on the bottom.

Generally, $U_{*}\mathrm{max}$ may be related to the maximum flow velocity, V_{max}, by a friction factor, f, as:

$$U_{*}\mathrm{max} = V_{max}\sqrt{f/2}$$

Using a typical f of 0.006 for steady flow over a sandy bottom yields δ = 6 m for the velocities observed on the 9th of October. Following Grant and Madsen's method of determining the friction factor for an oscillatory flow yields f = 0.06 and δ = 21 m, so that clearly the turbulent boundary layer at least approaches the full depth of the water column. Details of their analysis break down when the boundary layer becomes comparable to the water depth since they basically consider a modified form of the law of the wall, with only one sheared boundary. However, some qualitative conclusions may apply. In the constant stress region of a bottom boundary layer, an oscillatory flow at an angle to the steady flow will cause the steady flow to change direction with depth. This arises because stress is proportional to the square of the velocity so that the effects of the two flow vectors do not add up linearly. This may explain the rotation of the steady current vector observed on occasion but not the rotation of the oscillatory flow.

Regardless of bottom friction, nonlinear effects may come into play because of the sudden change in topography at station St3. In order to assess the potential for nonlinear effects we can evaluate the linear and nonlinear acceleration terms, $\frac{\delta \mathbf{V}}{\delta t}$ and $\mathbf{V}\frac{\delta \mathbf{V}}{\delta x}$, of the equation of motion. To a first approximation we can consider nonlinearity as a small perturbation to the normal seiche, especially in view of the very localized nature of the constriction at St3. Then, $\frac{\delta \mathbf{V}}{\delta t} \simeq \mathbf{V}\omega$ and from the solution for the linear seiche (figure 3.1a) $\mathbf{V}\frac{\delta \mathbf{V}}{\delta x} \simeq \mathbf{V}^2\, 5 \times 10^{-3}$ cm^{-1}, just north of the constriction. Substituting the maximum observed amplitude of the oscillating velocity (8 cm/sec) we obtain 0.0070 cm/sec^2 and 0.0032 cm^2/sec for the linear and nonlinear terms respectively. Both are of the same magnitude and nonlinear effects are likely to be felt. This will likely be enhanced by interaction with the steady flow which will amplify the nonlinear acceleration. The sheared background flow is the steady state circulation arising from the surface wind stress, and as such will be affected by topography in a very different way from the barotropic oscillation. In general, the wind-driven shear flow is proportional to channel depth while the inverse is true of the seiching motion. Also the effective drag at the bottom of the epilimnion may change abruptly when passing from a region where the surface is in contact with the bottom (South Basin) to a region where it overlaps a denser water mass (Central Basin), thus causing a sudden change in wind driven velocity. It is not clear how the two components of motion will interact, but it seems plausible that rotation of the oscillatory flow may occur if the wind stress is at an angle to the axis of the lake.

The fact that sheared oscillatory flow is observed during or near episodes of stratification at the mooring site, suggests that baroclinic waves (internal waves) may come into play. For long interfacial waves one may calculate the interface displacement, $\mathbf{D}$, corresponding to a given velocity amplitude $\mathbf{V}$ as:

$$\mathbf{D} = \mathbf{h_l} \frac{\mathbf{V}}{\mathbf{C_i}}$$

where $h_i = \frac{h_1 h_2}{h_1 + h_2}$ is an equivalent depth

h_1 and h_2 being the thickness of the top and bottom layers respectively

$C_i = \sqrt{g\, h_i \frac{\Delta\rho}{\rho}}$ is the phase velocity.

Assuming that the stratification structure occuring on October 10th is composed of two layers of temperatures, 14 °C and 6 °C, each layer 5 m thick, we obtain h_i = 250 cm and C_i = 12 cm/sec. Then for baroclinic waves to induce flow velocities of the same order as the surface seiche,they must have amplitude of order 120 cm. No temperature fluctuation at the 2.1 hour period are observed at St3 indicating that any vertical displacement is probably small. This, however, is inconclusive since we are probably very near regions of generation and reflection so that the waves are not progressive. Spectral analysis of temperature measurements in Central Basin show marked peaks near the surface seiching period (figure 3.1c). Cross spectral analysis shows the oscillations to be vertically coherent, confirming their interfacial nature. Because the thermocline is very sharp, with a thickness less than the 5 m spacing of the thermistor sensors, it is difficult to assess the amplitude of vertical displacement. Estimates assuming a linear temperature gradient between sensors, suggest an amplitude of order 100 cm (figure 3.1c). These internal waves can be generated by the interaction of the surface seiche with the abrupt change in topography near Skinner Island, much in the same way internal tides are generated at the continental shelf break by surface tides. Baines (1982) gives an excellent review of linear generation

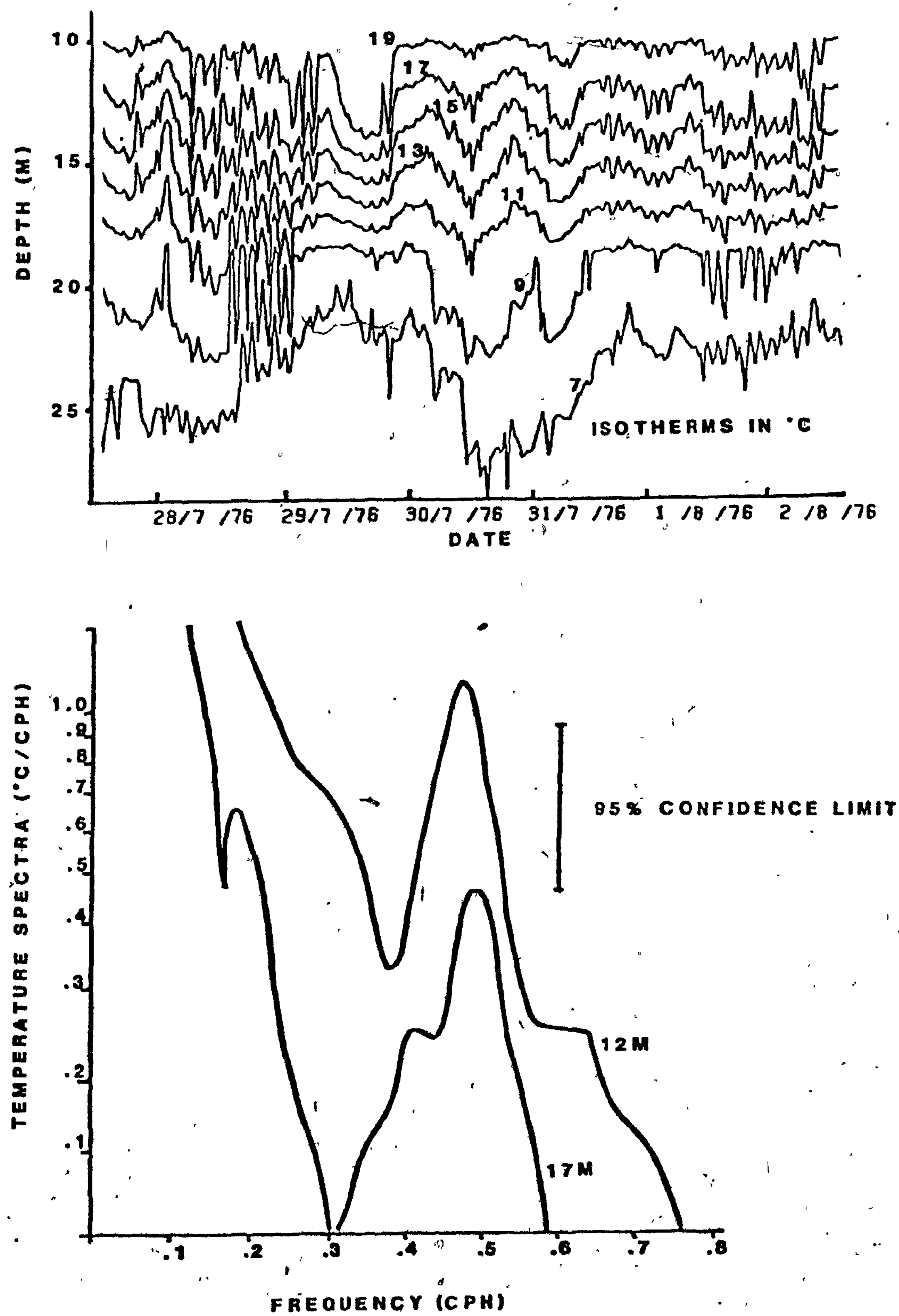

Figure 3.1c Isotherm plot and spectra of temperature showing internal waves at the frequency of the surface seiche in Central Basin.

mechanisms for internal tides. For the stratification used earlier and a sloping bottom with a 5% grade just north of St3, his solution predicts waves of 96 cm, for the seiche observed on October 10th. From observations in Central Basin the mean thermocline depth is about 14 m so that the interfacial depth must have varied in time before it was detected at the current meter level. According to Baines, the maximum amplitude of the internal waves (160 cm) would have occured when the thermocline passed the sill depth (10 m). These may therefore account for a considerable amount of shear. In view of the large amplitude of both the surface seiche and the internal waves it is probable that nonlinear effects come into play as generation mechanisms. For the October 1976 stratification another possibility is resonance with a transverse internal seiche. This might explain the transverse oscillation observed, but it is difficult to imagine how energy could be transfered from the surface longitudinal to the internal transversal seiche. Other generation mechanisms for the transverse internal seiche such as those described by Csanady (1973) rely on coriolis force to transfer longitudinal stresses into lateral motion, but they can only produce small displacements in a lake as narrow as Lake Memphremagog. Current meters were moored at station St3A and St3B to yield information on the lateral structure of flows near Skinner Island; they showed coherent oscillations with only insignificant amplitude differences across the channel.

It should be noted that the peak at the surface seiching period is the only significant peak in the temperature spectra, and the most prominent feature of the current spectra, for all of the data collected at the lake. Only the 2.1 hour seiching oscillation is apparent in visual inspection of the current meter data, the other spectral peaks were therefore interpreted as spurious response due to the clipping mentioned earlier.

In summary we can say that surface seiching is an important feature of the barotropic circulation of Lake Memphremagog. Because of the constriction at Skinner Island the flow is locally complex, being influenced by friction, nonlinear effects and the generation of internal waves. These internal waves are the only recognizable oscillatory feature of baroclinic motions. Internal waves are probably also generated at the constriction between Central and North Basins, in which case they would propagate in both basins. No temperature time series are available in North Basin to verify this assumption. Typical flows associated with the surface seiche have an amplitude of 3 cm/sec at Skinner Island. According to a solution obtained for the resonant oscillation of the lake, this corresponds to surface displacements of 1.25 cm and 1.90 cm at Newport and Magog respectively. Although the time history of atmospheric forcing would be important, comparison with the wind response computed for an idealized rectangular basin (Heaps and Ramsbottom, 1966) suggests, to a first approximation, that a surface stress of order 2.3 dynes/cm^2 (corresponding to a wind speed of 43 km/hr) lasting for about an hour would be required to produce the largest oscillations . The estimates of displacement and wind stress seem reasonable but remain unverified. It is probable that each basin of Lake Memphremagog can oscillate at its own resonant period (Murty, 1971), these motions would have to be detected by water level measurements as the associated current would be too small.

Cold Upwellings from Central into South Basins

Here we will discuss events in which sudden bursts of cold water are observed to flow along the bottom from Central to South Basin. Since during these events the equilibrium thermocline depth is below the level of the sill separating the two basins (10 m) and since most of the water thus transfered is not returned to the hypolimnion, they can be qualified as upwellings. During three mooring periods at stations St3, St3A or St3B, a total of 9 such events were detected. Figure 3.1d shows portions of current meter records extracted from each of the three mooring periods, and showing upwelling. In fall 1976 measurements at two levels permitted at least an estimate of the vertical extent of the cold water tongue. During the same period, temperature was recorded at 5 m intervals at St5, thus providing some insight into the accompanying baroclinic motions. In early summer 1977 a single current meter moored 1 m off the bottom recorded the largest number of upwelling events (5 in 34 days). At the same time another current meter was installed at the other extremity of Central Basin at St6. In August 1977 three current meters recording simultaneously at stations St3A, St3B and St4 provided information on the horizontal structure of the cold water flow.

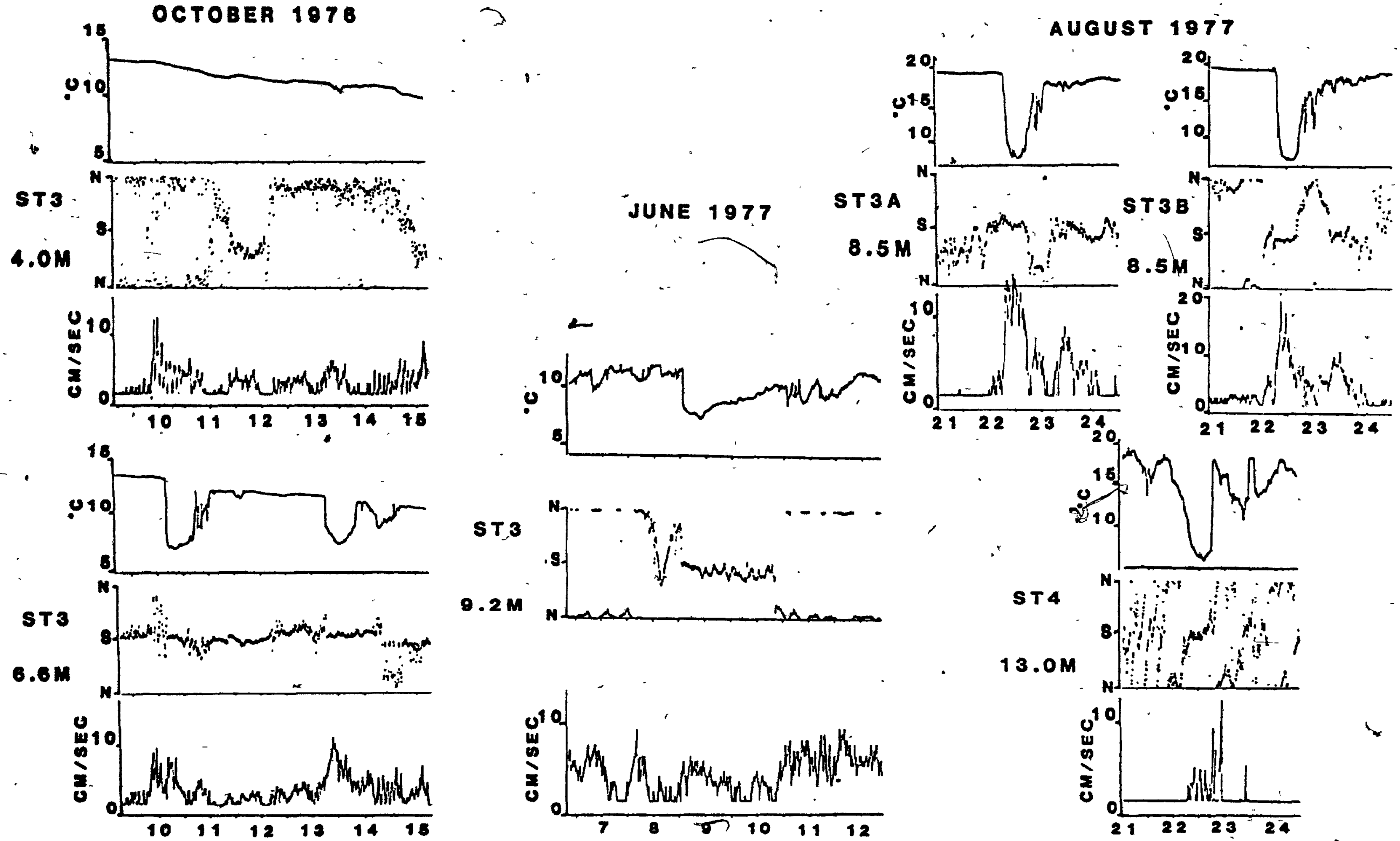

Figure 3.1d Current meter records showing upwellings of cold water from Central Basin to South Basin.

In the upcoming text we will first take a closer look at the relevant data, then consider what hydrodynamic processes may be involved and finally, estimate the importance of these events from a thermodynamic point of view.

The most interesting data is probably that collected in 1976. The current meters at St3 were at depths of 4.0 and 6.6 m in 10 m of water. The two cold water fronts detected by the lower current meter were not observed by the upper meter, thus the upwelling layer is known to have a thickness between 3.4 and 6.0 m. Temperature records at St5 show strong fluctuations associated with the upwelling. In one case a well-developed nonlinear undular bore of the type found in other long lakes (Hunkins and Fliegel, (1973), Thorpe (1971), Farmer (1978)) was observed. The high frequency internal waves which accompany this front are not well resolved and are subject to aliasing by our long sampling interval (10 min.). These oscillations, called solitons because of their similarity to solitary waves, result from the interaction of nonlinear steepening and dispersion of large amplitude disturbances (Zabusky and Kruskal, 1965). This internal front is shown in figure 3.1e together with the temperature fluctuations associated with another upwelling. In both cases the upwelling at St3 has been preceded by a gradual temperature drop at St5. It should be mentioned that temperature fluctuations recorded in Central Basin and smaller variations observed at the bottom current meter on October 6th suggest that at least one cold water intrusion of thickness less than 3.4 m may have gone undetected.

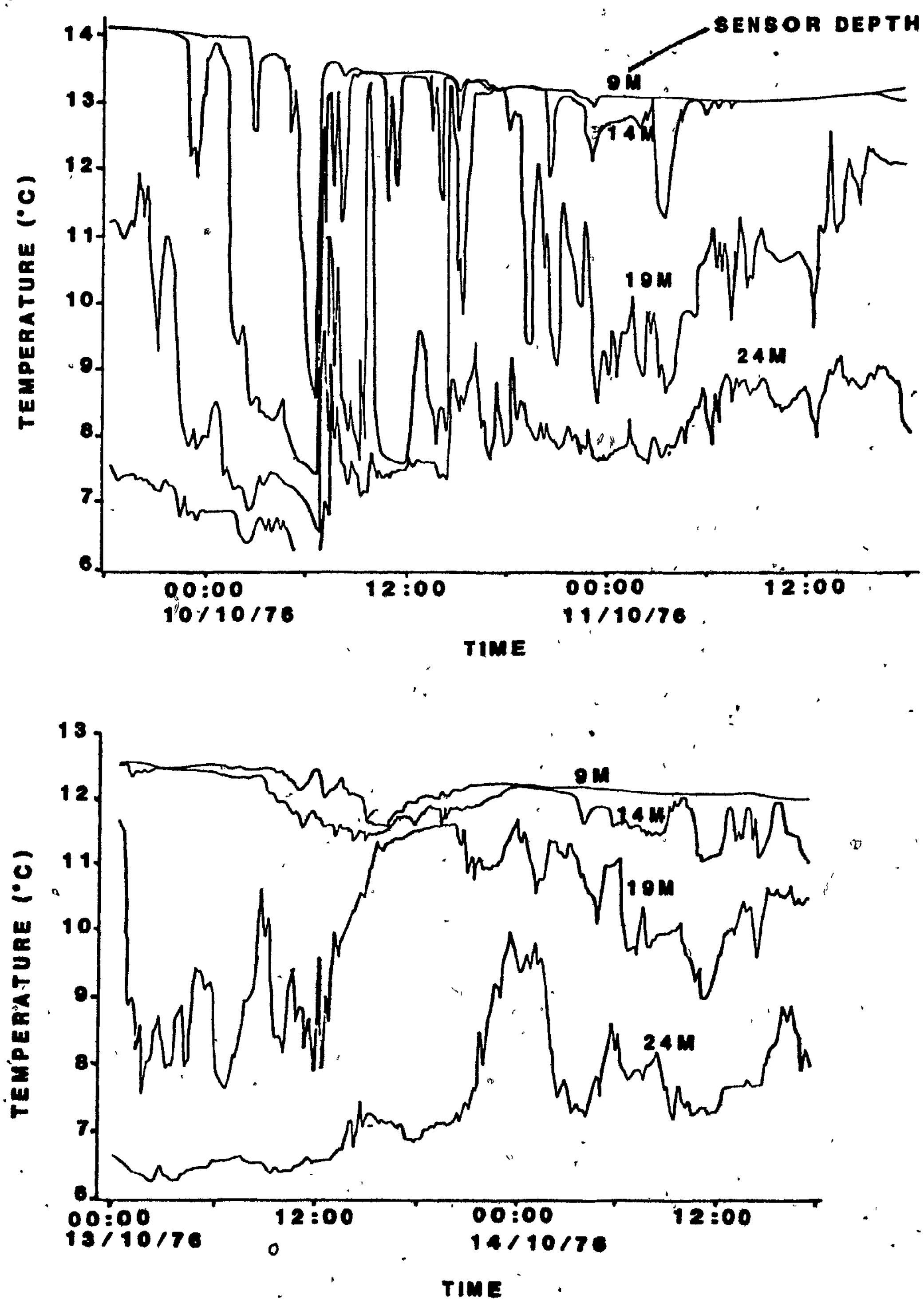

Figure 3.1e Temperature recorded in Central Basin at St5, during the upwelling events of October, 1976.

Comparison of the 1977 early summer record with the others shows the difference resulting from a weaker stratification period. During the major part of this mooring the thermocline depth was at or just below 10 m. Very small fluctuations in its level will therefore lead to upwelling. The temperature gradient in Central Basin was also weaker leading to a smoother variation of temperatures during upwelling, and in many cases the beginning and end of the events are not well defined. The current meter moored at St6 (not shown), 15 m deep, showed similar but more numerous temperature fluctuations. No systematic relationship seems to exist between the measurements at St3 and St6. Cold water exchanges probably occur between Central and North Basins, however because St6 is located in the lee of Lord's Island rather than in the interconnecting channels on either side of it, no currents are recorded and this transfer remains unverified.

The temperature measurements at St3A and St3B show that the cold water intrusion is laterally uniform. The sudden drop in temperature at the start of the upwelling occurs within the instrument sampling interval of 5 minutes on either side of the lake. The velocity differences may be attributed to the variations in bottom topography. Both instruments are 7.8 m deep but the total water depth is 8.5 m at St3B and 9.1 m at St3A. The time series at station St4, 1.5 km into Central Basin and 12 m deep, shows a gradual decrease in temperature before the upwelling and a very abrupt return to normal conditions afterwards. This abrupt change is reminiscent of the surge observed in October 1976. The highest velocities at St4 occur during a flow reversal accompanying this front.

Most upwelling events occur at the same time as surface seiching. The amplitude of the seiche varies considerably from one event to the next and strong seiching occurs with no upwelling. In the present discussion the two phenomena are assumed to be related only inasmuch as they both require strong winds along the axis of the lake. This is surely simplistic, especially in view of the interaction which can occur between the barotropic and baroclinic flow, but the present data base does not justify a more detailed analysis.

The gradual fall in temperature observed before and during the cold intrusions corresponds to a rise in the level of the thermocline. Since the measurement site (St4 or St5) is always nearest the southern extremity of Central Basin, this may be interpreted as the interface set up resulting in a southerly surface wind stress. According to Heaps and Ramsbottom (1966) the thermocline will sink at the down-wind end of the lake and rise at the upwind end in response to atmospheric forcing. For a steady uniform surface stress, τ , the interface between two liquids with a density difference, $\Delta \rho$ (small compared to unity), will reach an equilibrium tilt, $\frac{\partial \xi}{\partial x}$, of $\frac{\tau}{\Delta \rho g h_1}$, where g is gravitational acceleration and h_1 , the depth of the top layer. If the surface stress is imposed suddenly, the interface will start tilting, overshoot its equilibrium positions and oscillate at its natural resonant period, between the horizontal and twice its equilibrium position. Table 3.1B shows estimates of the tilt and wind stress needed to produce them, together with a

Table 3.18
Intrusion and stratification properties (for the thermocline at rest) during the nine observed upwelling events.

Properties of Cold Intrusions

	Duration	Temperature jump	Thickness of intrusion	Mean velocity	Volume transport	Heat transport
10/9/76	13 hrs	14.0° – 6.0°	>3.4 m <6.0 m	6 cm/sec	$>10\times10^6$ m^3> $<17\times10^6$ m^3<	80×10^{12} cal 136×10^{12} cal
13/9/76	14 hrs	12.0° – 7.0°		7 cm/sec	$>12\times10^6$ m^3> $<21\times10^6$ m^3<	60×10^{12} cal 105×10^{12} cal
1-2/6/77	24 hrs	10.0° – 6.0°	>1.0 m	9 cm/sec	$>8\times10^6$ m^3>	32×10^{12} cal
9/6/77	not well defined	13.5° – 8.0°		3 cm/sec		
17/6/77	28 hrs	14.5° – 8.0°		6 cm/sec	$>6\times10^6$ m^3>	39×10^{12} cal
24/6/77	not well defined	14.0° – 9.0°		6 cm/sec		
29/6/77	not well defined	15.5° – 7.5°		9 cm/sec		
22/8/77	11 hrs	19.5° – 6.0°	>1.5 m	12 cm/sec	$>7\times10^6$ m^3>	94×10^{12} cal
9/9/77	10 hrs	19.0° – 13.0°		12 cm/sec	$>6\times10^6$ m^3>	39×10^{12} cal

Properties of Central Basin Stratification

	Thermocline depth	Difference in mean density between epi- and hypolimnion	Phase velocity of long internal waves	First internal resonance period	Thermocline tilt required for observed upwelling	Surface stress required to produce a corresponding equilibrium tilt	Equivalent wind speed (drag coefficient = 1.3×10^{-3})
10/9/76	19 ± 3 m	0.70×10^{-3} g/cm^3	27 ± 2 cm/sec	24 ± 2 hrs	$2.1\pm0.6\times10^{-3}$	2.7 ± 0.8 g/cm sec^2	47 ± 6 km/hr
13/9/76	21 ± 3 m	0.44×10^{-3} g/cm^3	23 ± 2 cm/sec	30 ± 2 hrs	$2.3\pm0.6\times10^{-3}$	2.1 ± 0.8 g/cm sec^2	42 ± 5 km/hr
10/6/77	10 ± 1 m	0.50×10^{-3} g/cm^3	18 ± 1 cm/sec	42 ± 2 hrs	$>0.2\pm0.2\times10^{-3}$	>0.1 ± 0.1 g/cm sec^2	>9 ± 9 km/hr
20/8/77	13 ± 1 m	1.62×10^{-3} g/cm^3	37 ± 1 cm/sec	19 ± 1 hr	$>0.7\pm0.2\times10^{-3}$	>1.4 ± 0.4 g/cm sec^2	>34 ± 3 km/hr

$$* \text{ Tilt} = 2 \times \frac{\text{(mean depth of thermocline − layer depth at St3)}}{\text{Length of Central Basin}}$$

summary of the general intrusion and stratification properties for the nine observed events. The uncertainties originate primarily in the determination of thermocline depth with temperature measurement levels 5 m apart or from line angle when profiling from a boat. The calculated stresses are consistent with those required for the observed surface seiching. Assuming that no overshooting occurs, these would have to lastfor the time required for the thermocline to achieve the tilt, plus the duration of the upwelling. For a suddenly applied stress the time required to first reach the equilibrium is one quarter of the resonant period of the basin. Then for the fall 1976 and summer 1977 events a southerly wind blowing for a total duration of about 18 hours would have been needed.

In the vicinity of the junction between Central and South Basins, very little tilt could be sustained since the only boundary against which the cold water could accumulate is the southern extremity of the lake. Another balancing force for the pressure gradient imposed by the surface stress is the nonlinear acceleration. Neglecting the thermocline tilt compared to the local 5% bottom slope we can find, using the conservation of mass requirement, that this acceleration ($V \frac{\delta V}{\delta x}$) is given by 0.05 $\frac{V^2}{h_2}$, where h_2 is the thickness of the intrusion at St3. The pressure field imposed by the surface stress, τ , for a frictionless interface is given by $\frac{\tau}{\rho h_1}$, where ρ and h_1 are the density and thickness of the surface water. For a southerly wind and a south flowing intrusion the signs are such that for the two terms tend to balance out. In the fall 1976 events

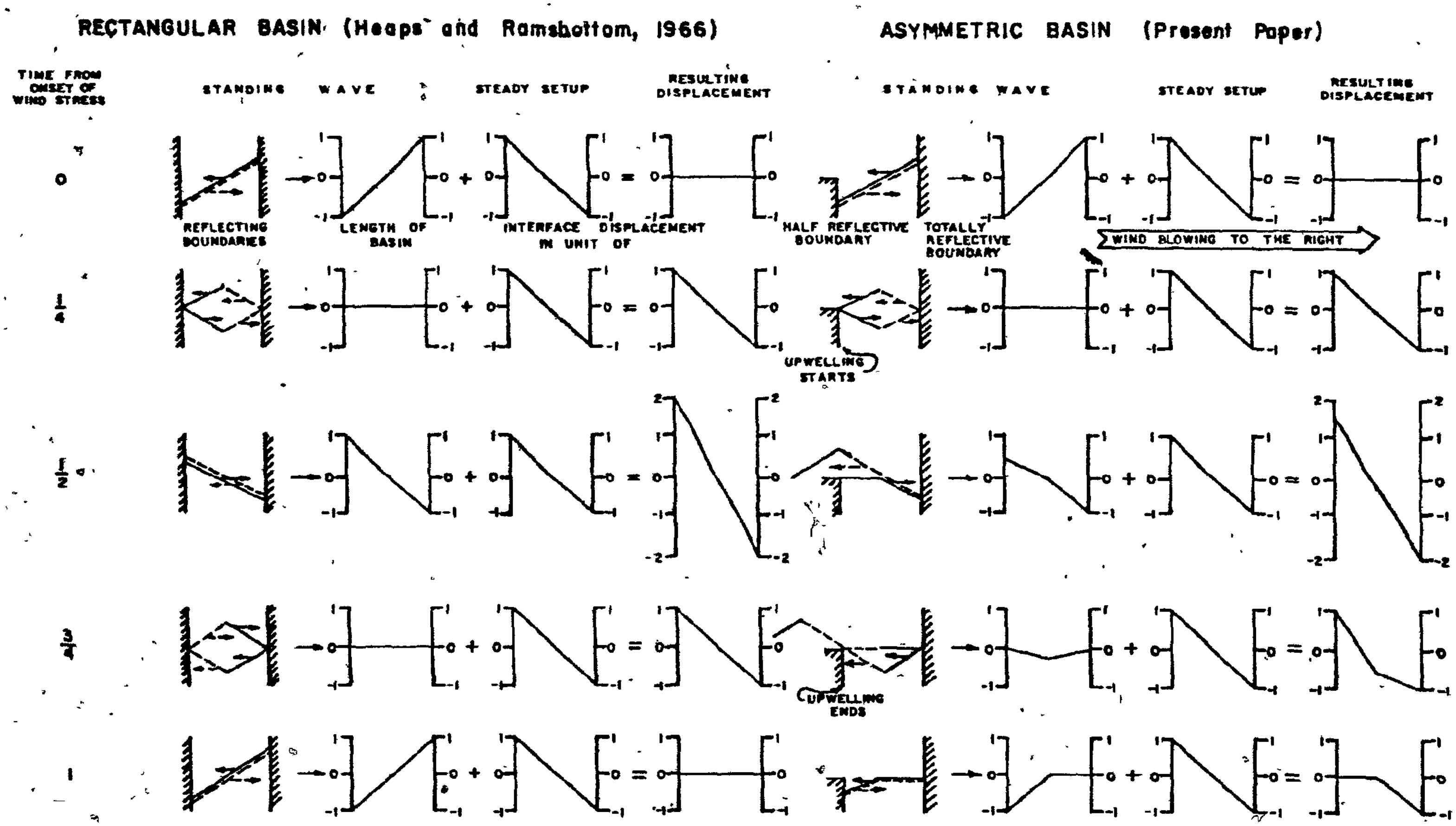

Figure 3.1f Schematic representation of the effect of steady setup and standing internal wave in response to a steady wind stress imposed at time 0. On the left is the case of a normal rectangular basin, on the right, for a rectangular basin with a partly reflecting boundary. In the first column, the full line represents the half of the standing wave initially travelling left, and the dashed line represents the half of the standing wave initially travelling right.

when the best estimates of h_1 and h_2 are available we find that the acceleration term could balance a surface stress of 1.2 to 4.0 g/cm sec^2 which is again consistent with other stress estimates. Further into South Basin a rapid decrease in intrusion thickness would be required to balance the surface stress on the flat bottom and widening channel. As the layer thins the velocity of internal waves it can sustain on its interface decreases and approaches the speed of the layer itself (ie. the layer Richardson number becomes small). This will cause shear instability and mixing. Neglecting the change in width we can find that the layer Richardson number will have decreased from 9 to 1 only 200 m downstream from St3. The widening of the lake will only enhance this effect. In addition to shear instability, mixing will occur due to entrainment. If surface agitation is assumed to provide energy for this mixing the rate of entrainment can be given by $\frac{\partial h_2}{\partial t} \simeq \frac{\rho \left(\frac{\tau}{\rho}\right)^{3/2}}{\Delta \rho \, g}$ (Niiler and Kraus, 1977). Using the stress estimates in table 3.1B we find that a rate of erosion of the cold water layer of about 25 cm/hr can be expected in every case except for the early summer 1977. This may have little effect at St3 where the intrusion layer may be relatively thick, however its importance will increase as the layer thins rapidly with distance into South Basin. The rapid mixing which is expected to occur within a few hundred meters after water enters South Basin explains why very little of the upwelled water is ever observed to flow back to Central Basin.

The sudden temperature rises observed in Central Basin during upwelling events correspond to abrupt depressions of the thermocline.

Their origin and the development, in one case, of an undular surge, is not as clear as the upwellings themselves. One problem is that at any one time there is only one measurement station in Central Basin, and we cannot directly ascertain the direction of propagation of any disturbance. At first it was thought that these disturbances were generated at the upwelling site as water was suddenly removed from the hypolimnion. Supporting this, the 1976 measurements show a difference in timing between the start of the surges at St3 and the passage of the disturbance at St4 equal to the amount of time required for a signal travelling at the speed of infinitesimal waves to travel the distance between the two stations. In this interpretation, however, it is not clear how the upwelling could result in a depression of the thermocline even if water is removed from the hypolimnion. Furthermore the 1977 observation of a temperature surge corresponding to the end of the upwelling and the flow reversal observed at St4 would suggest a south travelling pulse. An interpretation which can reconcile all observations is of an interfacial depression travelling southward. This deformation of the thermocline would first be detected at St4 and later cause the cold intrusion to cease as the interface is brought below the level of the sill. Using the end of the intrusion event (here defined as the time of the first rapid rise in temperature at St3) as the signal for the arrival of the surge, we can compute a transit time of 9 hours between St5 and St3 in fall 1976. Considering the 4.5 km separating the two sites the velocity of the surge can be computed as 14 cm/sec. This is considerably less than the phase velocities shown in table 3.1B, however we must consider that the thermocline is heavily tilted and that any disturbance travelling southward is effectively forced up an incline and slowing down. From the temperature profiles measured in Central Basin (figure 3.1e) we can compute the phase velocity of long waves just ahead and just behind the October 10^{th} surge. These are 22 cm/sec and 27 cm/sec respectively. Similarly the wave celerity at St3 can be calculated as 12 cm/sec. These values clearly show that the phase velocity for the thermocline at rest (Table 3.1B) used to support the north travelling pulse hypothesis are not applicable under severe tilt conditions. The values of the disturbance velocity based on the travel time is still relatively low but this may be due to the uncertainty in determining the arrival time of the pulse at St3.

A qualitative description of the generation mechanism for the upwelling and the internal surge can be given by looking at how the response of a rectangular two-layered basin is modified by allowing one discontinuous boundary. As illustrated in figure 3.1f the response is composed of a standing wave super-imposed on a steady tilt. The right side of the figure shows that as a result of the imperfect reflection steeper interfacial tilt occurs at the downwind end of the lake, at time $\frac{T_i}{2}$. This depression subsequently travels along the tilted thermocline, to the upwelling zone. This analysis makes no attempt to solve the boundary conditions exactly, but is conceptually correct. Following Farmer (1978) the distance required for an interfacial depression to evolve into a nonlinear surge is $x_b \simeq \frac{2}{3} \frac{h_1}{\delta\zeta/\delta x}$. For the 10^{th} of October 1976 this yields x_b = 9 km, thus a southward-travelling disturbance originating at the northern end of Central Basin could have degenerated into the observed surge at st5.

The idealized response illustrated in figure 3.1f is for a suddenly imposed wind stress, just sufficient for the thermocline to reach the sill at equilibrium. In a practical situation the amplitude of the southward pulse (therefore the formation of the surge) and the duration of the upwelling would depend on the time history and intensity of the forcing. Nonetheless, the present model explains the observation that the duration of upwelling is roughly proportional to the resonant internal period since it is not a steady state wind driven circulation.

Table 3.1B also gives estimates of volume and heat transport associated with upwelling. These were computed using the mean intrusion properties and assumes that no part of the water injected into South Basin flows back into Central Basin. For the spring 1977 observations these calculations must be considered very approximate since the water at St3 is probably always stratified and a profile of temperature and velocity would be required to properly compute the eddy fluxes. In most cases the intrusion is followed by a flow reversal which may carry some of the cold water back to Central Basin. The maximum amount of water observed to flow back was about 20%. A representative quantity of heat transported for the summer and fall events is 10^{14} cal. This corresponds to a cooling of 0.4 °C and a surface transfer of 250 cal/cm^2 for South Basin. Observed temperature drops before and after upwelling are typically

1.5 °C indicating that during these storm events atmospheric heat flux dominates over the effect of intrusion. Heat budget calculations to be outlined in chapter 4 support this conclusion, yielding surface heat loss ranging from 400 to 600 cal/cm^2 per day during the upwelling events. The volume of water removed from the hypolimnion of Central Basin would cause a drop in thermocline level of approximately 1 m. This is comparable to the deepening due to entrainment (0.05 m/hr for the stress found earlier) when the epilimnion, agitated by the surface wind, erodes the underlying stratification. The combined deepening is compatible with observations of the temperature profile in Central Basin.

On a day to day basis, the effect of upwelling on the heat budget and stratification of the basins of the lake is smaller but comparable to the effect of surface fluxes. Due to the low frequency of these events they probably have very little influence on the seasonal thermodynamic cycle of the lake. Perhaps a more important factor is that they provide a means by which the deep water, richer in nutrients, can be mixed in the euphotic zone. Previous calculations have shown that this water would mix vertically a short distance into South Basin. For the velocities usually observed in South Basin (see table 3.1A) a time scale for the horizontal dispersion of this enriched water over the whole South Basin is 4 days. There is no evidence for a persistent nutrient maximum near Skinner Island but a phosphorous rich bottom layer has been detected on occasion (Flett, 1977).Furthermore, this region in the lake is always a favorite fishing spot suggesting that biological activity may be enhanced locally. It should be mentioned that the combined effect of currents and wave motion would be vigorous enough at Skinner Island to transport sand particles and resuspend finer material (Grant and Madsen, 1979). This is supported by the fact that this region of South Basin, called Rocky Plateau, has very little fine sediment on the bottom, and may explain why the observed high phosphorous layer is usually more turbid. The resuspension of sediments in itself may be more important in enriching the water than the upwelling.

Non-periodic Current Structures

Here we will briefly look at current features of a non-periodic nature. These last for time scales of several days and their general character suggests a directly wind-driven circulation. Our purpose here is simply to describe the current structures which may be expected in the lake.

Figure 3.1g shows data recorded in summer 1976 and St2 in water 9.5 m deep. Two instruments were moored on a single line at 4.0 and 8.1 m. As may be seen, twice during this period, a stable stratification was formed and subsequently destroyed by wind mixing. These episodes are typical of stratified water bodies and are usually well explained by mixed layer dynamics, and in chapter 4 an attempt will be made to simulate the lake stratification using a numerical model. Some evidence of diurnal heating can be found during the periods of general homothermy. These

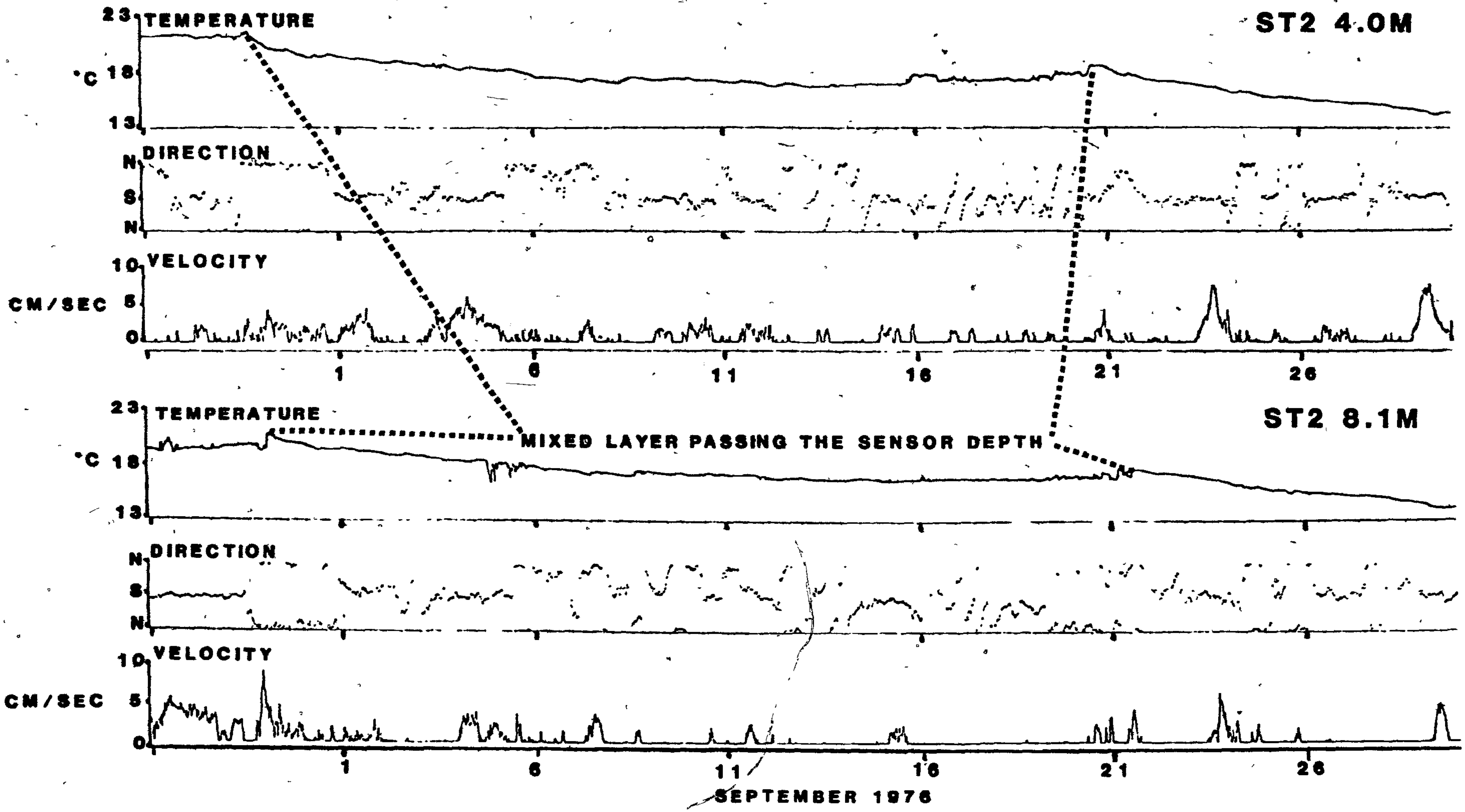

Figure 3.1g Current data record showing evidence of surface mixed layer deepening and entrainment.

however, cannot result from direct solar radiation since the maximum effect felt at 8.1 m usually occurs near midnight. They are caused instead by the formation and subsequent destruction of daily thermoclines.

An important feature of this data record is the difference in current regime between the stratified and unstratified conditions. Currents are usually vertically uni-directional with amplitude decreasing with depth during periods of homothermy. Otherwise the flow is in opposite directions and stronger near the bottom. The fact that the current at 4 m is lower during periods of stratification may be due to the position of the instrument near the middle of the water column and possibly close to a level of minimum current, where the flow reverses direction.

In order for the flow to maintain a steady direction with no bottom return flow, large scale horizontal circulation must exist. The only time during which such horizontal flow pattern could be monitored was during the 1977 experiments at St3A and St3B. Other moorings in this region have shown that the flow in this region is usually vertically sheared with surface flows opposing bottom currents. The fall 1977 moorings show that, on occasions, the flow may also be laterally sheared. The currents during these episodes are lower than average but still measurable (2.5 cm/sec). One period of laterally sheared flow lasted for 4 days, indicating the steady state nature of this circulation. The observations show mostly northerly currents on the east side and southerly flow on the west side, resulting in a cyclonic circulation. The observation period is much too short to determine if this is a persistent feature.

These observations confirm earlier measurements using profiling current meters, and point to a complex, spatially varying circulation pattern. For practical purposes it probably makes more sense to look at the horizontal current in South Basin as a turbulent flow. Scaling a horizontal eddy diffusion coefficient to the mean observed absolute velocity (Table 3.1A) and to the mean width of the basin we obtain a coefficient of 1.2×10^6 cm^2/sec. This would yield a time scale of 17 days for the longitudinal mixing of South Basin. This can only be considered as an order of magnitude estimate since choosing the length instead of the width of the basin as a dimension scale results in a coefficient 3 times larger and a mixing time 3 times smaller. Furthermore during storm conditions the maximum observed velocities could momentarily increase the diffusion by a factor of five.

3.2 Thermodynamics

In this section we will present data which will support a heat budget and stratification model for Lake Memphremagog in chapter 4. Since the model is not valid for the ice-covered season, special attention will be given here to the implication of winter observations. The data in itself is of interest in defining the basic physical environment and its variability in the lake.

Figure 3.2a summarizes temperature profile data collected between 1972 and 1977. Each data point represents the mean of all observations

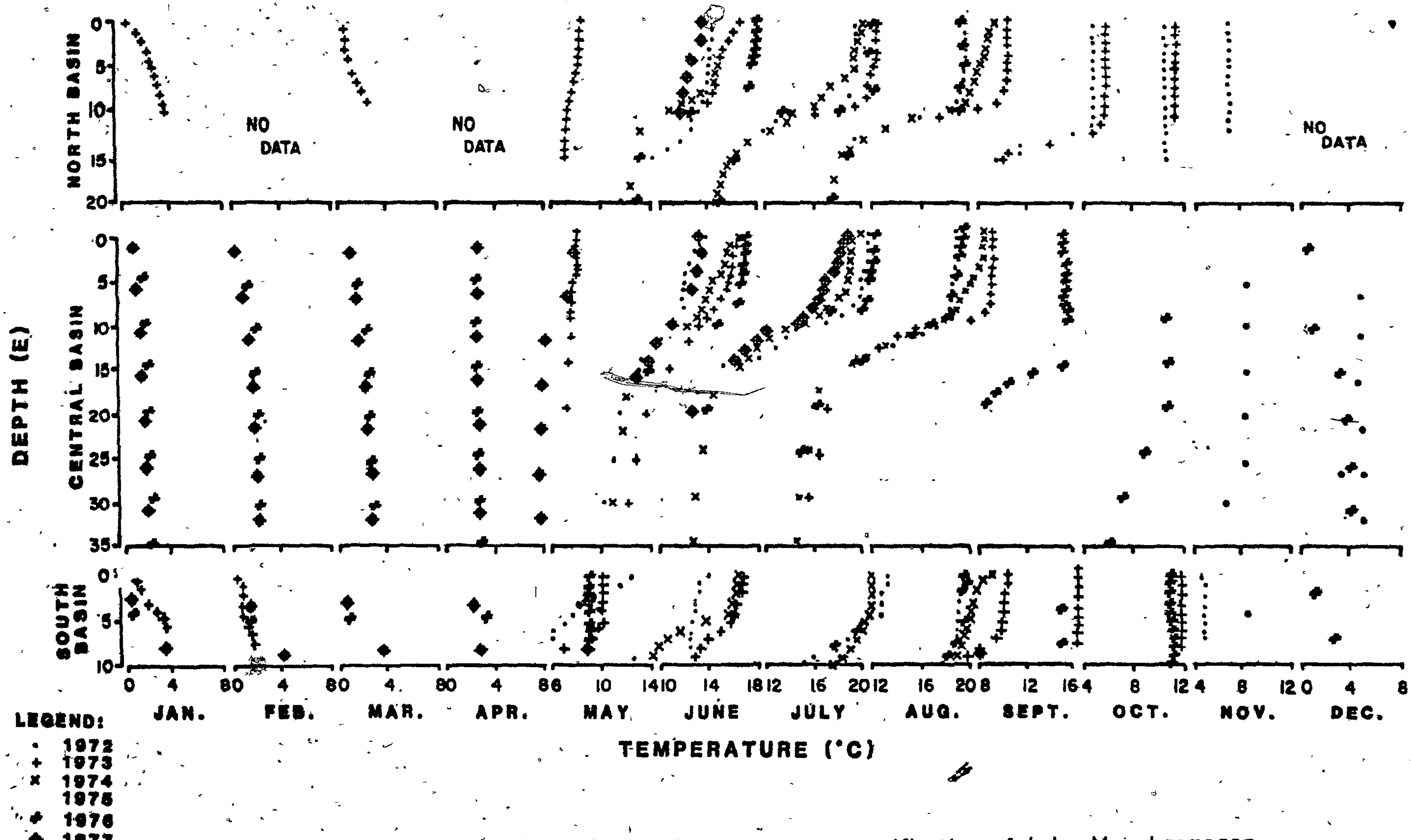

Figure 3.2a Seasonal temperature stratification of Lake Memphremagog.

taken during the two-week period centered on the middle of each month. Most data points result from averaging at least three profiles taken either on different days or at different stations within a basin and contamination of the signal by baroclinic motions is negligible. The variations shown are therefore truly representative of seasonal and interannual variability. One problem with the averaging process is that it effectively smooths out the thermocline during periods of rapid change but comparison with the raw data reveals that two-week averaging still reproduces all significant features.

Overall Thermal Cycle

As mentioned earlier this lake follows a typically dimictic cycle, with the seasonal warming and cooling being the predominant feature. Interannual variation for the ice-free season can be quite large (~ 4 °C). Comparing data for the three basins we find that the main lake response to surface heat fluxes is unimodal, i.e. the lake warms and cools as a whole. Following the progression of stratification through each season it can be seen that any year is not consistently warmer or cooler but that from month to month they change position on the graph. This is consistent with earlier results which shows that meteorological conditions were quite variable on a time scale of a day to a month.

Examining the data more closely we can also detect a bimodal thermal response as expected in an asymmetric basin. There is often a slight temperature gradient along the lake, with Central Basin having a temperature intermediate between those of South and North Basins.

Ice breakup usually occurs simultaneously over the whole lake, in the later part of April. The inverse stratification in South Basin breaks down immediately and the water warms to above 4 °C within a few days, while Central Basin reaches the temperature of maximum density only a week later. During this period, cabelling must occur where the warm water (> 4 °C) meets cooler water (< 4 °C), forming a denser mixture which sinks to the bottom of the lake. The resulting feature called a thermal bar is commonly observed in large lakes. This phenomenon was not studied in detail in Lake Memphremagog, however, the position of the thermal bars is regulated by local water depth (Sundaram, 1974), and it is probable that the downwelling region remains near the junction of Central and South Basins, where the depth rapidly changes.

After the thermal bar period, Central Basin stratifies rapidly, as evidenced by summer bottom temperatures near 4.5 °C, but by mid-May, South Basin is still vertically uniform and 0.5 to 2.0 °C warmer than the rest of the lake. In June, stratification is quasi-continuous up to the surface, for the whole lake. Warming occurs primarily in a near surface layer so that depth differences become irrelevant and temperatures are near horizontally homogeneous. In July and August a thermocline forms near 10 m, which is almost twice the mean depth of South Basin. During these months the southern end of the lake is on some occasions warmer and on others cooler, with typical differences of 0.5 °C. The response remains mostly bimodal, with one extremity of the lake warmer than the other and the temperature fluctuations reflect short term variations in surface heat flux. The stabilization of the thermocline near 10 m may be in part due to increased dissipation and mixing at the depth of the sills, for baroclinic motions of a shallower thermocline.

By mid-September the cooling trend is well established and the thermocline has deepened to 12 m. South Basin remains colder than the rest of the lake for the fall season. The temperature difference reaches about 2 °C by the end of October. In November the fall thermal bar forms, with South Basin up to 4 °C cooler than Central. Because of the larger temperature differences, the fall thermal bar lasts longer (2 to 3 weeks) than its spring counterpart, and in 1976 South Basin was ice-covered by the time it ended. In 1976 current meters at St3 did not show increased horizontal heat flux compared to the rest of the year, suggesting that the thermal bar has little effect on the heat or water budget of each basin.

Freeze-up in Central Basin occurs in late December or early January, roughly a month after South Basin. Very few observations are available for North Basin but satellite photographs show that it also freezes over before Central Basin, indicating that at least in late fall depth differences between these basins become important. During winter the water temperature at the ice interface must be 0 °C everywhere. South Basin has a bottom temperature near 4 °C , and its water column as a whole warms between December and March. In Central Basin the temperature at 10 m depth is between 2.0 °C and 1.5 °C during this time, creating a horizontal change in temperature at the level of the sill. During spring runoff (end of March and beginning of April), the temperature under the ice decreases slightly due to the large inflow of melt water near 0 °C. In 1976 a homogeneous mixed layer formed in Central Basin at this time. This was initially interpreted as a convective layer resulting from solar radiation (Farmer, 1975), but more careful considerations showed that the rate of deepening of the layer was more related to the volume of runoff than to shortwave radiation flux. It can be speculated that during this record runoff year, velocities were high enough to cause turbulent mixing of the water column as it passed the constriction at Skinner Island, resulting in an homogeneous layer flowing into Central Basin. A mixed layer was also observed intermittently between 17 m and 22 m in 1977, but again it cannot be accounted for by local solar heating and must be advected from elsewhere in the lake. Towards the end of the spring freshet, the temperature of both South and Central Basins rises, in response to increased solar input and perhaps warmer river inflow. When the ice breaks up, South Basin is already at 4 °C throughout most of the water column while Central Basin is near 3 °C.

Thermal Convection

The pressure gradients due to horizontal temperature differences in Lake Memphremagog are typically 0.5×10^{-4} g/(cm^2 sec^2) and during the ice-free season the wind stress due to the slightest breeze will suffice to offset this. In winter, before the spring runoff these pressure gradients are the only forces which can generate baroclinic motions, for which much evidence has been found.

Figure 3.2b shows monthly temperature profiles measured with a thermistor chain at St5 in 1976 and St4 in 1977. The instrument manufacturer claims an absolute accuracy of 0.1 °C. For a small temperature range, such as observed in winter, the relative error of any one sensor will be nearer the resolution of the data logger (0.02 °C). The observed heating between January and March represents about 20% of the incident solar radiation at the surface. Such high transmission rates by the ice and snow cover have been observed by other authors (Farmer, 1975), however in our case the heating rate departs markedly from the exponential curve expected for the direct absorption of solar radiation. In 1976 the heating below 25 m would imply an unreasonable water transparency with an extinction coefficient five times smaller than observed values (0.3 to 0.5 m^{-1}). Vertical molecular diffusion would have a negligible effect on the observed temperature profile and throughflow is too small to generate turbulence (Ri 100). The temperature changes which occur below the ice cover in Central Basin must therefore be due to the advection of warm water ~~from~~ elsewhere in the lake.

In 1980 a winter survey was undertaken to determine if the differences between the 1976 and 1977 profiles could be due to spatial variation, and perhaps linked to dynamic processes. The results shown in

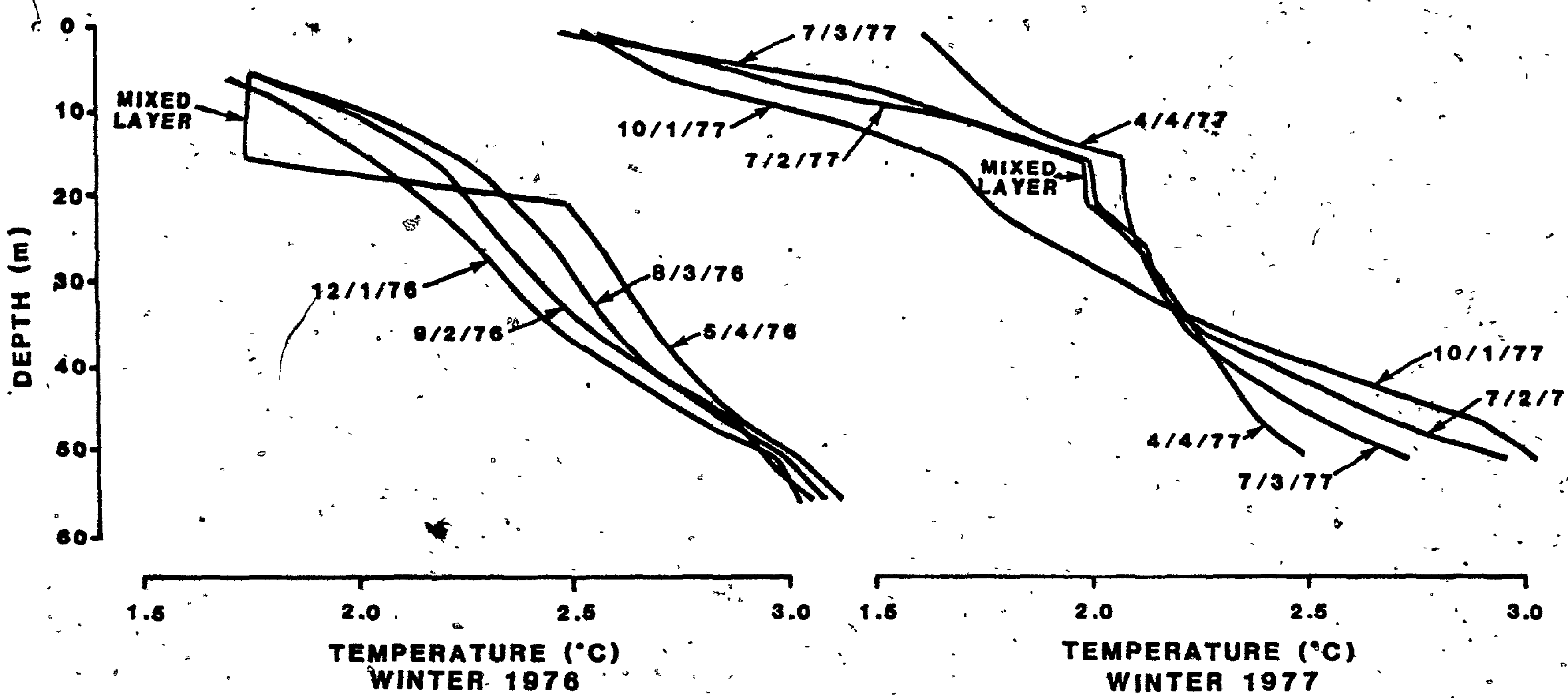

Figure 3.2b Under-ice temperature changes in Lake Memphremagog.

figure 3.2c were obtained with a thermistor probe with an accuracy of 0.1 °C. Both samples were taken for conductivity determination which showed variations of less than 2 , corresponding to a salinity of 1 ppm, which would have a negligible effect on water density. The results therefore confirms that the difference between 1976 and 1977 may be due to horizontal variations. Furthermore since temperature is the only important factor determining water density, the horizontal structure cannot be in static equilibrium and some motion must exist below the ice cover.

As mentioned earlier, current meter data at St3 show that, although the velocities are below measurement level, the flow is directed towards the north at 8.5 m and south at 2.8 m. This suggests that some convective heat exchange is occurring between South and Central Basin, with cooler water entering South Basin near the surface and warm water leaving along the bottom. Late in the season the flow direction near the surface reverses in response to higher runoff, indicating that convection velocities are smaller than those associated with throughflow during the freshet (0.8 cm/sec).

Solar radiation throught the ice cannot be dismissed as a possible energy source for convection, as it could cause more intensive heating of the shallower South Basin. It is difficult to estimate its effect since the transparency of the snow and ice cover may easily vary by an order of magnitude, and no radiation measurements below the ice are available. Another source of energy which may be assessed with some confidence is the release of the heat absorbed by the sediments during the summer months. In chapter 4 it will be shown that the sediments of South Basin

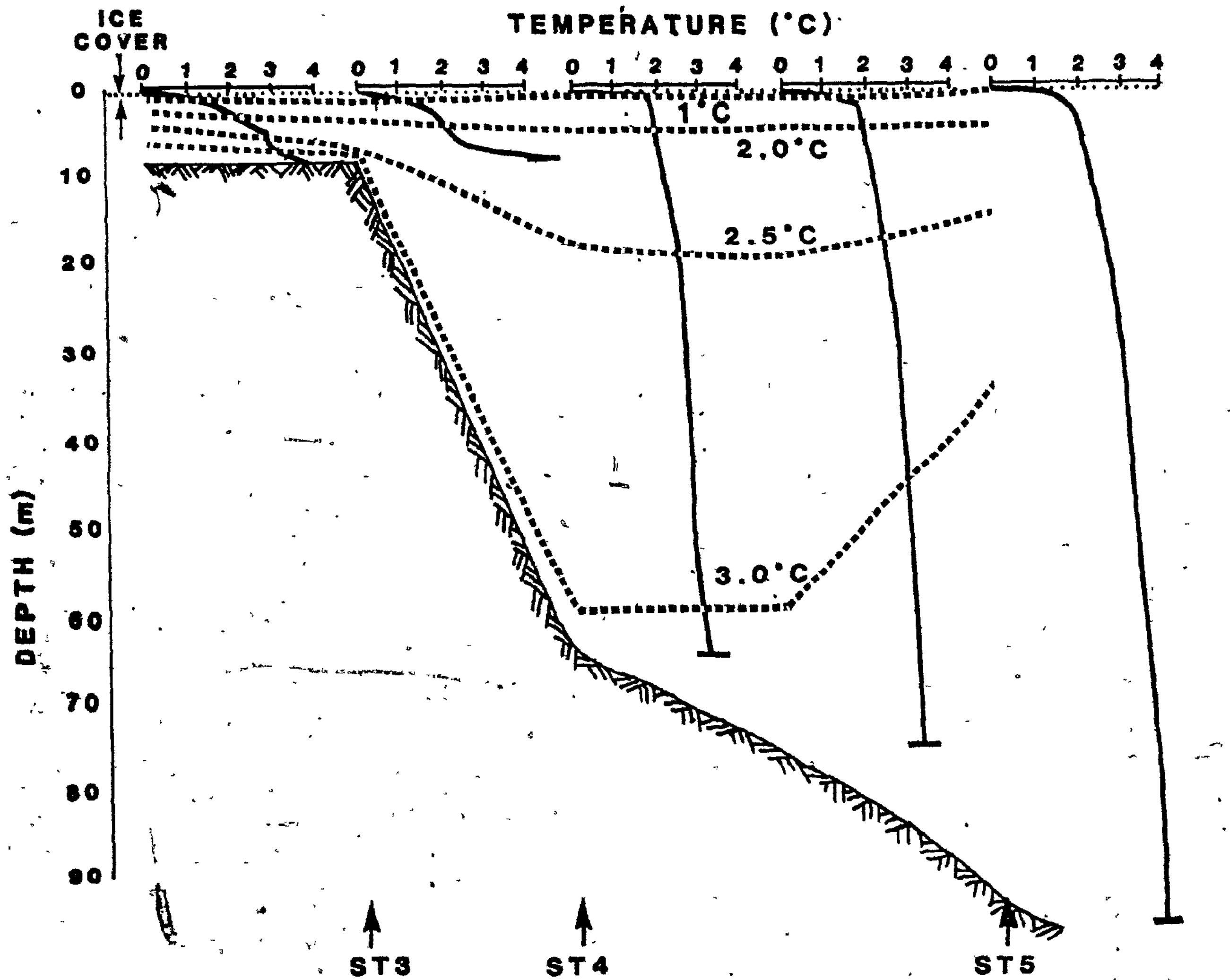

Figure 3.2c Horizontal temperature structure under the ice on March 18, 1980.

can take part in 30% of the local heat budget. To verify the importance of this in winter, a simple one-dimensional thermal model for the water column and underlying sediments was devised. During the ice-free season the water of the basin is assumed to be homogeneously mixed so that the sediment surface is subjected to the summer temperature cycle, and absorbs heat. The temperature profile of the sediment is computed by applying a finite difference integration scheme to the heat equation, using the sediment properties to be discussed in chapter 4. As soon as ice covers the water column, molecular diffusion and thermal convection are assumed to the only transport mechanism. The water surface temperature is fixed at 0 °C and both the sediment and water profiles are determined by the heat equation. Due to the heat released by the sediment, the bottom water may reach 4 °C. Any further heating will result in an unstable stratification as the bottom water becomes lighter than that directly overlying it. In such circumstances a convectively mixed layer of 4 °C would form on the bottom and grow vertically as Farmer (1975) proposed for solar heating under ice. Numerically this is simulated by mixing two adjacent water layers if they become unstable. Figure 3.2d shows the results of the simulations. The depth of the convective layer is very sensitive to the temperature of water at the time of freeze-up, and several runs were done to examine this dependence. As can be seen, a mixed layer of 1 m forms even for an initial winter temperature of 0 °C. For 1 °C, which is more realistic, the mixed layer grows to more than half the mean depth of South Basin. The error in sediment heat flux is ± 20%

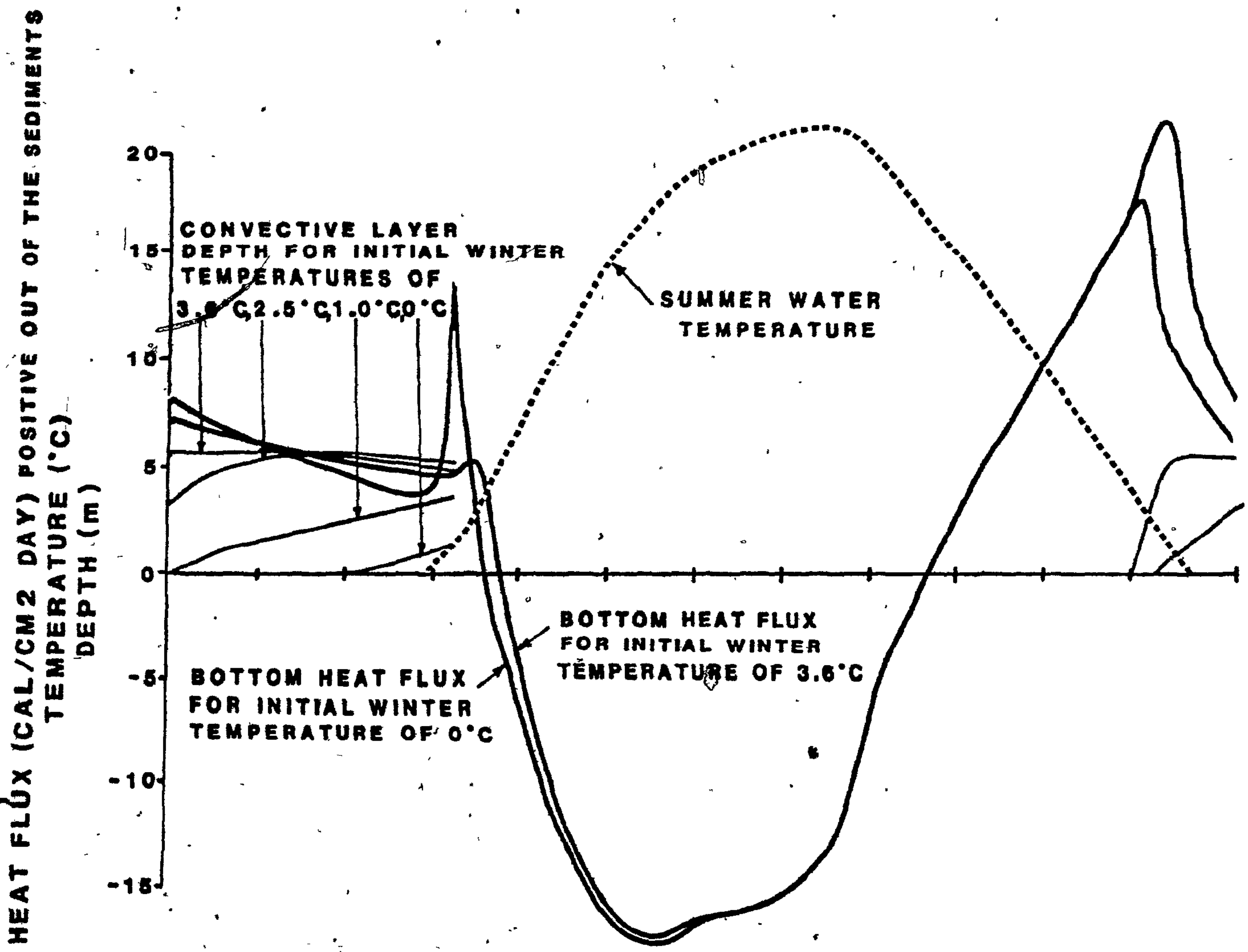

Figure 3.2d Result of simple heat sediment heat storage and release model.

and since the data shows no sign of such a mixed layer we must conclude that the heat is transported out of the basin. The mean under-ice sediment heat release of 5 cal/cm^2 per day is sufficient to account for the observed warming of both South and Central Basins from January until the start of runoff (mid-May). As for North Basin, few observations are available, but its smaller volume implies that it would account for only a small fraction of the thermal energy.

As seen in figure 3.2c the isotherm slopes down between St3 and St4, and we can infer that a density current flows down the slope. The temperature minimum between St4 and St5 in 1980, and the cooling observed near the bottom in 1977 may be interpreted as a depression in the isotherms, resulting when the density current, carried by its momentum, passes its equilibrium position and is subsequently deflected up again. This stationary wave has dimensions comparable to the length of Central Basin and exact computations of heat transport are impossible without temperature profile measurements at several locations along the lake, for the whole ice-covered season.

Summary

Recapitulating, the thermal cycle of Lake Memphremagog is dimictic and primarily uniform over the length of the lake. The main interest in the slight temperature variations that may be detected along its length is in the insight these may give us into exchange rates of water properties between the basins. During the ice-free season currents due to atmospheric forcing will dominate exchange processes, and it will be shown in chapter 4 that a simple turbulent exchange coefficient adequately models the interbasin transport rate. During most of the winter thermal convection is the only driving force for internal circulation in the lake. Observations and consideration of the heat released by the sediment suggest that a significant amount of water is exchanged between the basins. The under-ice temperature distribution in Lake Memphremagog is more complex than that observed in basins of simpler geometry (Stewart, 1972) and an exact determination of transport rate would require more data. As the end of winter approaches river runoff plays an important role in the hydrodynamic and thermodynamic behaviour of the lake. Just before ice breakup the temperature of South Basin is heated almost uniformly to 4 °C, suggesting that internal heating of the water column and perhaps warmer river inflow may be important in triggering removal of the ice cover.

4. THERMAL STRATIFICATION MODEL FOR LAKE MEMPHREMAGOG

In this chapter a numerical model for the temperature stratification of Lake Memphremagog will be presented. The thermal stratification of a water body is the most obvious expression of the interaction between the water and the atmosphere, for time scales over a few days. It will determine the properties of shorter time scale phenomena such as the size of wind rows and the period of internal seiches, and define the physical setting in which biota will evolve. In addition, within a lake, the transport mechanisms controlling temperature distributions are likely to be important for other properties such as solute or particulate matter concentration; the understanding of stratification thus provides knowledge applicable in other branches of limnology.

Numerical modeling has found applications in most aspects of scientific research as a tool to test and further our understanding of nature. In environmental sciences an additional incentive is the need for predictive capabilities to help in planning the development of natural resources with the minimum detrimental effect. In the last decade several lacustrine stratification models have been developed, which can quantitatively simulate the thermal cycle of lakes. The main area of application of these models is in reservoir management where the effect of changes in water level, or the choice of inflow/outflow locations on the thermal regime of the basin itself and its discharge, may be simulated. In cases where the sources and sinks of other conservative properties are not far removed from those of heat (i.e. near the water surface), minor modifications of thermal stratification models will suffice to predict their vertical distribution.

In the first section of the present chapter a review of current stratification models is presented. In the second section the use of a one-dimensional model for Lake Memphremagog is justified and a final choice is made on the type of model to be used. Section three looks at the boundary condition to be imposed on a model of the lake. In the last part the final modeled stratification is compared to observations and conclusions are reached on the usefulness and limitations of this model.

4.1 Review of Present Thermal Stratification Models

Much of the work on stratification effects has been concerned with the ocean where the density is a function of temperature, salinity and pressure. In lakes and in the thermocline regions of the ocean, the depth is small enough for the pressure dependence to be neglected. As for salinity, excluding salt fingering, its effect is homologous to that of temperature so that consideration of one or the other can be sufficient (Munk and Anderson, 1948). Here we will consider heat to be the only source of buoyancy with no loss of generality.

In lakes and parts of the ocean where mean currents are small and the surface condition uniform, isotherms will, on the average, be nearly horizontal. This permits the use of one-dimensional equations to describe the thermal structure of these bodies. Neglecting molecular diffusion compared to turbulent transport the conservation of heat for a basin of varying cross-section is (Tzur, 1973):

$$\frac{\delta}{\delta t}\rho C\overline{T} = -\frac{1}{A}\frac{\delta}{\delta z}\rho CA\overline{W'T'} - \frac{1}{A}\frac{\delta}{\delta z}\rho CA\overline{W}\,\overline{T} + Q_i \qquad 4.1.1$$

In oceans the large horizontal dimensions allow one to neglect the variation of **A** so that 4.1.1 reduces to:

$$\frac{\delta}{\delta t}\rho C\overline{T} = -\frac{\delta}{\delta z}\rho C\overline{W'T'} - \frac{\delta}{\delta z}\rho C\,\overline{W}\,\overline{T} + Q_i \qquad 4.1.2$$

where:

τ = time

ρ = density (ML^{-3})

C = heat capacity ($QC^{-1}M^{-1}$)

T = temperature (C)

A = cross sectional area at a given depth (L^2)

z = vertical coordinate; zero at the surface, and positive upward (L)

W = vertical velocity (LT^{-1})

Q_i = internal heat sources ($QT^{-1}L^{-3}$), in the ocean is given by:

$$Q_i = \beta \Phi_p e^{\beta z}$$

and in closed basins by:

$$Q_i = \beta \Phi_p e^{\beta z} + \frac{\Phi_b}{A} \frac{\partial A}{\partial z}$$

where:

β = extinction coefficient (L^{-1})

Φ_p = penetrating component of short wave radiation flux ($QL^{-2}T^{-1}$)

Φ_b = heat flux through the bottom ($QL^{-2}T^{-1}$)

Overbars denote mean components and primes denote fluctuating components.

The second right-hand term in these equations represents vertical advection due to upwelling and can often be neglected. It can be determined in the oceans by overall dynamical consideration and in lakes it is the result of inflows and outflows below the surface which are part of the boundary conditions. Φ_p and Φ_b are also given by boundary conditions while β is a property of the water. It therefore remains to determine the first right-hand term, the turbulent heat flux, in order to solve for $\overline{T}$.

Two methods are widely used to find a solution, turbulence closure models and mixed layer models. In the turbulence model, by analogy to molecular diffusion the turbulent flux is often represented by:

$$\rho C \overline{W'T'} = -\rho C K_T \frac{\partial \overline{T}}{\partial z} \qquad 4.1.3$$

K_T is the eddy diffusion coefficient for T with dimensions (L^2T^{-1}). K_T is related through an empirical or semiempirical relationship to the density and velocity structure of the water column. It is therefore generally necessary to solve the equation of motion in order to determine $\bar{T}$.

In mixed layer models one assumes a priori the existence of a homogeneous surface layer in which all mixing takes place. One can then easily integrate equation 4.1.1 or 4.1.2 from the surface ($z = 0$) to the bottom of the mixed layer ($z = -h$). Then $\rho C \overline{W'T'}\big|_{z=0}$ is the surface heat flux prescribed by the boundary condition. At the bottom of the mixed layer when h increases the heat flux is used to bring the underlying water to the temperature of the mixed layer, therefore:

$$\rho C \overline{W'T'}\big|_{-h} = \rho C W_e \left(T_0 - T_{-h} \right) \qquad 4.1.4$$

where:

$W_e = H\left(\frac{\delta h}{\delta t}\right) \frac{\delta h}{\delta t}$

T_0 = temperature of the mixed layer

T_{-h} = temperature just below the mixed layer

$H(\ )$ is the Heaviside function defined as:

$$H(x) = \begin{matrix} 1, x > 0 \\ 0, x < 0 \end{matrix}$$

When h decreases there is no entrainment and $\overline{W'T'}\big|_{-h} = 0$. The turbulent kinetic energy (TKE) equation, which is also integrated from $z = 0$ to $z = -h$, is then used to evaluate W_e so that there is sufficient mechanical energy generated to maintain the mixing in the layer. Since one source of TKE is the instability of the mean shear, we must again solve the equations of motion.

Decomposition of the motion into its mean and fluctuating components and the subsequent manipulation to obtain the equations of mean momentum, continuity and TKE, are given in many textbooks (Phillips, 1966, for example). Here we shall just give the resulting relations after using several simplifying assumptions. The Boussinesq approximation neglects variation of density except in the pressure terms. The pressure is given hydrostatically; this holds if the mean vertical velocity is much smaller than its horizontal counterpart and if the vertical component of coriolis force is neglected. We can neglect nonlinear terms and horizontal Reynolds stresses assuming small currents compared to the wave speed and horizontally isotropic turbulence.

The governing equations are then,

for momentum conservation:

$$\frac{\delta \underline{\overline{V}}}{\delta t} + \underline{F} \times \underline{\overline{V}} + \frac{1}{\rho} \underline{\nabla} P + \frac{\delta}{\delta z} \overline{W' \underline{V}'} = 0 \qquad 4.1.5$$

$$\frac{\delta P}{\delta z} = -\rho g$$

for mass conservation (assuming incompressibility):

$$\underset{\rightarrow}{\nabla} \bullet \underset{\rightarrow}{\overline{V}} + \frac{\delta}{\delta z}\overline{W} = 0 \qquad 4.1.6$$

$$\underset{\rightarrow}{\nabla} \bullet \underset{\rightarrow}{V'} + \frac{\delta}{\delta z}W' = 0$$

for TKE:

$$\underset{(E)}{\frac{1}{2}\frac{\delta}{\delta t}q^2} = \underset{(A)}{\overline{W'V'}\frac{\delta \underset{\rightarrow}{\overline{V}}}{\delta z}} + \underset{(B)}{g\,\alpha\,\overline{W'T'}} - \underset{(C)}{\frac{1}{2}\frac{\delta}{\delta z}\left[\overline{W'(W'^2 + V'^2)} + \frac{\overline{W'P'}}{\rho}\right]} \qquad 4.1.7$$

$$- \underset{(D)}{\gamma\left[(\underset{\rightarrow}{\nabla}\bullet\underset{\rightarrow}{V'})^2 + (\frac{\delta}{\delta z}W')^2\right]}$$

where:

V is the horizontal velocity (LT^{-1})

$F = \sin(\varphi) \times 2\pi$ / day and

is the coriolis parameter, (T^{-1})

φ is the latitude

ρ is the density (ML^{-3})

P is the pressure $(MT^{-2}L^{-1})$

g is the gravity (LT^{-2})

$\frac{q^2}{2} = W'^2 + \underset{\rightarrow}{V'}\bullet\underset{\rightarrow}{V'}$ is the TKE per unit mass (L^2T^{-2})

$\alpha = \frac{1}{\rho}\frac{\delta\rho}{\delta T}$ is the coefficient of thermal expansion (C^{-1})

γ is the molecular viscosity (L^2T^{-1})

Arrows denote vector quantities, while primes and overbars have the same meaning as before.

The meaning of equations 4.1.5 and 4.1.6 is straightforward but equation 4.1.7 merits term by term explanation:

(A) - the shear production term; as the kinetic energy of a shear flow is always greater than that of a uniform flow with the same momentum, any decrease in shear by mixing must generate an equivalent amount of turbulent energy.

(B) - the buoyancy production term; any change in the stratification by the mixing brings about a change of potential energy which must also be balanced by turbulent kinetic energy.

(C) - the turbulent energy flux expressed the transport of turbulent energy by the turbulence itself.

(D) - the dissipation by viscosity.

(E) - the rate of change of TKE is usually negligible and the equation is considered in its balanced form most of the time.

The only term in equations 4.1.5 to 4.1.7 which involves horizontal coordinates is $\frac{1}{\rho}\underline{\nabla} P$ in 4.1.5. It is not generally feasible to solve the three-dimensional equation of motion unless we are interested in the velocity structure *per se*, and in some way equation 4.1.5 must be one-dimensionalized. Since we are concerned with velocity shear, only the baroclinic pressure warrants consideration. It can be shown that it will act on a scale equal to the time it takes for long internal waves to travel the length of the basin:

$$t = \frac{L}{\sqrt{g' h}} \qquad 4.1.8$$

where L is the horizontal dimension of the basin

h is the depth of the thermocline

$g' = g(\nabla \rho / \rho)$

$\nabla \rho$ is a characteristic density difference between the top and bottom waters.

In oceans and in lakes larger than 100 km, this time scale is usually larger than the dominant 2-3 day period of atmospheric events. The pressure force therefore never has the time to fully develop in response to surface wind stress, and can be neglected.

In small lakes the pressure term is usually computed approximately by dimensional considerations, or the shear production term in 4.1.7 is neglected altogether.

In the following pages we will review different versions of both types of one-dimensional models and see how different authors apply them to small basins. These are presented roughly in chronological order of their publication to show the evolution of ideas on the stratification process. The papers discussed were chosen to be representative of the work in this field, and are but a subset of a large amount of literature. A more complete list of publications on the subject is included in the bibliographical section.

Turbulence Closure Models

As mentioned earlier most of these models postulate the following form for the turbulent fluxes:

$$\overline{W'T'} = -K_T \frac{\delta\overline{T}}{\delta z} \qquad 4.1.9$$

$$\overline{W'V'} = -K_V \frac{\delta\overline{V}}{\delta z}$$

This subset of turbulence closure models can be called eddy coefficient models. The eddy coefficients are usually taken to be of the form:

$$K_T = K_{T,O}\, F_T \qquad 4.1.10$$

$$K_V = K_{V,O} \cdot F_V$$

where noughts indicate coefficients for neutral stability.

The F functions depend on both stratification and shear. Dimensional analysis shows that if the F's are to be dimensionless they must be functions of the Richardson number,

$$Ri_G = \frac{g\,\alpha\,\delta T/\delta z}{\rho(\delta V/\delta z)^2} \qquad 4.1.11$$

where Ri_G denotes the gradient Richardson number.

Similarly it can be argued that $K_{T,0}$ and $K_{V,0}$ must depend on some Reynolds number (Re) which expresses the ratio of inertia to viscosity, the only two forces that come into play in an homogeneous flow. This formulation permits a separate evaluation of the effect of varying Ri and Re.

The first realistic model of the upper ocean stratification was that of Munk and Anderson (1948). Based on the then available observational evidence, they assumed $K_{T,0}$ and $K_{V,0}$ to be equal. They obtained values for K_0 as a function of wind speed from a graph in Sverdrup et al (1942). For the F functions, they chose:

$$F_V = (1 + \beta_V Ri_G)^{-h_V} \qquad 4.1.12$$

$$F_T = (1 + \beta_T Ri_G)^{-h_T}$$

where β_V, β_T, n_V, m_T are semiempirical constants chosen as 10, 10/3, 1/2, 3/2 respectively.

Their limited computational facilities permitted only a steady state solution to the set of equations 4.1.2, .5, .9, .10, .11 and .12. The agreement of their calculations for thermocline depths with observations in Sweetwater Lake was probably fortuitious since they neglected the effect of pressure gradients and varying cross-sectional area. When applied to oceanic situations their technique underestimates the depth by a factor of one half. However, their model suitably describes the qualitative features of stratification in these water bodies (see figure 4.1a): a relatively uniform surface layer separated by a thin region of sharp temperature gradient from the underlying water, with little mixing occurring at depth.

In 1973 Sundaram and Rehm used a modified form of this model applied to a lake. They reasoned that due to continuity, currents must be very small in lakes, so more energy would be transfered from the wind to direct mechanical mixing by interaction with the surface waves, than to the mean current flow. Then a more appropriate velocity to scale the Richardson number would be the frictional velocity:

$$u_* = \sqrt{\frac{\tau_o}{\rho}} \qquad 4.1.13$$

τ_o is the surface wind stress

so that

$$Ri_* = -\frac{g\,\alpha\,z^2}{\rho\,u_*^2}\,\frac{\delta T}{\delta z} \qquad 4.1.14$$

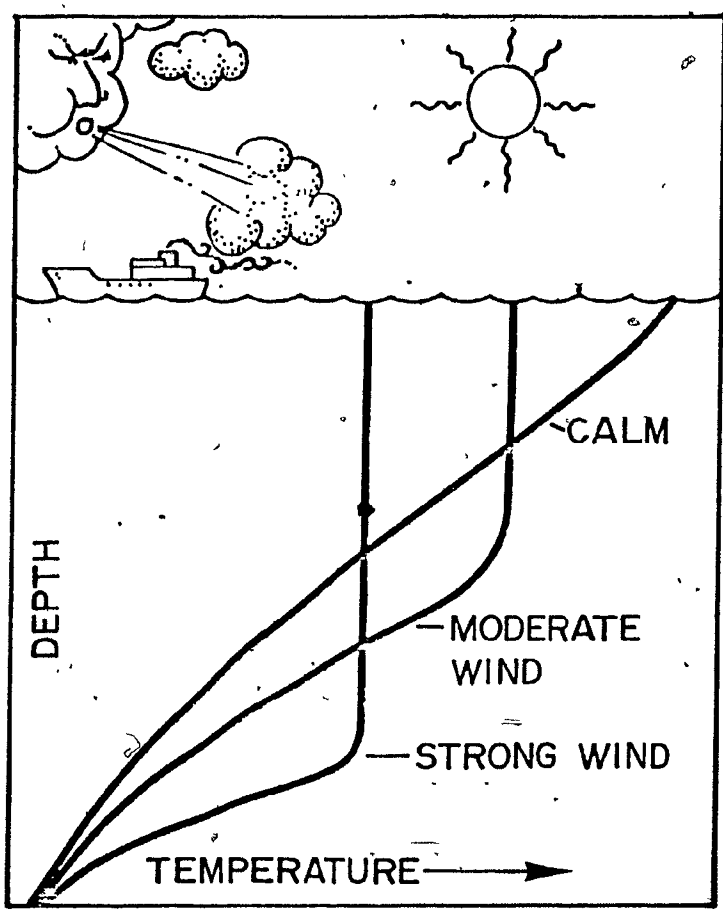

Figure 4.1a). Schematic representation of the development of a wind stirred layer and thermocline (redrawn from Munk and Anderson, 1948)

It should be pointed out that this will be equivalent to Ri_G for a uniform surface layer for times long compared to $L/\sqrt{g'h}$, when the internal oscillations of the lake will have attenuated and the only current that can remain is the surface boundary flow.

They put

$$K_{T,0} = c' u_*$$

where c is an empirical constant.

There are two regions in which this formulation is not expected to be valid: the region below the thermocline (the depth where $\partial^2 T/\partial z^2 = 0$), which is effectively shielded from surface disturbances by the stratification; and the region above the convection depth during periods of cooling. K_T is assumed to be constant in these zones and equal to the value at the higher and lower limit of these regions respectively. They solved the time dependent problem (equations 4.1.2, .9, .10, .14) iteratively, using $n_T = 1$ and $\beta_T = 0.1$ approximating the seasonal change in surface heat flux and wind stress by sinusoidal functions. They give results for $c = 2.82 \times 10^{-3}$ m, presumably chosen to give the best fit for conditions over Cayuga Lake, New York. Their model agrees well with observation; predicted thermocline depths are probably within observational error, and temperature prediction is within a few degrees. It should be noted that consideration of the variation in cross-sectional area by the use of 4.1.1

could considerably distort their computed profiles. The authors point out that their model predicts well the uniform temperature gradient observed in spring, a feature that mixed layer models cannot predict since they assume a discontinuous stratification at the start.

Mellor and Yamada (1974) have developed a hierarchy of the turbulence closure model. Equations 4.1.1 to 4.1.7 plus equations for $W'V'$ and $W'T'$ do not form a closed set unless some behaviour is assumed for the third order moments like $W'V'V'$ in term (C) of 4.1.7. Alternatively another set of equations can be derived to describe these third order moments, but these will introduce fourth order components. These in turn can be assumed functions of lower moments or can be given as a function of even higher fluctuating moments and so forth. In the lowest level of their system, they neglect terms (C) and (E) in 4.1.7 and set term (D) proportional to q^3/ℓ. They show that this is equivalent to an eddy coefficient model where $K_{T,O} = K_{V,O} = \ell q$ and F_V and F_T are fixed functions of the Richardson number, given graphically in figure 4.1b (which also shows the functions used by Munk and Anderson, Sundaram and Rehm, and mixed layer models). The mixing length ℓ can be defined as:

$$\ell = \frac{1}{10} \frac{\int_{-\infty}^{0} |z|\, q\, dz}{\int_{-\infty}^{0} q\, dz} \qquad 4.1.15$$

In 1975 Mellor and Durbin used this model to predict the behaviour of the upper ocean. Their results agree quantitatively with a month and a

Figure 4.1b) F_T and F_V used by various authors and in mixed layer models. The Richardson numbers are defined differently in each case so that the horizontal scale may not be the same for each curve. However, the shape of the curves can be compared.

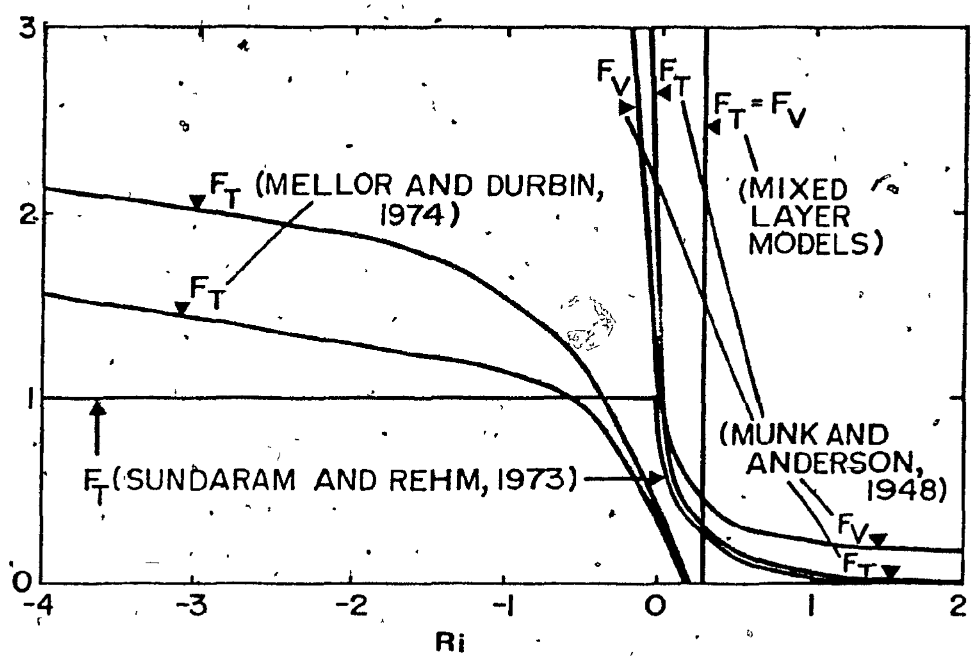

half of observations at station Papa (50° N, 145° W.), without any adjustment of constants being needed to fit the data. Their computations also agree well with laboratory results by Kato and Phillips (1969). Unfortunately this model is not directly applicable to lakes unless the full dimensional equations of motion are solved, since it relies uniquely on shear for the generation of turbulence.

Svensson (1978) also used a model which would correspond to level 1 in Mellor and Yamada's scheme, but assumes that the turbulent transport of energy, term (C) in 4.1.7 and dissipation, term (D), are given by a diffusion equation similar in form to 4.1.9, with appropriate eddy coefficients K_T and K_V. He approximated the effect of pressure by:

$$\frac{\partial}{\partial t} \vec{\nabla} P = C_p \vec{\underline{V}} \qquad 4.1.16$$

where C_p is a constant which depends on the dimensions of the lake. This formulation is valid only for $t < L/\sqrt{g'h}$ or if $L/\sqrt{g'h} > 2\text{-}3$ days, since it does not include baroclinic pressure. In this model **V** is not a velocity at a specific point, but is a representative value of velocity at a given depth for the whole lake. The success of his model is comparable to that of Mellor and Durbin except below the thermocline where mixing is consistently underestimated. The main object of his paper was to investigate by numerical experiments the effect of varying crosssectional area, pressure, and absorption of short wave radiation below the surface, all of which are neglected in the previously discussed models. The results for a basin of 100 km by 20 km showed that pressure will have a negligible effect, this is to be expected as the coriolis force will dominate the pressure term for baroclinic motions in large basins. However, consideration of both change in horizontal area with depth and variation in the extinction coefficient can change thermocline depth and temperature differences by as much as 100%.

Other models such as that of Hüber and Harleman (1972) which consider only molecular diffusion could be included here but they deal with basins having a large through flow, with inlets and outlets at different depths. They are dominated by vertical advection, and will not be considered here.

Mixed Layer Models

Mixed layer models depend critically on the assumption that the mixing occurs only in the homogeneous surface layer. In the previous section we have seen that this is reasonable except as pointed out by Sundaram and Rehm for periods of rapid change in heat flux. They show that the determining parameter is Π, the ratio of the time scale for variation in surface condition to the time scale for the formation of a new thermocline in response to these variations. The latter can be given by:

$$t = \frac{10\ u_*^2}{\alpha g\ \frac{\Phi_0}{\rho C}} \tag{4.1.17}$$

Using representative values for seasonal surface heat flux Φ_o and wind stress u_*^2 of 200 cal/cm^2 day and 10 cm^2/sec^2, respectively, we find the scale to be 5 days. Mixed layer models are therefore most useful for describing seasonal cycles. They are not applicable during a few weeks in early spring when a combination of small Φ_o, small α and large $\frac{\partial \Phi_o}{\partial t}$ combine to make H less than one.

Following from the above discussion we shall examine seasonal mixed layer models in oceans and lakes, relying on Niiler and Kraus (1978) for the derivation of the general theory.

As discussed earlier, the heat flux at the bottom of the mixed layer is given by:

$$\rho C \, \overline{W'T'}|_{-h} = -W_e \, \rho \, C \, \Delta \bar{T} \qquad 4.1.18$$

Similarly the momentum flux at the bottom of the layer can be given by:

$$\overline{W'\underline{V}'}|_{-h} = -W_e \, \underline{\bar{V}} - C_d \, \Delta \underline{\bar{V}} \, |\Delta \underline{\bar{V}}| \qquad 4.1.19$$

where Δ denotes the difference of a variable across the discontinuous interface at the bottom of the mixed layer.

The first right-hand term is the momentum flux needed to bring entrained water to the velocity of the mixed layer. The second term accounts for momentum lost to internal waves, C_d being a generalized drag coefficient. This parametrization for internal wave radiation loss is rather crude and others have been proposed (Kantha, 1977).

At the surface these fluxes are given by the boundary conditions:

$$\rho C \overline{W'T'}|_o = -\Phi_o \qquad 4.1.20$$

$$\overline{W'V'}|_o = -\frac{\tau_o}{\rho} = -u_*^2$$

τ_o is the wind stress ($ML^{-1}T^{-2}$).

Integrating 4.1.1 and 4.1.2 from $z = -h$ to $z = 0$, neglecting W and using the previously obtained values of flux at $z = -h$ and $z = 0$, we get for a lake:

$$\frac{\delta T_o}{\delta t}\int_{-h}^{0} A = -W_e\,\Delta T\,A_{-h} + \frac{\Phi_o}{\rho C}A_o + \frac{\Phi_p}{\rho C}\beta\int_{-h}^{0} A\,e^{\beta z} + \int_{-h}^{0}\frac{\delta A}{\delta z}\frac{\Phi_p}{\rho C} \qquad 4.1.21$$

and for the ocean:

$$h\,\frac{\delta T_o}{\delta t} = -W_e\,\Delta T + \frac{\Phi_o}{\rho C} + \frac{\Phi_p}{\rho C}(1 - e^{-\beta h}) \qquad 4.1.22$$

The noughts now denote surface values, while -h subscripts denote values at the bottom of the mixed layer.

For now, let us neglect the pressure gradient term in 4.1.5 and also integrate it over the mixed layer:

$$h \frac{\delta \underline{V}_0}{\delta t} + h \underline{F} \times \underline{V}_0 = u_*^2 - W_e \Delta \underline{V} - C_d \Delta \underline{V} |\Delta \underline{V}| \qquad 4.1.23$$

The only unknown in 4.1.22 and 4.1.23 is W which we will obtain by integrating the TKE. We will proceed term by term; for clarity each is tabulated with a brief description in table 4.1A.

- The general heat conservation equation in the absence of advection (valid only for a lake with a small throughflow) can be given as:

$$\frac{\delta T}{\delta t} = -\frac{\delta}{\delta z}\overline{W'T'} - \nabla \overline{V'T'} + \beta \frac{\Phi_p}{\rho C} e^{\beta z} \qquad 4.1.24$$

Mixed layer models assume a vertically constant T in the surface layer. We can therefore expect horizontal turbulent fluxes $\nabla \overline{V'T'}$ to be constant also. Integrating this equation between -h and 0 and again between a depth z and 0, the two resulting equations can be used to eliminate $\frac{\delta T}{\delta t}$ and $\nabla \cdot \overline{V'T'}$, to give:

$$\overline{W'T'} = \frac{\Phi_0}{\rho C}\left(1 + \frac{z}{h}\right) + \frac{\Phi_p}{\rho C}\left(1 + \frac{z}{h} - e^{\beta z} - \frac{z}{h} e^{-\beta h}\right) - \frac{z}{h} W_e \, \Delta T \qquad 4.1.25$$

Integrating again we obtain the integral of term (B) in (5):

$$g \alpha \int_{-h}^{0} \overline{W'T'} \, \delta z = g \alpha \left[\frac{\Phi_0 h}{2 \rho C} + \frac{\Phi_p}{\rho C}\left(\frac{h}{2} - \frac{1}{\beta} + e^{-\beta h}\left(\frac{h}{2} + \frac{1}{\beta}\right)\right) + \frac{h W_e \Delta T}{2} \right] \qquad 4.1.26$$

As $\frac{1}{\beta}$ is usually much smaller than h, the term containing $e^{-\beta h}$ is often neglected. In the ocean and in lakes when T > 4 °C, α is negative.

TABLE 4.1A

LIST AND DESCRIPTION OF TERMS

IN THE TURBULENT KINETIC ENERGY (TKE) EQUATION

	Term	Description
(A)	$\overline{W'V'}\,\frac{\delta \overline{V}}{\delta z}$	Shear production term
(B)	$g\,\alpha\,\overline{W'T'}$	Buoyancy production term
(C)	$-\frac{1}{2}\frac{\delta}{\delta z}[\overline{W'(W'^2+V'^2)}+\frac{\overline{W'P'}}{\rho}]$	Turbulent energy flux
(D)	$-\nu[(\nabla\cdot V')^2+(\frac{\delta}{\delta z}W')^2]$	Viscous dissipation
(E)	$\frac{1}{2}\frac{\delta}{\delta t}q^2$	Rate of change of turbulent energy

Since Φ_p is always positive the second right-hand term is a sink of energy (except in fresh water when $T < 4\,^{\circ}C$). Φ_0 can have either sign and can therefore be a source or a sink. As for the last term in a stable stratification it is always a sink.

- Integrating term (A), $\overline{W'V'}\,\frac{\delta V}{\delta z}$, is not so simple since the velocity gradient tends to infinity at the base of the mixed layer. We can get around this by allowing the velocity to vary linearly in a thin transition zone between $z = -h$ and $z = -h'$ ($h' > h$). Then using our previously obtained value for $\overline{W'V'}\big|_{-h}$ we get:

$$\lim_{(h'-h)\to 0} \int_{-h'}^{-h} -\overline{W'V'}\,\frac{\delta V}{\delta z}\,dz = \frac{1}{2} W_e\, |\underline{\vec{V}}|^2 + \frac{1}{3} C_D\, |\underline{\vec{V}}|^3 \qquad 4.1.27$$

- Shear within the layer is limited to a mean surface wave drift zone. From dimensional arguments, $\overline{W'V'}$ near the surface must be proportional to u_*^2 and the velocity gradient to u_* so that the integral of term (B) is:

$$\int_{-h}^{0} -\overline{W'V'}\,\frac{\delta V}{\delta z} = m_0\, u_*^3 + \frac{1}{2} W_e\, |\underline{\vec{V}}|^2 + \frac{1}{3} C_D\, |\underline{\vec{V}}|^3 \,. \qquad 4.1.28$$

where m_0 is a proportionality constant.

Each of these terms is positive and therefore a source term.

- The flux term (C) in the TKE equation has to be evaluated at the top and bottom of the mixed layer. At the surface this flux must equal the rate of working by wind velocity over the surface. Since the friction velocity is linearly related to the wind velocity we have:

$$-\frac{1}{2}\left[\overline{w'(w'^2 + v'^2)} + \frac{1}{\rho}\overline{w'p'}\right]\Big|_{z=0} = m_2 \frac{\tau_0}{\rho} W_{air} = m_1 u_*^3 \qquad 4.1.29$$

m_1 and m_2 are proportionality constants,

and W_{air} is the wind speed.

This term is a source of turbulent energy.

At the bottom of the layer the flux must equal the rate at which turbulent energy has to be supplied to make the entrained water as agitated as the mixed water, then:

$$-\frac{1}{2}\left[\overline{w'(w'^2 + v'^2)} + \frac{1}{\rho}\overline{w'p'}\right]\Big|_{z=-h} = -\frac{1}{2} W_e\, q^2 \qquad 4.1.30$$

which is a sink term.

- The most criticized part of mixed layer models is the specification of dissipation term (D) which we will now label ϵ. Most often $\int_{-h}^{0} \epsilon$ is assumed to be proportional to the active turbulence generating processes (the source term previously discussed), so that:

$$-\int_{-h}^{0} \epsilon = (1-n)\frac{g\alpha}{\rho C}\left[H(\alpha\Phi_0)\frac{\Phi_0 h}{2} + H(\alpha\Phi_p)\Phi_p\left(\frac{h}{2} - \frac{1}{\beta} + e^{-\beta h}\left(\frac{h}{2} + \frac{1}{\beta}\right)\right)\right] \qquad 4.1.31$$

$$+ (m_0 + m_1 - m)u_*^3 + (1-s)\frac{1}{2} W_e |\underline{V}|^2 + \left(\frac{C_D}{3} - c\right)|\underline{V}|^3$$

The Heaviside function is used to account for the buoyancy terms which may be either sources or sinks.

The notation for the proportionality constants m, n, s and c is used for convenience.

- We can now add all these equations to obtain the integrated equation of TKE. Factoring ~~out~~ W_e we have:

4.1.32

$$\underset{(a)}{\tfrac{1}{2} W_e\Big(q^2} + \underset{(b)}{c_i^2} - \underset{(c)}{s|\underline{V}|^2}\Big) = \underset{(d)}{m\, u_*^3} + \underset{(e)}{J_o\big(1 - \mathbb{H}(J_o)(1-n)\big) + J_p\big(1 - \mathbb{H}(J_p)(1-n)\big)} + \underset{(f)}{C_D\,|\underline{V}|^3}$$

where we have used the following abbreviations:

$c_i^2 = g\,\alpha\, h\,\Delta T$ is the internal wave speed squared for a deep basin

$J_o = \dfrac{g\,\alpha\, h}{2}\,\dfrac{\Phi_0}{\rho C}$ is the potential energy available from surface heat flux

$J_p = g\,\alpha\, h\,\dfrac{\Phi_0}{\rho C}\left(\dfrac{h}{2} - \dfrac{1}{\beta} + e^{-\beta h}\left(\dfrac{h}{2} + \dfrac{1}{\beta}\right)\right)$ is the potential energy available from penetrating solar radiation

Table 4.1B lists the meaning of each term.

The first term, involving q^2 is usually small and often neglected. If not, q^2 can be parametrized in terms of u_* and the buoyancy fluxes (Zeeman and Tennekes, 1977).

There are other possible parametrizations for the dissipation $\int_{-h}^{0} \epsilon$, but this one has the advantage that the efficiencies (m, n, s and c) with which different processes affect the entrainment velocity (W_e) can be

TABLE 4.1B

LIST AND DESCRIPTION OF TERMS

IN THE INTEGRATED TURBULENT KINETIC ENERGY (TKE) EQUATION

	Term	Source	Description	Remark
(a)	$\frac{1}{2} W_e\ q^2$	sink	Rate of increase of total TKE due to increasing layer thickness.	negligible
(b)	$\frac{1}{2} W_e\ c_i^2$	sink	Rate of increase of potential energy of the stratification due to entrainment.	
(c)	$-\frac{1}{2} W\ \ s\,\lvert\underline{V}\rvert^2$	source	Shear production term at the base of the entrainment layer.	may include the effect of term in addition to dissipation
(d)	$m\ u_*^3$	source	Primarily direct wind mixing term, due to agitation of the surface, but also includes shear production by surface drift.	
(e)	$J_0\left(1 - \mathbb{H}(J_0)(1-n)\right) + J_p\left(1 - \mathbb{H}(J_p)(1-n)\right)$	either	Potential energy available from atmospheric heat fluxes.	source for cooling; sink for heating, except in fresh water when 4 °C
(f)	$C_D\,\lvert\underline{V}\rvert^3$	sink	Radiation loss due to internal waves.	This term is rarely explicitely included.

considered individually. Experiments and observations where only one generating process is at work (Kato and Phillips, 1969; Farmer, 1975, etc.) confirm that the dissipation integral is reasonably independent of the mixed layer thickness **h**. It is not yet sure however that the dissipation effect on the different energy generating processes can be added linearly.

Equations 4.1.21, .22, .23 and .32 form a closed set which is most often solved by finite difference methods. If the change in **h** and τ_o, from one iteration to the next is small, then nonlinear interactions of the terms may be neglected on the scale of the time step. Entrainment velocities (W_e) can be calculated for the individual source terms and then added. Most authors have found that a time step of a day or less yields adequate results. The iteration usually starts in spring when the thermal structure is vertically uniform. As the heating starts a thermocline forms at a certain depth **h** . Since there is no entrainment, **h** is found by solving 4.1.32 with the left-hand side set to zero. At each iteration the rate of heating is generally increasing at this time of the year. The third right-hand term therefore grows and **h** decreases while the temperature of the mixed layer increases. Progressively shallower and warmer thermoclines are formed, leaving behind a series of fossil interfaces. If an analytical solution was found, a continuous stratification would result with only discontinuous first derivative at the mixed layer base. When the surface heat flux finally levels off at the height of summer and starts decreasing, the wind mixing and shear terms in 4.1.21 gradually gain over the buoyancy terms so that the left hand side becomes positive. Then entrainment starts eating at the underlying stratification even though the surface water might still be warming. During entrainment a characteristic discontinuous interface is formed. When heating converts to cooling in late fall the positive buoyancy flux will contribute to the erosion process and the mixed layer will rapidly grow until once again a uniform stratification is reached (see figure 4c). In fresh water α changes sign when the water has cooled to 4 °C so that an inverse temperature stratification starts developing. The surface mixing process is however soon arrested by ice formation when the surface temperature becomes zero.

Several authors have contributed to the development of this model. In early applications all but one or two terms in the integrated TKE equation were retained (Kraus and Turner, 1967; Pollard, Rhines and Thompson, 1973). In recent years the trend has been to include more and more of the terms and to refine their parametrization. We will not review this progression here as it would largely be repetitious of the previous derivations, the reader may refer to the bibliography for a list of papers on the subject. It is worthwhile however to consider two recent papers concerned with the use of mixed layer models in closed basins.

Spigel and Imberger (1980) have used equations 4.1.21 and 4.1.32 to simulate the stratification of a reservoir. In their analysis they neglected the rate of change in TKE (a), the effect of penetrative solar radiation (f) and ~~the~~ internal wave losses (g), but included the shear production term (c) by coupling the stratification model with a simple hydrodynamic model. The latter approximates the basin by a box containing two

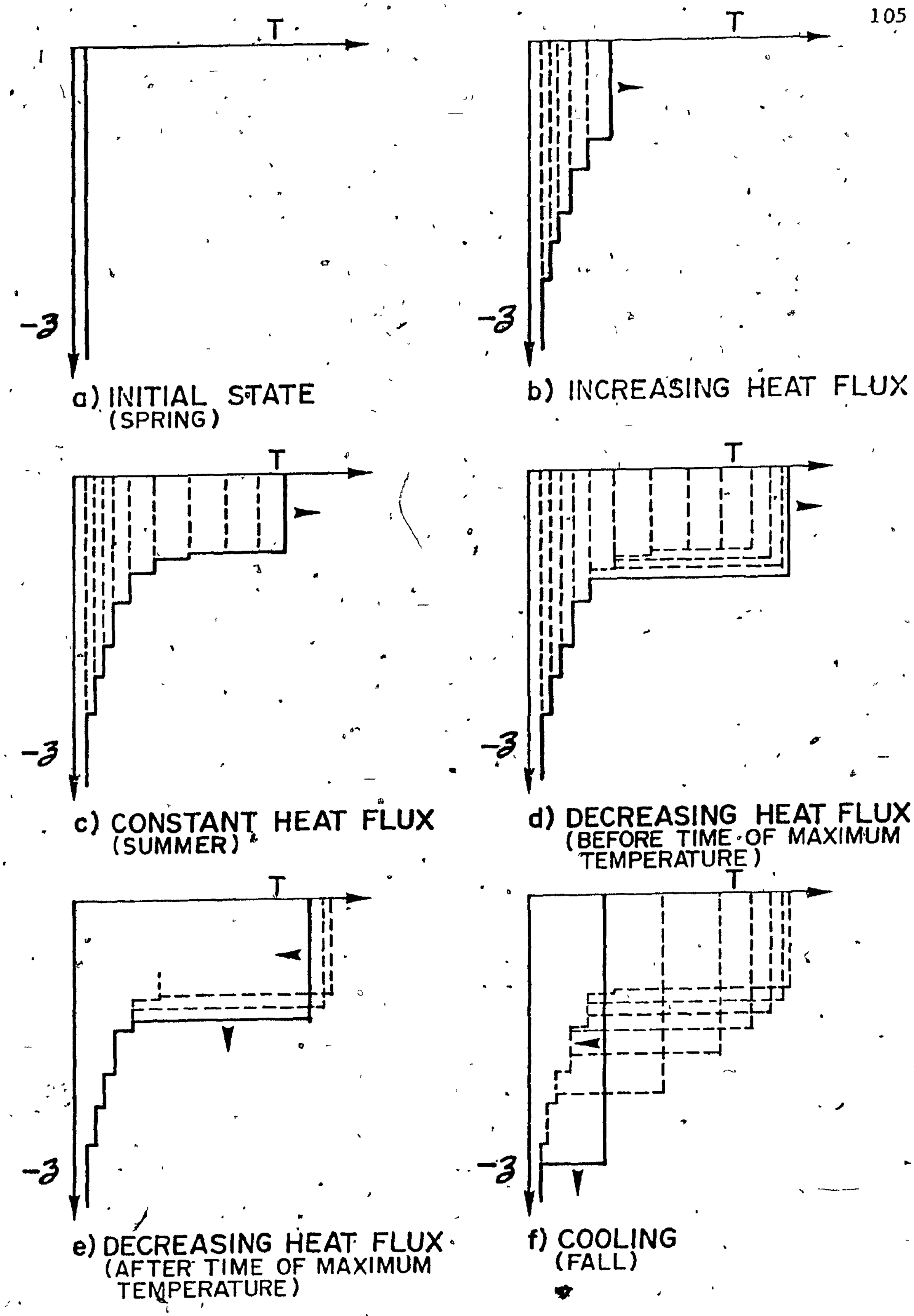

Figure 4.1c) Schematic representation of the response of a mixed layer model to a seasonally varying heat flux with constant wind stress. (The full line is the profile of the current iteration; the dashed line is the profile of previous iterations; arrows indicate the direction of progress.)

layers of liquid with a density difference $\Delta\rho$. The top layer has a depth h equal to the mixed layer depth and the bottom layer occupies the remainder of the basin, which has a total depth H. Coriolis force is not included but it is pointed out that for very large lakes it can be taken into account by replacing T_i (the period of the first internal resonance mode) by F^{-1} (the inertial period) in the upcoming derivations.

In the dynamical model, after the onset of a wind stress, the velocity difference between the layers increased linearly until a time:

$$t = \frac{L}{2c_i} \tag{4.1.33}$$

when it reached its maximum value:

$$\Delta V_{max} = \frac{u_*^2 L}{2hc_i} \tag{4.1.34}$$

where $c_i^2 = g\,\frac{\Delta\rho}{\rho}\,\frac{h(H-h)}{H}$

The velocity then oscillated about zero with a period of:

$$T_i = \frac{2L}{c_i} \tag{4.1.35}$$

The interface moved with the same period but out of phase by a quarter cycle. The equilibrium tilt was given by the inverse of a Richardson number characterizing the mixed layer:

$$Ri_L = g \frac{\Delta \rho}{\rho} \frac{h}{u_*^2} \qquad 4.1.36$$

Energy considerations show that the time constant for damping is:

$$T_d = T_i \frac{H}{X} \qquad 4.1.37$$

The thickness of the bottom turbulent boundary layer, X, being given by an empirical formula:

$$X = V_{max} \; T_i^{1/2} \; (0.11 \; sec^{1/2}) \qquad 4.1.38$$

The behaviour of the solution is illustrated in figure 4.1d). To analyze their effect on mixing the authors defined four regimes with respect to Ri_L but other equivalent classifications are possible (see Thompson and Imberger, 1980). The range and main features of these regimes are given in table 4.1C. Following the notation of the authors we will now examine each regime starting with the one where wind mixing is the least intense.

- In regime IV, buoyancy is strong enough to inhibit large seiching and the shear at the interface is too weak to contribute to entrainment. In this regime mixing energy is just sufficient to keep the surface layer agitated.

- In regime III wind energy will significantly contribute to

TABLE 4.1C

REGIME	RANGE	PRINCIPAL PROCESSES AT WORK	MAIN FEATURES
IV	$Ri_L > \frac{1}{4}\left(\frac{L}{h}\right)^2 \frac{H}{H-h}$	Only wind mixing through surface agitation.	Sharp thermocline; small internal seiches; almost no deepening.
III	$\frac{1}{4}\left(\frac{L}{h}\right)^2 \frac{H}{H-h} > Ri_L > \frac{1}{2}\frac{L}{h}\left(\frac{H}{H-h}\right)^{\frac{1}{2}}$	Only wind mixing through surface agitation.	Sharp interface; large seiches; slow deepening.
II	$\frac{1}{2}\frac{L}{h}\left(\frac{H}{H-h}\right)^{\frac{1}{2}} > Ri_L > 1$	Shear induced mixing and overturning due to upwelling.	Diffuse interface; no seiching due to large damping; horizontal temperature gradient.
I.	$Ri_L < 1$	All of the above.	Vertical uniformity; small to no horizontal temperature gradient.

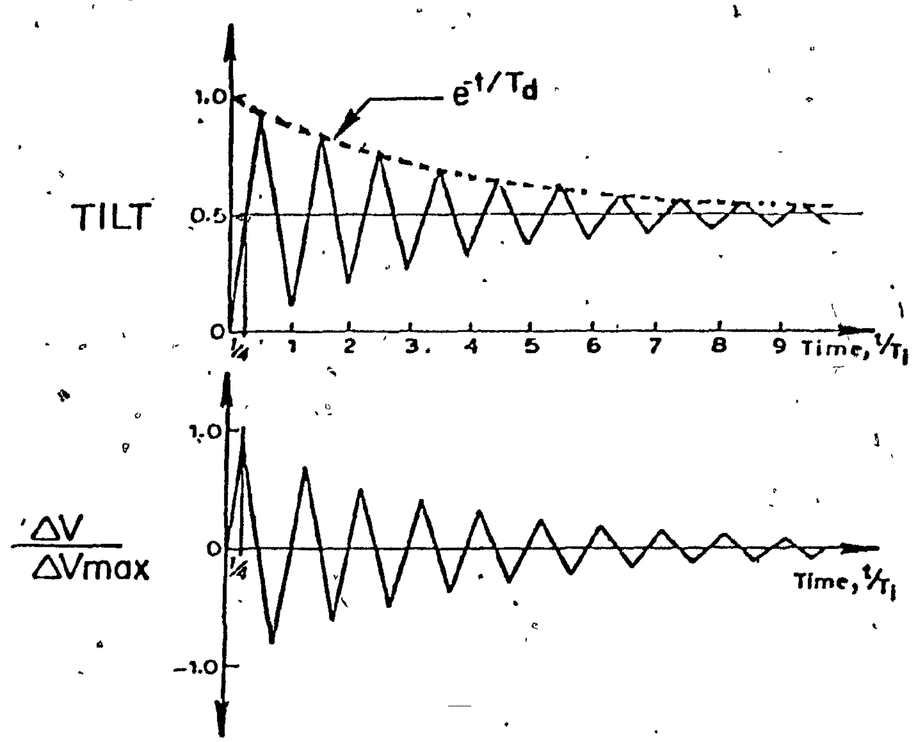

Figure 4.1d) Internal oscillations of a rectangular basin, without entrainment, after the onset of a constant wind stress. The tilt is defined as the difference of the lake, divided by the length of the lake.

entrainment. Although internal waves and seiching will be induced by the wind stress, their amplitudes are still too small to affect entrainment.

- Comparing terms (b) and (c) in 4.1.32, where we have replaced $|\bar{V}|$ by ΔV_{max} and let $s \sim 1$ we obtain the criterion for entrainment due to shear, which is also the upper bound of regime II.

$$Ri_L = \frac{1}{2}\frac{L}{h}\left(\frac{H}{H-h}\right)^{1/2}$$

Therefore in this regime shear can be great enough to induce deepening. This is important when the velocity is near its maximum value at every interval $\frac{1}{2}\,T_i$. These events are maintained until either entrainment has increased h or damping decreased ΔV_{max} , so that the system reverts to regime III (this is illustrated in figure 4.1e).

Their model has the peculiarity that it simulates Kelvin Helmholtz billowing which makes part of the energy from the shear available for turbulent production. In the absence of surface stirring this process will diffuse the interface symmetrically rather than cause entrainment in one direction or the other. Therefore the shear produced TKE is used to smooth out the interface linearly about h and over a thickness equal to $s\left(\Delta V_{max}\right)^2/g\,\frac{\Delta\rho}{\rho}$. This, up to a certain point, will simulate the finite thickness interface which is occasionally observed.

- In regime I, the time scale for the mixing of the whole basin, both vertically and horizontally, is a few hours. In view of this, the previous scheme does not apply and the authors use a model of a constant vertical eddy diffusivity of 6.25 $u_* H$. The water becomes uniform a very

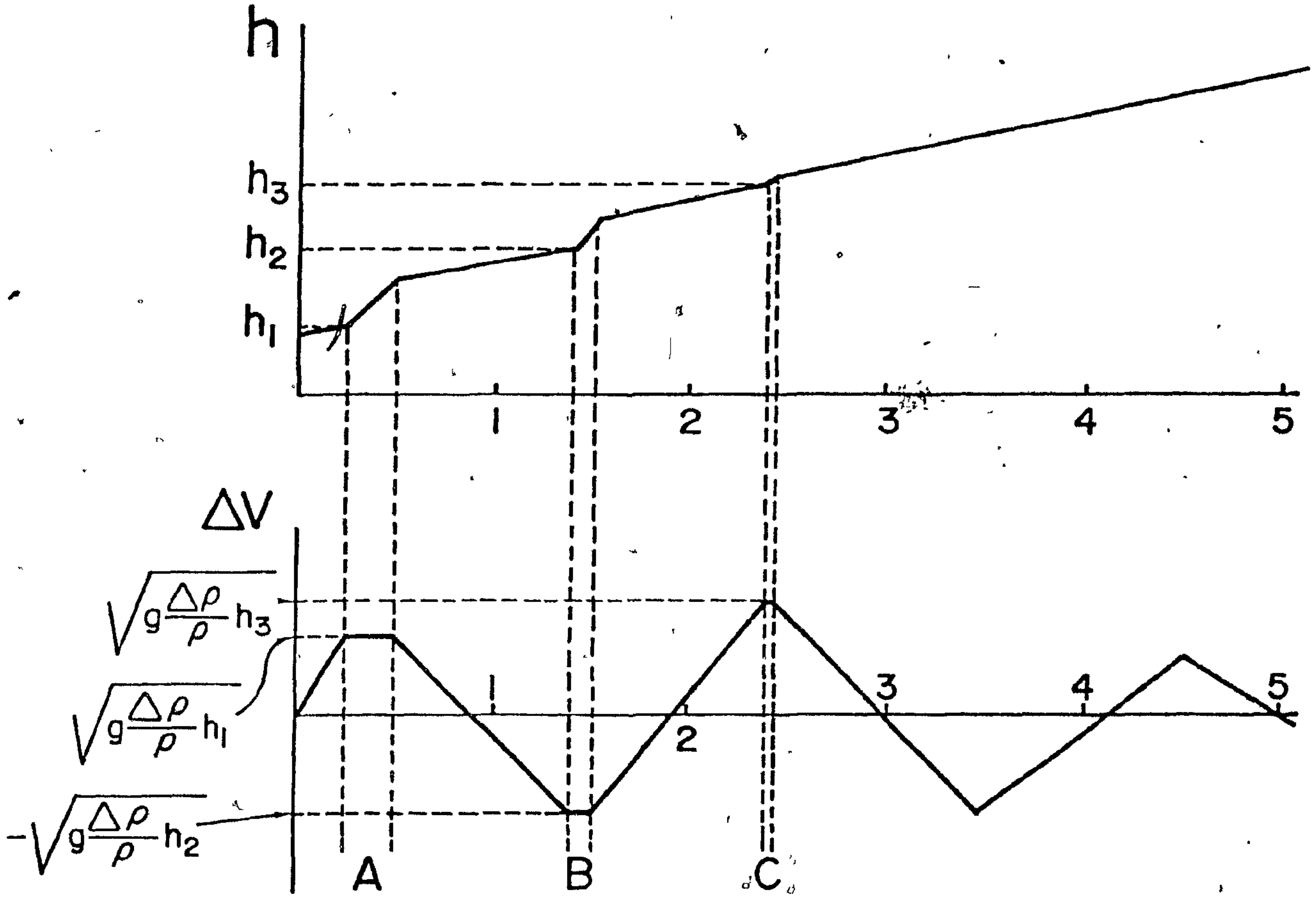

Figure 4.1e) Effect of oscillation on mixed layer deepening. During shear induced entrainment periods, the kinetic energy of the oscillation is used to produce TKE rather than accelerating the fluid (episodes A, B and C).

short time after entering this regime.

When applied to a warm monomictic basin (a basin that retains a positive temperature gradient, never falling below 4 °C) in Western Australia over a period of a year, it was found that regimes III and IV dominate, and that the effects of a shear remained small. Regime II only occurred with exceptionally high wind. Inasmuch as these events are rare and short a simple model not considering regimes I and II may be adequate for the seasonal cycle of many lakes. Comparison of model prediction with observations show only marginal improvement over an earlier version, neglecting shear (Imberger et al, 1978).

Bloss and Harleman (1980) have developed a model that, in contrast to the one discussed above, considers all terms of the TKE equation except the shear production term. In their analysis they parametrize terms (a) and (g) as $C_T\, q^2\, \frac{\partial h}{\partial t}$ and $C_D\, q^2 \,(g\,h\, \frac{\Delta\rho}{\rho})^{1/2}$ respectively. In their algorithm entrainment due to thermal convection (terms (e) and (f)) is treated separately so that the velocity scale q is simply set equal to u_*. Generally, however, we may scale q^3 to the sum of terms (d), (e) and (f) as:

$$q^3 = u_*^3 + \frac{n}{m}\,(J_O + J_P) \qquad 4.1.39$$

Then the buoyancy term will be implicitely included in term (d) if we replace $m u_*^3$ by $m q^3$. Defining a layer Richardson number as:

$$Ri_L = \frac{g \Delta \rho h}{\rho q^2},$$

the TKE equation can be manipulated to yield:

$$\frac{g \Delta \rho h}{2 \rho q^3} \frac{\delta h}{\delta t} = \frac{1}{2} Ri_L \frac{m - C_D \sqrt{Ri_L}}{C_T + Ri_L} \tag{4.1.40}$$

Noting that the numerator of the left-hand side is equal to the potential energy change associated with entrainment while the denominator is the turbulent kinetic energy input we see that this expression gives the conversion rate of TKE into potential energy of stratification. Bloss and Harleman have solved the above equation for three lakes of widely varying properties, using the constants obtained by Zeeman and Tennekes (1977). Temperature predictions are within one degree Celsius in most cases. In order to verify the importance of various components of the TKE equation they did several model runs neglecting one term or the other each time. The conclusion reached was that over the wide range of conditions presented by the three lakes each one became important at one time or another.

Some other three-dimensional effects not included in these analyses are discussed by Tucker and Green (1977) and Sundaram (1977). They are mainly the effects of thermal bars in dimictic lakes during turnover, and the effect of fetch on the wind stress. The first will last for only a short period, compared to the yearly cycle when the system is likely to be in regime I or II, and thus can have only a limited effect on the seasonal thermocline. As for fetch effect they may be included in the coefficients s and m, or included in the calculation of u_* .

Many mixed layer models, although they are successfully used for oceans and lakes, are not strictly predictive because some of the constants in the TKE equation are left as free parameters to obtain a best fit. Sherman et al (1978) review the values for the coefficients used by different authors and propose a representative set of constants that best fit the body of data available to date. Although there are great variations in the values used, several experiments (Thompson, 1976; Niiler, 1975) have shown that mixed layer models are relatively insensitive to the particular constants utilized. This gives us confidence in model prediction but leaves much of the theoretical speculation on the partitioning of TKE unverified. There is little point in further refining the TKE equation until this can be resolved. The danger of using model results to support theoretical speculation can be illustrated by comparing the turbulence closure model of Mellor and Durbin (1975) and the mixed layer model by Denman and Miyake (1973). The former model neglects transport of TKE from the surface wave region to the thermocline, while the latter relies entirely on this process to provide energy for entrainment. However both give results that agree well with the same set of observations at ocean station PAPA.

The experiment of Bloss and Harleman (1980) is important in giving predictive credibility in these models, as it is one of the only ones in which a model was applied successfully to three completely different lakes, without any need for adjustment or calibration.

4.2 A System of Interconnected Basins

As seen earlier Lake Memphremagog can be divided into 3 distinct basins. One of them, South Basin, is different from the others by having a much larger surface to volume ratio.

To investigate the effect of such asymmetry on the application of a one-dimensional model, let us consider the simple system illustrated in figure 4.2. It comprises two basins which are joined by a channel, where heat enters through the surface. The temperature of the water in the two basins is given by:

$$
\begin{aligned}
T_1 &= \frac{1}{C\rho} \int \left(\frac{1}{h_1} \Phi_o - \frac{1}{V_1} Q_{ex} \right) dt \\
T_2 &= \frac{1}{C\rho} \int \left(\frac{1}{h_2} \Phi_o - \frac{1}{V_2} Q_{ex} \right) dt
\end{aligned}
\qquad 4.2.1
$$

T_1 and T_2 are the temperatures of each basin, above an initial state of isothermy (C).

h_1 and h_2 are the depths of the thermocline or the total depth of each basin, depending on whether they are stratified or not (L).

V_1 and V_2 are the volumes of the epilimnion of each basin (L^3).

Φ_o is the atmospheric surface heat flux ($Q^2L^{-2}T^{-1}$).

Q_{ex} is the rate of heat exchange between basins (QT^{-1}).

t is the time from the state of isothermy. (T)

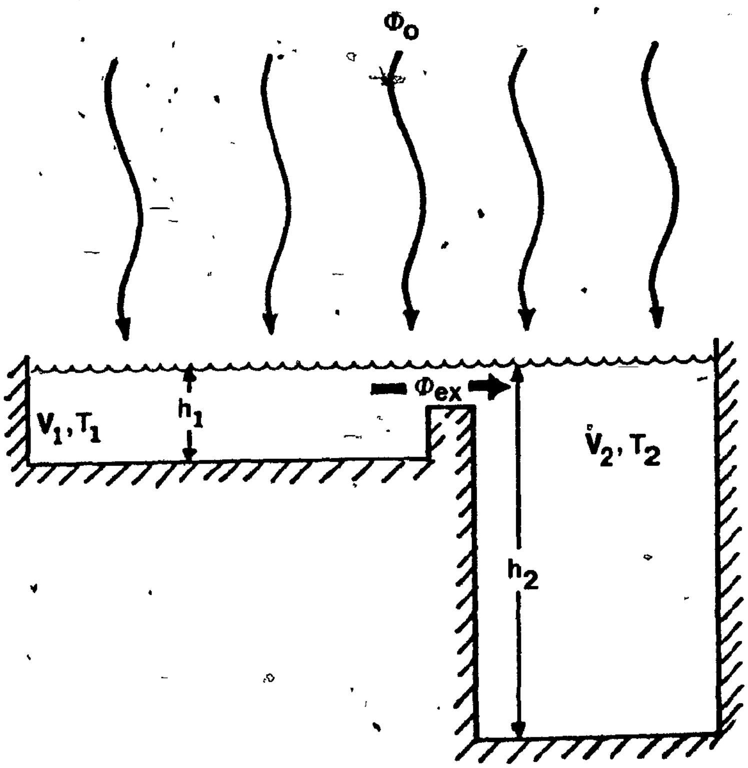

T_1, T_2 - temperatures

V_1, V_2 - basin volumes

h_1, h_2 - basin depth

Φ_o - uniform surface heat flux.

Figure 4.2 Definition sketch for a simple two-basin system to illustrate the effect of lake asymmetry.

ρ is the density of water (ML^{-3})

C is the specific heat of water ($QC^{-1}M^{-1}$)

The rate of heat exchange through the channel can be expressed in a form analogous to Fickian diffusion:

$$Q_{ex} = X\,(T_1 - T_2) \qquad 4.2.2$$

where X is an exchange coefficient ($QC^{-1}T^{-1}$)

Using the two previous equations to eliminate T_1 and T_2 we get:

$$Q_{ex} = X \frac{1}{C\rho}\left(\frac{1}{V_1} + \frac{1}{V_2}\right) \int \Phi_0 \frac{\left(\frac{1}{h_1} - \frac{1}{h_2}\right)}{\left(\frac{1}{V_1} + \frac{1}{V_2}\right)} - Q_{ex}\, dt \qquad 4.2.3$$

The time scale for interbasin heat exchange is $\left(\frac{X}{C\rho}\left(\frac{1}{V_1} + \frac{1}{V_2}\right)\right)^{-1}$. For events much longer than this the basins have plenty of time to exchange water, the rate of heat transfer will rapidly reach an equilibrium and temperature difference between basins will be small. For events much shorter than this, the basins are effectively disconnected, their stratification evolving independently. In this case the temperature difference between basins may be large compared to the change in temperature induced by the surface heat flux.

In the above equations two cases can be identified when heat exchanges are always negligible. First if the mean depth of the two epilimnion basins are similar ($h_1 \simeq h_2$), they will both behave similarly whether or not they are connected. Secondly, if one basin has a much larger volume than the other ($V_1 \gg V_2$), it will not be affected by the smaller one, the heat gained through interbasin exchange being negligible compared to the surface heat flux.

Now let us look at Lake Memphremagog's basins. Central and North Basins are deep enough so that the thermocline is usually above their mean depth. They are likely to have similar stratifications, leading to the first case mentioned above with negligible heat transfer. This is not so for Central and South Basins, as the thermocline is generally well below the mean depth of South Basin. The volumes of the three basins are comparable so that the second criteria for negligible heat exchange does not apply. Heat exchange between South and Central Basins may therefore be important.

To evaluate the time scale of interbasin heat exchanges, $\left(\frac{X}{C\rho}\left(\frac{1}{V_1}+\frac{1}{V_2}\right)\right)^{-1}$, one needs to know X, the exchange coefficient. Ideally it could be computed from a horizontal diffusion coefficient, but we lack adequate data to estimate one. Alternately an approximate value of X can be obtained directly from current measurements in the boundary region between South and Central Basins. Assuming that any water parcel crossing this boundary is immediately and completely mixed in the basin it enters, then:

$$X = C\rho a v \qquad 4.2.4$$

where a is the cross-sectional area of the boundary (9000 m^2)

and v is the scale of currents normal to the boundary.

From a total of 5 ice-free months of current observation near Skinner Island, the RMS north-south velocity was found to be 4 cm/sec. Using this value for v we obtain:

$$X = 3.6 \times 10^8 \frac{\text{Cal}}{^\circ\text{C sec}} \qquad 4.2.5$$

This represents a maximum value, as there are several ways in which heat or water entering a basin could be returned before being completely absorbed. However on a few occasions temperature differences were large enough to clearly identify a water mass entering South Basin, and during these events, only a small portion of the water was observed to flow back into Central Basin (section 3.2). Using this value of X, together with the epilimnion volume of Central Basin, corresponding to a 10 m thermocline, for V_1 and the total volume of South Basin for V_2, we obtain:

$$\left(\frac{X}{C\rho}\left(\frac{1}{V_1}+\frac{1}{V_2}\right)\right)^{-1} = 4.2 \text{ days} ,$$

in the case of no stratification; with V_1 equal to the full volume of Central Basin:

$$\left(\frac{X}{C\rho}\left(\frac{1}{V_1}+\frac{1}{V_2}\right)\right)^{-1} = 8.0 \text{ days}$$

Therefore the time scale for interbasin heat exchange is rather short compared to the seasonal cycle. This means the whole lake could be considered to be horizontally homogeneous, and the overall seasonal cycle would be well simulated. Rough calculations, however, will show that for typical seasonal heat fluxes a temperature difference of 1 to 2 °C may still occur between Central and South Basins. This is larger than the accuracy claimed by most contemporary models; therefore to use them to their full capacity the lake assymetry should be considered.

In order to include the effect of assymetry between different parts of Lake Memphremagog, the model developed here will treat the heat and TKE equations separately for each basin. At each iteration the basins will be allowed to exchange heat among themselves through equation 4.2.2 using the X defined above. In the model the lake is divided into a series of horizontal slabs of uniform thickness whose temperatures we seek to determine. In order to preserve the stratification we will allow heat exchange between slabs at the same level in each basin. For each of these the value X defined by 4.2.4 will change as a function of depth according to the cross-sectional shape of the interconnecting channel, as:

$$a_i = \Delta z \ B(i\Delta z) \qquad 4.2.6$$

a_i is the cross-sectional area of the i^{th} slab at the junction of two basins.

Δz is the thickness of each slab.

$B(i\Delta z)$ is the width of the interconnecting channel at the depth of the i^{th} slab.

In this analysis we neglect the interleaving which is likely to occur when two water masses of different temperatures meet. When the thermocline is above the depth of the junction between two basins, the epilimnion of each basin will have similar mean depths and as seen earlier little heat exchange will occur. In the case when the thermocline is below the junction depth, all of the exchange will occur within the wind-mixed surface layer and it is assumed that any stratification due to local convection will quickly be obliterated by mixing and be confined to a small region near the junction. Potential energy which may be exchanged for kinetic energy during such a convective process is not considered in the TKE equations. This is equivalent to saying that all of the energy released by convection is used locally in mixing.

This model does not apply if convection becomes the main driving force for heat exchange. It has been shown in chapter 3 that during the ice-free season convective effects would be small compared to wind forces. This is supported by the observation that no significant change in heat exchange, between South and Central Basin, occurs during the thermal bar periods.

It must be remembered that the above scheme, although idealized, can only help improve model resolution for small time scales since as shown earlier the seasonal cycle should be well simulated anyway.

A yet unanswered question is what type of model will be used to solve the TKE equation. A mixed layer model has been chosen simply because they are generally easier to implement than turbulence closure model. In particular, contemporary versions of the latter require a detailed determination of the shear structure while the former considers simple two layer flow. As seen in Bloss and Harleman's paper, model formulation can be quite simple if shear is neglected. Their results and those of Spigel and Imberger seem to indicate that this is a reasonable assumption, however the basins they have considered are at least half the size of Lake Memphremagog. The criterion for neglect of shear turbulence production given in the last section can be given as:

$$L < 2\ Ri_L\ h \sqrt{\frac{H}{H-h}} \qquad 4.2.7$$

Inserting $H = 17$ m (mean lake depth), $h = 8$ m (typical observed thermocline depth) and using $W_* = 0.2$ cm/sec (corresponding to the typical wind speed over the lake, see section 2.4) and $\Delta\rho = 0.001$ g/cm^3 (corresponding to a difference in mean temperature of 5 °C which is commonly observed between the summer epi- and hypolimnion) to compute Ri_L, we resolve that the length of the lake must be less than 300 km to neglect shear. In spring and fall, however, stratification may be temporarily weaker, bringing the critical lake length down by an order of magnitude. The shear term will not included in the model as the wind information is not of sufficient quality to solve the equation of motion for the lake. However, periods when inequality 4.2.7 does not hold will be flagged in the computational results. It can be shown that the criterion for shear induced mixing is also a criterion for upwelling at the extremities of a basin, and the finding in chapter 3 that upwelling had only a small overall effect can help justify the neglect of shear.

The formulation of the TKE equation to be used is very similar to that used by Bloss and Harleman presented in section 4.1. The only difference is the parametrization of internal wave radiation losses is more general, applying to both sharp or diffuse interface. The following is from Sherman, Imberger and Corcos (1978):

$$\frac{g \Delta \rho h}{2 \rho q^3} \frac{\delta h}{\delta t} = \frac{1}{2} \frac{C_k - C_D R_s^3/(R_s - Ri_L)^2}{\left(1 + C_t / Ri_L\right)} \qquad 4.2.8$$

where $q^3 = \left(\frac{m}{n}\right) W_*^3 + J_o + J_p$

$$R_s = \frac{h}{q} \sqrt{\frac{g}{\rho} \left.\frac{\delta \rho}{\delta z}\right|_h}$$

where $\left.\frac{\delta \rho}{\delta z}\right|_h$ is the density gradient just below the mixed layer, and other variables have the same meaning as before.

For the five constants used in this equation we will use the values determined by the same authors as the best fit to six independent sets of experiments. These are:

$$\frac{n}{m} = 1.8$$

$$C_k = 0.38$$

$$C_t = 2.25$$
$$C_D = 0.04$$

The time step used for data input is one day. This permits the use of readily available daily meteorological observations from government operated weather stations and provide a fine enough resolution to distinguish major weather systems. The temperature profiles are computed at 50 cm intervals, which is the intended vertical resolution of the model. An integration time step of one day was used, as reducing it showed only negligible changes in the results.

4.3 The Boundary Conditions for Lake Memphremagog

The boundary conditions for stratification modeling consist of specifying heat and momentum fluxes across the exterior surfaces of a body of water. In general fluxes may exist at the surface as well as along the bottom. For momentum the only sources other than surface wind stress are inflows and outflows. In Lake Memphremagog, however, these would cause currents below 0.6 cm/sec, which is well below the magnitude of observed currents. Surface stress must then be the principal source of momentum and turbulent kinetic energy. In a similar way it may be shown that river inflow will affect water temperatures only by a fraction of a degree. The present model therefore neglects the effects of throughflow. This may not be adequate during the spring snow melt during which river discharge can be very large, but this lasts only for a few weeks, at or near the time of turnover when other model assumptions break down. This will have little effect the rest of the year.

Momentum fluxes through the surface are entirely due to the action of turbulence near the air water interface. Heat fluxes are composed of turbulent and radiative components. The turbulent fluxes are calculated using the bulk aerodynamic method, as:

$$\tau = C_d \rho_a U_{10}^2 \quad 4.3.1$$

$$\Phi_q = C_q C_a \rho_a U_{10} \Delta T_{10} \quad 4.3.2$$

$$\Phi_e = C_e L U_{10} \Delta e_{10} \quad 4.3.3$$

where τ is the surface stress or momentum flux $(ML^{-1}T^{-2})$

Φ_q is the sensitive heat flux, transfered by thermal conduction. $(QL^{-2}T^{-1})$

Φ_e is the evaporative heat flux, corresponding to the water vapour flux. $(QL^{-2}T^{-1})$

C_d, C_q and C_e are exchange coefficients for momentum, heat and vapour.

$\rho_a = 1.2 \times 10^{-3}$ g/cm^3 is the density of air

$C_a = 0.24$ cal/g °C is the specific heat of air

$L = 590$ cal/g is the latent heat of evaporation of water

U is the wind speed (LT^{-1})

ΔT is the difference between air and water surface temperatures (C)

Δe is the difference in specific humidity between air and the water surface. (ML^{-3})

The subscript 10 in the above equations refers to a measurement level of 10 m above the water surface. In order to apply the above formulae, a correction factor of 1.07 (Deacon and Webb, 1962) was applied to lake measurements which were at 7 m. The coefficient C_d was set to 1.2×10^{-3}, a value which Bengtsson (1978) found representative of lake conditions. Following the results of Pond et al (1971) from heat and vapeur fluxes above water, C_q and C_e are set equal to 1.3×10^{-3}.

Two windows in the electromagnetic spectrum transfer significant amounts of heat to and from water bodies. The sum is the primary source of short wave radiation while long wave or thermal radiation emanates from the atmosphere and the water surface itself.

Although incident short wave radiation is measured near the lake. The amount that is reflected and back-scattered by the water must be estimated. The albedo of water surface to diffuse sky radiation was taken as 0.066 (Kondratyev, 1969). The albedo for direct solar radiation can be calculated from an empirical formula derived for a natural water surface (Grey, 1970), as $1.18\ S_A^{-0.77}$, where S_A is the angular elevation of the sun in degrees. The ratio of diffuse to direct radiation depends on cloud cover and to a first approximation is linearly related to cloudiness (Neumann and Pierson, 1966). The global albedo is then given by:

$$A = (0.008 + 0.057\,c + 1.03\,(1-c)\,S_A^{-0.77})$$

where c is the fractional cloud cover.

The instantaneous radiation flux absorbed by the water can then be given by:

$$\Phi = \Phi_{incident}\,(1 - A)$$
$$= \Phi_{incident}\,(0.992 - 0.057\,c - 1.03\,(1-c)\,S_A^{-0.77})$$

The solar angle can be calculated by geometry at any time and the diurnal fluctuation of $\Phi_{incident}$ is well approximated by the positive half of a sinusoidal curve, so that the above relationship may be easily integrated over a day to yield an expression of the form:

$$\Phi_{sw} = \Phi_{sw\,incident}\,(0.934 - (1-c)\,G) \qquad 4.3.4$$

where Φ_{sw} are daily fluxes

and G is a fixed function of the time of year.

Ivanoff (1977) shows that this flux decreases exponentially with depth, past a few meters. In the top layer, however, absorption is much stronger. This can be approximated by letting 55% (Ivanoff, 1977) of the radiation flux be absorbed near the surface. The penetrative component of short wave radiation is thus given by:

$$\Phi_p = 0.45\,\Phi_{sw}\,e^{-\beta z}$$

Mean extinction coefficients for South, Central and North Basins determined using light measurement data provided by R. Flett, are 0.52 m^{-1}, 0.36 m^{-1} and 0.39 m^{-1} respectively. These values vary considerably in response to suspended sediment concentrations or algae blooms, but the extinction cefficients are so large that most of the radiation will be absorbed in the first few meters of the water column, with very little effect on stratification.

Water surfaces radiate long wave radiation nearly as black bodies. The radiative properties of the atmosphere, however, depend strongly on its vapour content and on cloud cover. Recently Arnfield (1979), has evaluated the merit of several empirical formulae for computing atmospheric radiation by comparing them to measurements. He found that many of them yielded values within instrumental error. Combining the one he favoured to the black body formulae for water we can get the relationship for the net long wave radiation flux:

$$\Phi_{LW} = \sigma \left\{ \theta_a^4 \left(1 - 0.261\ e^{-0.777 \times 10^{-3} T_a^2}\right) (1 + Kc) - 0.98\ \theta^4 \right\} \qquad 4.3.5$$

where $\sigma = 1.35 \times 10^{-12} \dfrac{cal}{cm^2\ {}^oK^4\ sec}$ is the Boltzman constant

θ_a is the air absolute temperature

T_a is the ordinary air temperature

θ is the water surface absolute temperature

c is the fractional cloud cover

K depends on the cloud type and can be computed from:

$$K = \sum_{i=1}^{m} k_i c_i$$

where k_i is the proportion of certain cloud type

and c_i is a constant corresponding to that cloud type.

In order to estimate k_i computations were done using a list of given by Kondratiev and cloud cover information covering seven years from the "General Summaries of Hourly Observations in Canada". Variations in k from station to station in south-eastern Quebec were found to be insignificant and seasonal changes were small. The mean value of k is 0.18 and its standard deviation is 0.01. This mean value will be used in the above equation.

Since cloudiness is not recorded at Sherbrooke or Lennoxville, fractional cloud cover, which enters the equations for both Φ_{LW} and Φ_{SW}, will be approximated by the idealized relationship (1 - s) where is the relative insolation (defined in section 2.5). Kondratiev points out that several factors may cause deviations from this relationship. As a check comparison with seven years of monthly mean observation at Dorval airport in Montreal revealed a standard error of ± 0.1 in cloudiness, which is considered acceptable in view of the low sensivity of Φ_{LW} and Φ_{SW} to this variable.

Another possible source of heat flux in lakes is through the sediment water interface. Normal geothermal heat is of the order of 1 N cal/cm^2 sec (Hart and Steinhart, 1965) and is clearly insignificant, seasonal heat exchanges between the sediment and the water are potentially more important. Following Likens and Johnson (1969) the relative importance of sediments in the seasonal heat budget of shallow basins is roughly given by:

$$\frac{Q_s}{Q_{total}} = \frac{2}{\overline{H}} \left(\frac{1 \text{ year} \quad \rho_s \, k_s \, C_s}{2\pi} \right)^{1/2} \qquad 4.3.6$$

where $\overline{H}$ is the mean basin depth

ρ_s is the density of the sediments (ML^3)

k_s is the thermal conductivity of sediments $(QT^{-1}L^{-3}C^{-1})$

C_s is the heat capacity of the sediments $(QC^{-1}M^{-1})$.

For k_s, ρ_s and C_s we will use 2.2×10^{-3} (cm sec °C), 1.52 g/cm^3 and 0.54 cal/(°C g) respectively. These are values corresponding to sediments containing 65% water (Bullard, 1963). This is a representative water content for surficial sediments in Lake Memphremagog (Flett, 1978). From the above relationship we obtain that 30% of the annual heat budget of South Basin may involve the sediment. To include this in our model the area of bottom in contact with each of our horizontal slabs is computed and the heat flux through this surface is computed by numerically solving the heat equation for the sediments. Before a simulation run the model is exercised through several mean yearly cycles so that the sediment may reach an equilibrium temperature profile. As seen in the previous chapter bottom fluxes can cause convective motion. This, however, is ignored and the sediment exchanges heat with water at the same depth. This will have little effect since most of the heat transfer will occur in shallow regions where mixing will overcome convection.

Recapitulating the content of this section, the momentum flux into the lake is entirely through the surface and may be expressed simply by equation 4.3.1. The heat budget is more complex and can be given by:

$$Q_{total} = A\left(\Phi_{SW} + \Phi_{LW} + \Phi_q + \Phi_e\right) + Q_s \quad 4.3.7$$

where A is the surface area of the lake.

In order to compute these fluxes we need to know the weather conditions over Lake Memphremagog. As mentioned in section 2.4, except for short wave radiation, meteorological observations at the lake are available only for a short time, and we must rely on data from Sherbrooke airport. Linear least squares fit was used to relate observations at the weather station to those taken over the lake. Since the two data sets were found to have greater correlation for averaging periods longer than a day, 5 day averages were used for the regressions. This offered the optimum balance between high correlation and number of data points, minimizing the uncertainty in the coefficients. There is the possibility that the variations of weather variables are interrelated and because turbulent fluxes depend on the product of two variables it is preferable to find relationships among the products directly. Table 4.3 lists the formulae obtained and the equations for which they are used. In addition to these, measured incident short wave radiation flux is used in equation 4.2.4, and the relative insolation in equations 4.2.4 and 4.2.5 is taken from Lennoxville data.

TABLE 4.3

FORMULAE TO CONVERT METEOROLOGICAL OBSERVATIONS AT SHERBROOKE AND LENNOXVILLE USED TO COMPUTE FLUXES THROUGH THE LAKE SURFACE

Formula	$U^2_{lake} = 98\ km^2/hr^2 + 2.3\ U^2_{Sher}$	$(\Delta TU)_{lake} = -15^{\circ}C\ km/hr + 1.9\ (\Delta TU)_{Sher}$	$(\Delta eU)_{lake} = 0 + 1.6\ (\Delta eU)_{Sher}$	$\Delta T_{lake} = -1.5\ ^{\circ}C + 0.93\ \Delta T_{Sher}$
Equation Used in	4.2.1 for surface shear stress	4.2.2 for sensible heat flux	4.2.3 for latent heat flux	4.2.5 long wave radiation flux
RMS deviation between 98 daily estimates and observations	115 km^2/hr^2	29 °C km/hr	2.7 10^{-7} (g km)/(cm^3 hr)	1.1 °C
and between 15 five-day averages	52 km^2/hr^2	22 °C km/hr	1.1 x 10^{-7} (g km)/(cm^3 hr)	0.8 °C

To investigate the error caused by using transformed Sherbrooke weather data rather than lake observations, the fluxes were computed using both methods, for the 98 days of meteorological observations at the lake. It was found that for daily fluxes the standard errors were about twice as great as the accuracies of the flux formulae as claimed by their authors. When grouped into 5 day averages, however, errors dropped to below the formula accuracy. This is in agreement with results in chapter 2 which showed that standard deviations decreased while correlation increased with longer averaging time. Therefore for time scales longer than a few days, the formulae themselves, rather than the lack of continuous site specific observation, imposes a limit on precision. The accuracies for Φ_{sw}, Φ_{Lw}, Φ_q and Φ_e are then 2%, 20%, 20% and 20% respectively. For sediment heat flux, accuracy is limited by the knowledge of the water content of bottom materials, and from observed variations in the quantity, Φ_s may be expected to vary by $\pm$ 15%. Because for the ice-free season Φ_{Lw}, Φ_q, Φ_e and Φ_s are almost always of the same sign (i.e. loss terms) and the error in the balancing term, Φ_{sw}, is small, the former will control the accuracy of the global heat budget which is expected to be within 20%. The accuracy in the long term surface stress is about 20% also.

As mentioned in section 2.5 another source of error is the possibility of systematic deviations between weather conditions over the whole lake from those measured in South Basin. Because South Basin comprises almost 50% of the lake surface area we may expect the total heat budget to be reasonably accurate. The turbulent energy generated by surface stresses, however, is assumed to be dissipated or consumed locally and is therefore independent of surface area. This means that the predicted vertical temperature distributions in basins other than South Basin might deviate from reality. In order to check this the next section will compare predicted and observed heat content and vertical temperature distributions for all three basins.

4.4 Modeling Results

The modeling results using mean seasonal meteorological conditions as input are presented in figure 4.4a. Comparing the computed temperature profiles with the data presented in chapter 3 we can see two principal disparities. First, the predicted summer surface temperatures are two degrees short of the mean observed value. Secondly, the depth of the thermocline is overestimated by about 50%. Some experimenting of wind mixing indicated a reduction of the mixing energy by half provided a better fit for thermocline depth but had little effect on surface temperature. The reason for this is that the surface heat flux budget is a self-regulating system and summer water temperatures are near the equilibrium point (Sundaram and Rehm, 1973). The balance between heat loss and heat gain terms are changed if the wind speed is modified since both and are proportional to wind velocity. Reducing the wind velocity by one half resulted in a better agreement for both surface

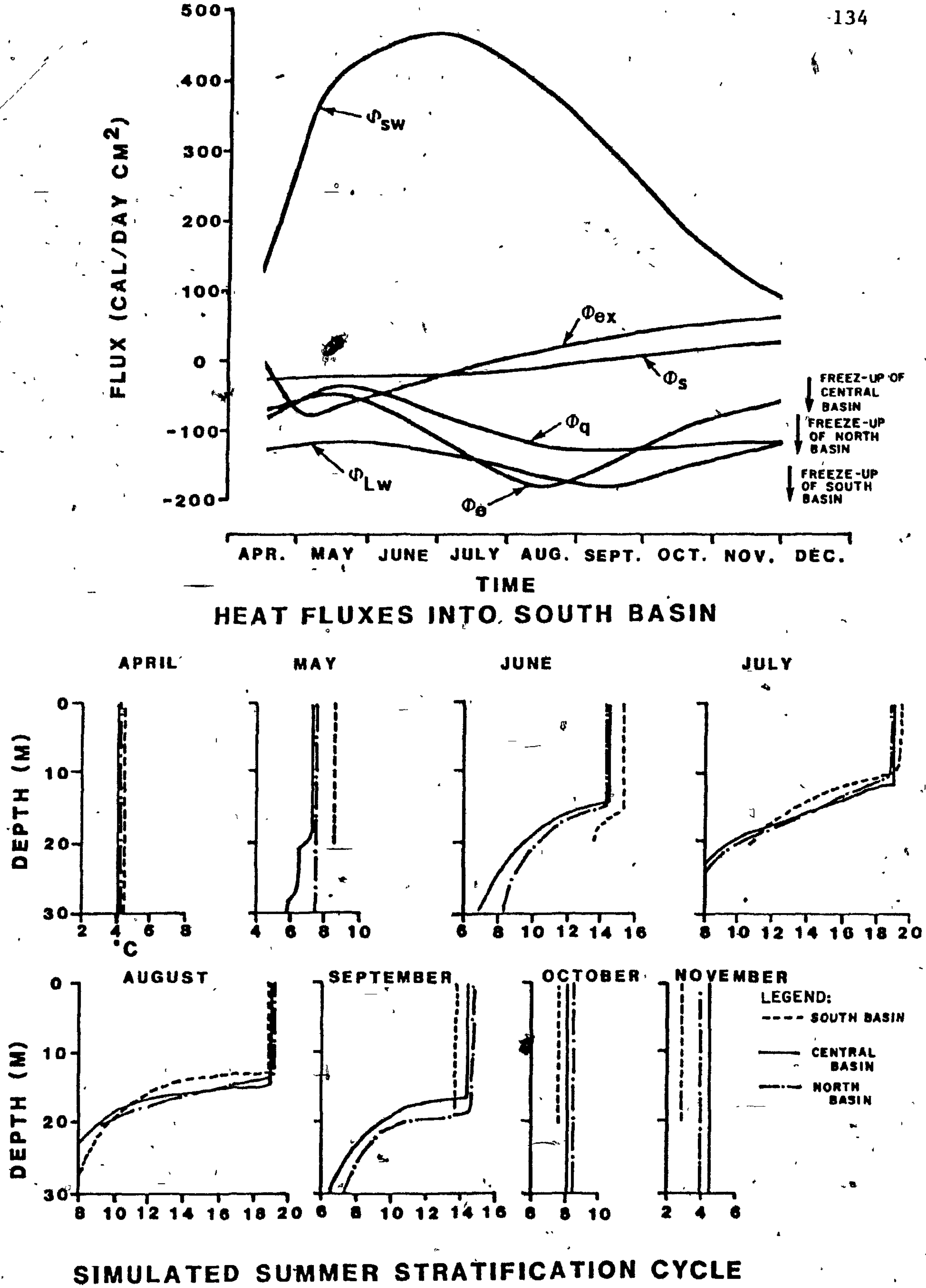

Figure 4.4 Numerical modeling results for the stratification of Lake Memphremagog.

temperature and thermocline depth. It is therefore probable that the wind speed used to drive the model is too high and that any error in prediction is due to this rather than a faulty parametrization of turbulent kinetic energy. This is consistent with the fact that the recording meteorological station was installed in a region which is less sheltered from winds than other parts of the lake. Because this cannot be verified without installing several wind speed recorders along the length of the lake, it was decided not to modify model parameters instead of speculating on the cause of discrepancies.

The model does predict the observed temperature gradients along the lake. Comparing the heat transfered between South Basin and Central Basin (Φ_{ex}) with the other heat sources in figure 4.4a we see that its seasonal variation has the same amplitude as other surface heat flux terms. The calculated time of freeze-up for Central Basin is the 15^{th} of December, lagging South Basin by two weeks.

The sediment heat flux remains a small portion of the total lake heat budget, but in South Basin it accounts for up to 25% of the net heat flux. It is interesting to note that the model predicts some cooling of the bottom water of South Basin when it is stratified. This results, not from heat exchange with the rest of the lake, but from the absorption of heat by the sediment. This would explain the lower temperatures and gradual rise in isotherm level observed as we go from Central to South Basin (see sections 3.1 and 3.3), without recourse to upwelling which was shown to have a more local effect.

Although shear is not included as a turbulent energy source in our model, the criteria discussed earlier to assess its importance was evaluated. Shear was found to play a role in vertical mixing during the months of April, May and November. Because the shear production term in the TKE equation depends on the fourth power of the wind speed, a reduction in wind velocity would greatly reduce the importance of shear.

In summary, the present model reproduces the qualitative features of the seasonal stratification cycle in Lake Memphremagog. The main obstacle for quantitative agreement between the simulation and observations is the availability of wind data at different points along the lake. If this information becomes available, the computer program given in the appendix could be easily modified to incorporate it.

BIBLIOGRAPHY

Arnfield, A.J. (1979), Evaluation of empirical expressions for the estimation of hourly and daily totals of atmospheric longwave emission under all sky conditions, Quart. Jour. R. Met. Soc. 105, 1041-1052.

Baines, P.G. (1982), On internal tide generation models, Deep Sea Research, Vol. 29, no. 3A, 307-338.

Bengtsson, Lars (1978), Wind induced circulation in lakes. Nordic Hydrology, 9, (1978), 75-94.

Benjamin, T.B. (1966), Internal waves of finite amplitude and permanent form, Jour. Fluid Mech. Vol. 25, part 2, 241-270.

Blackford, B.L. (1978), On the generation of internal waves by tidal flow over sills - A possible nonlinear mechanism, Jour. Mar. Res. August.

Bloss, S. and Harleman, R.F. (1980), Effect of wind-induced mixing on the seasonal thermocline in lakes and reservoirs, Second International Symposium on Stratified Flows, The Norwegian Institute of Technology Trondheim, Norway, 24-27 June 1980.

Bullard, E.C. (1963), The flow of heat through the floor of the ocean, The Sea, Vol. 3, M.N. Hill, ed., Interscience Publishers, N.Y.

Clark, Thomas H. (1967), Appalachian Tectonics, University of Toronto Press, Toronto, Canada.

Csanady, G.T. (1973), Transverse internal seiches in large oblong lakes and marginal seas, Jour. of Phys. Ocean., Vol. 3, no. 4, 439-447.

Dake, J.M.K. and Harleman, D.R.F. (1969), Thermal stratification in lakes: Analytical and laboratory studies, Water Resources Research, Vol. 5, no. 2, 484.

Darbyshire, J. and Edwards, A. (1972), Seasonal formation and movement of the thermocline in lakes, Pageoph. Vol. 93, part 1, 141-150.

Darbyshire, J. and Jones, G.L. (1974), A further note on the seasonal formation and movement of the thermocline in lakes, Pageoph. Vol. 112.

Deardorff, J.W., Willis, G.E. and Lilly, D.K. (1969), Laboratory investigation of non-steady penetrative convection, Jour. Fluid Mech. Vol. 35, part 1, 7-31.

Denman, K.L. (1973), A time-dependent model of the upper ocean, Jour. Phys. Ocean. Vol. 3, 173-183.

Denman, K.L. and Miyake, M. (1973), Upper layer modification at ocean station PAPA: Observations and simulation, Jour. Phys. Ocean. Vol 3, April, 185-196.

Dillon, T.M. and Powell, T.M. (1979), Observations of a surface mixed layer, Deep Sea Res. 26A, 915.

Dutton, J.A. and Bryson, R.A. (1962), Heat flux in Lake Mendota, Limnol. and Ocean. 7, 80-97.

Emery, K.O. and Csanady, G.T. (1973), Surface circulation of lakes and nearly land-locked seas, Proc. Nat. Acad. Sci. USA, Vol. 70, no. 1, 93-97.

Farmer, D.M. and Spearing, L.A.F. (1975), Isotherm plots of Babine Lake during the ice-free season, Pacific Mar. Science Report. 75-9, Institute of Ocean Sciences, Patricia Bay, Victoria, B.C., Canada.

Farmer, David M. (1975), Penetrative convection in the absence of mean shear, Quart. Jour. R. Met. Soc. 101, 869-891.

Farmer, D.M. (1978), Observation of long nonlinear internal waves in a lake, Jour. Phys. Ocean. Vol. 8, no. 1.

Farmer, David M. (1980), Mixed layer dynamics in a lake near temperature of maximum density, Unpublished Report, Institute of Ocean Sciences, Victoria, B.C.

Fischer, Gunter (1965), In a finite difference scheme for solving the non-linear primitive equations for a barotropic fluid with application to the boundary current problem, Tellus XVII, 4, 405-412.

Flett, R. (1977), Studies in the lake physics, in Progress Report no. 2, Lake Memphremagog Project, Limnology Research Group, Dept. of Biology, McGill University, Quebec, Canada.

Flett, R. (1978), Phosphorus sedimentation in Lake Memphremagog, Progress Report no. 3, Lake Memphremagog Project, Limnology Research Group, Dept. of Biology, McGill University, Quebec, Canada.

Fliegel, M.H. (1973), Temperature measurements and internal waves in Seneca Lake, N.Y., Tech. Report # 9, Lamont-Doherty Geological Observatory of Columbia University.

Friehe, Carl A. and Schmitt, Kurt F. (1976), Parameterization of air-sea interface fluxes of sensible heat and moisture by the bulk aerodynamic formulas, Jour. Phys. Ocean. Vol. 6, November, 801-809.

Gadd, N.R., B.C. McDonald and W.W. Shilts (1971), Deglaciation in Southern Quebec, Geological Survey of Canada, paper 71-47.

Gargett, A.E., Sanford, T.B. and Osborn, T.R. (1979), Surface mixing layers in the Sargasso Sea, Jour. Phys. Ocean. 9, November, 1090-1111.

Germeles, A.E. (1970), A new method for the computation of seiches in oblong basins, Tellus XXII ,6.

Grant, W.D. and Madsen, D.S. (1979), Combined wave and current interaction with a rough bottom, Jour. Geophys. Res. Vol. 84, no. C4, April 20, 1979, 1797-1808.

Gray, D.M. (1970), Handbook on the Principles of Hydrology, Canadian National Committee for the International Hydrological Decade.

Hamblin, P.F. (1976), Seiches, circulation and storm surges of an ice-free Lake Winnipeg, Jour. Fish. Res. Board Canada, 33, 2377-2391.

Hansen, N-E.O. (1978), Mixing processes in lakes, Nordic Hydrology, 9, 57-74.

Hart, S.R. and Steinhart, J.S. (1965), Terrestrial heat flow: Measurement in lake bottoms, Science, 149, September, 1499.

Heaps, N.S. and Ramsbottom, A.E. (1966), Wind effects on the water in a narrow two-layered lake, Phys. Trans. Royal Soc. Lon. Vol. 259A, 391.

Heidt, F.D. (1977), Development of a free convection layer in stably stratified water, Symp. on Modeling of Transport Mechanisms in Oceans and Lakes, M.S.D. D.F.E. no. 43.

Huang, J.C.K. (1972), The thermal bar, Geophysical Fluid Dynamics, Vol. 3, 1-25.

Huber, W.C., Harleman, D.R.F. and Ryan, P.J. (1972), Temperature prediction in stratified reservoirs, Jour. of the Hydraulics Division, Proc. of the American Soc. of Civil Engineers, April, HY4, 645-666.

Hunkins and Fliegel, Myron (1973), Internal undular surges in Seneca Lake: A natural occurence of Solitons, Jour. Geophys. Res. 78, no. 3.

Idso, Sherwood B. and Jackson, Ray D. (1969), Thermal radiation from the atmosphere, Jour. Geophys. Res. Vol. 74, no. 23, October 20, 5397-5403.

Ivanoff, Alexandre (1977), "Oceanic Absorption of Solar Energy" in <u>Modelling and Predictions of the Upper Layers of the Ocean</u>, ed. by E.B. Kraus, Pergamom Press.

Kadomtsev, B.B. and Karpman, V.I. (1971), Nonlinear waves, Soviet Physics Uspekhi, Vol. 14, no. 1, August.

Kalff, J., Leggett, W.C. and Peters, R.E. (1976, 1977 and 1978), Studies on the nutrient dynamics of a transboundary lake, Progress Rep. nos. 1, 2 and 3, Lake Memphremagog Project , Limnology Research Group, Dept. of Biology, McGill University, Quebec, Canada.

Kanari, Sei-Ichi (1970), Internal waves in Lake Biwa (I) - The responses of the thermocline to wind action, Bull. of the Disas. Prev. Res. Inst. Kyoto U., Vol. 19, part 3, no. 161, February.

Kanari, Sei-Ichi (1973), Internal waves in Lake Biwa (II) - Numerical experiments with a two-layer model, Bull. of the Disas. Prev. Res. Inst., Kyoto U., Vol. 22, February.

Kanari, Sei-Ichi (1974), Some results of observations of the long-period internal seiches in Lake Biwa, Jap. Jour. Limnol. 35, 4, 136-147.

Kanari, Sei-Ichi (1975), The long-period internal waves of Lake Biwa, Limnol. Ocean. Vol. 20, no. 4, July.

Kato, H. and Phillips, O.M. (1969), On the penetration of a turbulent layer into a stratified fluid, Jour. Fluid Mech. 37, 643.

Killworth, D. Peter, and Carnack, Eddy C. (1979), A filling-box model of river-dominated lakes, Limnol. Ocean. 24(2), 201-217.

Kraus, E.B. and Rooth, C. (1961), Temperature and steady state vertical heat flux in the ocean surface layer, Tellus, XIII, 2, 231-238.

Kraus, E.B. and Turner, J.S. (1967), A one-dimensional model of the seasonal thermocline, II. The general theory and its consequence, Tellus XIX, 1, 98-105.

Lee, Chi-Yuan and Beardsley, Robert C. (1974), The generation of long nonlinear internal waves is a weakly stratified shear flow, Jour. Geophys. Res. Vol. 79, no. 3, January.

Likens, Gene E. and Johnson, Noye M. (1969), Measurement and analysis of the annual heat budget for the sediments in two Wisconsin lakes, Limnol. Ocean. 14, 115-135.

Likens, Gene, E. and Rajotzkie, R.A. (1965), Vertical water motions in a small ice-covered lake, Jour. Geophys. Res. 70, no. 10, 2333.

Linden, P.F. (1975), The deepening of a mixed layer in stratified fluid, Jour. Fluid Mech. 71(2), 385-405.

Long, Robert R. (1965), On the Boussinesq approximation and its role in the theory of internal waves, Tellus XVII, 1, 46-52.

Maxworthy, T. (1978), A mechanism for the generation of internal solitary waves by tidal flow over submarine topography, Ocean Modeling, 14, May.

McDonald, BC. (1967), Pleistocene Events and Chronology in the Appalachian Region of Southeastern Quebec, Canada, Yale University, Ph.D. dissertation.

Mellor, G.L. and Durbin, P.A. (1975), The structure and dynamics of the ocean surface mixed layer, Jour. Phys. Ocean. 5, 718-728.

Mortimer, C.H. and Mackereth, F.J.H. (1958), Convection and its consequences in ice-covered lakes, Verh. Internat. Ver. Limnol. XIII, 923-932.

Mortimer, C.H. (1954), Models of the flow-pattern in lakes, Weather, Vol. IX, 177-185.

Munk, W.H. and Anderson, E.R. (1948), Notes on a theory of the thermocline, Jour. of Mar. Res., Vol. 7, no. 3, 276-295.

Murthy, C.R. and Miners, K.C. (1978), Turbulent diffusion processes in the Great Lakes, Scientific Series No. 83, Inland Water Directorate CCIW.

Murty, T.S. (1971), The response of a lake with a depth-discontinuity to a time-dependent wind-stress, Arch. Met. Geoph. Biokl., Ser. A, 20, 50-66.

Neumann, G. and Pierson, W.J. Jr. (1966), Principles of Physical Oceanography, Prentice-Hall, Inc. Englewood Cliffs, N.J., USA.

Niiler, P.P. (1977), One-dimensional models of the seasonal thermocline in "Marine Modeling", The Sea, Vol. 6, John Wiley & Sons, Inc.

Niller, Pearn P. (1975), Deepening of the wind-mixed layer, Jour. Mar. Res. 33, 3, 405-422.

Niiler, P.P. and Kraus, E.B. (1977), "One-dimensional Model of the Upper Ocean" in Modelling and Predicton of the Upper Layers of the Ocean, ed. by E.B. Kraus, Pergamon Press.

Pollard, R.T., Rhines, P.B. and Thompson, R.O.R.Y (1973), The deepening of the wind mixed layer, Geophys. Fluid Dynamics, Vol. 4, 381-404.

Pond, S., Phelps, G.T. and Paquin, J.E. (1971), Measurements of the turbulent fluxes of momentum, moisture and sensible heat over the ocean, Jour. Atmos. Sc. Vol. 28, no. 6, 901-917.

Prest, V.K. (1969), "Quaternary Geology" in Economic Minerals of Canada, ed. R.J.W. Douglas, Geological Survey of Canada, Queen's Printer of Canada, Ottawa.

Price, J.F., Mooers, C.N.K. and Van Leer, J.C. (1978), Observation and simulation of storm-induced mixed-layer deepening, Jour. Phys. Ocean. 8, 582-599.

Rattray, M. (1960), On the coastal generation of internal tides, Tellus XII 1.

Sam, J.F.T. and Anderson, E.R. (1956), The heat budget of a body of water of varying volume, Limnol. & Ocean. 1, 247

Sherman, F.S., J. Imberger and G.M. Corcos (1978), Turbulence and mixing in stably stratified waters, Ann. Rev. Fluid Mech. Vol. 10, p. 267.

Smith, J.D. (1977), Modeling of sediment transport on continental shelves, The Sea, Vol. 6, 539-577.

Spigel, R.H. and Imberger, Jörg (1980), The classification of mixed-layer dynamics in lakes of small to medium size, Jour. Phys. Ocean. 10, 1104.

Stewart, K.M. (1972), Isotherm under ice, Verh. Internal. Verein. Limnol. 18, November, 303-311.

Sundaram, T.R. (1977), Some remarks on the influence of basin-wide effects on the formation and maintenance of stratification in lakes, Symp. on Modeling of Transport Mechanisms for Oceans and Lakes, M.S.D. D.F.E.

Sundaram, T.R. and Rehm, R.G. (1973), The seasonal thermal structure of deep temperate lakes, Tellus XXV, 2.

Sundaram, T.R. (1974), Transient thermal response of large lakes to atmospheric disturbances, Proc. 17th Conf. Great Lakes Res., 801-810.

Svensson, Urban (1978), Examination of the summer stratification, Nordic Hydrology, 9, 105-120.

Thendrup, Arve (1978), A one-dimensional numerical model for temperature studies in lakes, Nordic Hydrology, 9, 95-104.

Thompson, R.O.R.Y. (1976), Climatological numerical models of the surface mixed layer of the ocean, Jour. of Phys. Ocean., Vol. 6, p.496.

Thompson, R.O.R.Y. and Imberger, J. (1980), Response of a numerical model of a stratified lake to wind stress, Second International Symposium on Stratified Flows, The Norwegian Institute of Technology, Trondheim, Norway, 24-27 June, 1980.

Thorpe, S.A. (1971), Asymetry of the internal seice in Loch Ness, Nature, Vol. 231, June 4.

Tucker, W.A. and A.W. Green (1977), Thermocline formation in large and small lakes, Symp. on Modeling of Transport Mechanisms for Oceans and Lakes, M.S.D.D.F.E.

Turner, J.S. (1969), A note on wind mixing at the seasonal thermocline, Deep Sea Research, Supplement to Vol. 16, 297-300.

Turner, J.S. and Kraus, E.B. (1967), A one-dimensional model of the seasonal thermocline, I. A laboratory experiment and its interpretation, Tellus XIX, 88.

Tzur, Y. (1973), One-dimensional diffusion equations for the vertical transport in an oscillating stratified lake of varying cross section, Tellus XXV, 3, 266-271.

Wu, J. (1969), Wind stress and surface roughness at air-sea interface, Jour. Geophys. Res. 74, 444.

Zabusky, N.J. and Galvin, C.J. (1971), Shallow-water waves, the Korteweg-de Vries equation and solitons, Jour. Fluid Mech. Vol. 47, no. 4, 811- 824.

Zabusky, N.J. and M.D. Kruskal (1965), Interaction of "Solitons" in a collisionless plasma and the recurrence of initial states, Physical Review Letters, Vol.. 15, no. 6, p. 240.

Zeeman, O. and Tennekes, H. (1977), Parametrization of the turbulent energy budget at the top of the daytime atmospheric boundary layer, Jour. Atmos. Sc., 34, 111-123.

Ziegenbein, J. (1969), Short internal waves in the Strait of Gibraltar, Deep Sea Research, Vol. 16, 479-487.

APPENDIX

```
      PROGRAM LMOD(TAPE5,TAPE11,TAPE12,TAPE13,TAPE14,OUTPUT)
C
C
C           STRATIFICATION MODEL FOR LAKE MEMPHREMAGOG
C           =========================================
C                    BY SYLVAIN DE MARGERIE
C
C
C      A STANDARD MIXED LAYER MODEL IS APLIED TO EACH OF THE LAKES THREE
C     BASINS INDIVIDUALY. THEIR THERMAL REGIME IS THEN LINKED TOGETHER THROUGH
C     AN EXCHANGE EQUATION. IN THE MODEL EACH BASIN IS DIVIDED INTO HORIZONTAL
C     SLABS EACH 50 CM THICK.
C
C     *********
C     *       *
C     *  I/O  *
C     *       *
C     *********
C      ALL OUTPUT (TAPE11) IS WRITEN WITHOUT FORMAT AND THEREFOR NEEDS A
C     POST-PROCESSOR TO BE OF ANY USE (FOR LISTING, PLOTS, ETC..).
C      TAPE12 CONTAINS INITIAL VALUES OF WATER AND SEDIMENT TEMPERATURE
C     PROFILES. THIS INFORMATION IS REPLACED EACH TIME THE MODEL GOES THROUGH
C     A COMPLETE YEARLY CYCLE.
C      TAPE13 CONTAINS SEASONAL METEOROLOGICAL DATA
C      TAPE14 CONTAINS MORPHOMETRIC INFORMATION.
C      TAPE5  CONTAINS CONTAINS DAILY METEOROLOGICAL OBSERVATIONS FROM
C     SHERBROOKE, LENNOXVILLE, AND THE LAKE.
C
C
C     ALL UNIT ARE CGS
C     ================
C
C     ALL VARIABLES ARE STORED IN COMMON BLOCKS FOR EASE OF COMMUNICATION:
C
C      /GEN/----------GENERAL VARIABLES------------
C           DZ - DEPTH INTERVAL
C           CE - TURBULENT EXCHANGE COEFFICIENT FOR WATER VAPOR
C           CQ - TURBULENT EXCHANGE COEFFICIENT FOR HEAT
C         QLAT - LATENT HEAT OF EVAPORATION FOR H2O
C       F7TO10 - FACTOR RELATING WEATHER AT A 10M LEVEL TO OBSERVATIONS AT 7M
C           CA - HEAT CAPACITY OF AIR
C           CD - WIND DRAG COEFFICIENT
C        ROAIR - DENSITY OF AIR
C        TKSED - THERMAL CONDUCTIVITY OF SEDIMENTS
C        ROSED - DENSITY OF SEDIMENTS
C         CSED - HEAT CAPACITY OF SEDIMENTS
C          DAY - # OF SECONDS IN A DAY
C           XV - INTERBASIN EXCHANGE VELOCITY
C         BINT - WIDTH OF INTERCONECTING CHANELS
C           RO - MEAN WATER DENSITY
C            G - GRAVITATIONAL ACCELERATION
C           C - HEAT CAPACITY OF WATER
C          ETA - CONSTANT IN MIXED LAYER MODEL
C           CK - CONSTANT IN MIXED LAYER MODEL
C           CL - CONSTANT IN MIXED LAYER MODEL
C           CT - CONSTANT IN MIXED LAYER MODEL
C           CS - CONSTANT IN MIXED LAYER MODEL
C           JD - JULIAN DAY
C         H2OK - THERMAL CONDUCTIVITY OF WATER
C
C     /BASIN/-------INFORMATION RELATING TO EACH BASIN--------
C           BD - TOTAL DEPTH
C           SA - SURFACE AREA
```

```
C           VO - TOTAL VOLUME
C         BETA - EXTINCTION COEFFICIENTS
C          ICE - ICE COVER FLAG
C          IZM - MIXED LAYER DEPTH / DZ
C      TKELEFT - TURBULENT KINETIC ENERGY LEFTOVER FROM PREVIOUS STEPS
C         QTMX - TURBULENT KINETIC ENERGY INTENSITY AT THE LAST STEP.
C       ISHEAR - FLAG ,SINGNALS POSSIBLE IMPORTANCE OF SHEAR WHEN =1
C
C  /VOL/--------MORPHOMETRY------------
C        VS,VC,VN - VOLUME OF EACH SLAB OF WATER FOR SOUTH, CENTRAL,
C                   NORTH, AND THE WHOLE LAKE.
C
C  /TEMP/-----------WATER TEMPERATURE PROFILES-------------
C          TS,TC,TN, FOR SOUTH, CENTRAL, AND NORTH BASINS
C
C  /BOT/----------SEDIMENT TEMPERATURE PROFILES------------
C          SS, SC, SN, FOR SOUTH, CENTRAL, AND NORTH
C
C  /FLUX/---------EQUIVALENT SURFACE FLUXES----------------
C          TAU - MOMENTUM
C        PHILW - NET LONG WAVE RADIATION
C        PHISW - NET SHORT WAVE RADIATION
C       PHILAT - LATENT HEAT
C       PHISEN - SENSITIVE HEAT
C       PHISED - SEDIMENT HEAT
C        PHIEX - INTERBASIN HEAT EXCHANGE
C
C  /HEAT/---------NET SURFACE HEAT FLUX (EXCLUDING FENETRATING SW RAD)--
C          QS, DC, QN FOR SOUTH, CENTRAL, AND NORTH
C
C  /YEAR/-----------SEASONAL ATMOSPHERIC DATA--------------
C        ASTRO - SOLAR INCLINATION, MAXIMUM NUMBER OF HOUR OF SUNSHINE PER
C                DAY, AND ALBEDO FUNCTION FOR EACH DAY OF THE YEAR.
C        TAM,TIM,RAM,RIM,WM,HM - NORMAL DAILY MAXIMUM AND MINIMUM TEMPERATURE
C                , AND RELATIVE HUMIDITY, WIND SPEED AND HOURS OF INSOLATION
C                AT THE BEGUINING OF EACH MONTH.
C
C
C
      COMMON /GEN/DZ,CE,CQ,QLAT,F7TO10,CA,CD,ROAIR,TKSED,ROSED,CSED,
     %DAY,XV,BINT(2,30),RO,G,C,ETA,CK,CL,CT,CS,JD,H2OK
C
      COMMON /BASIN/BD(3),VO(3),BETA(3),ICE(3),IZM(3),TKELEFT(3),QTMX(3)
     % ,ISHEAR(3)
C
      COMMON /VOL/VS(42),VC(216),VN(70)
C
      COMMON /TEMP/TS(42),TC(216),TN(70)
C
      COMMON /BOT/SS(10,42),SC(10,216),SN(10,70)
C
      COMMON /FLUX/TAU(3),PHILW(3),PHISW(3),PHILAT(3),PHISEN(3),
     %PHISED(3),PHIEX(3)
C
      COMMON /HEAT/QS,QC,QN
C
      COMMON /YEAR/ASTRO(3,366),TAM(12),TIM(12),RAM(12),RIM(12),
     %WM(12),HM(12)
C
C
C****TOTAL STORAGE****
      REAL AGEN(81),ABASIN(15),AVOL(328),ATEMP(328),ABOT(10,328),
     %AFLUX(21),AHEAT(3),AYEAR(1170)
```

```
      EQUIVALENCE (AGEN,DZ),(ABASIN,BD),(AVOL,VS),(ATEMP,TS),(ABOT,SS)
     %,(AFLUX,TAU),(AHEAT,QS),(AYEAR,ASTRO)
C
C
C
C****INITIALIZE VARIABLES*****
      DZ=50.
      CE=1.3E-3
      CQ=1.3E-3
      CLAT=590.
      F7TO10=1.07
      CA=.24
      CD=1.2E-3
      ROAIR=1.2E-3
      TKSED=2.2E-3
      ROSED=1.52
      CSED=.54
      DAY=84600.
      XV=4.
      DO 1001 I=1,18
 1001 BINT(1,I)=100000.
      DO 1002 I=19,30
 1002 BINT(1,I)=0.
      DO 1003 I=1,30
 1003 BINT(2,I)=3000.*(31-I)
      RO=1.
      G=981.
      C=1.
      ETA=1.8
      CK=.38
      CL=.04
      CT=2.25
      CS=.3
      H2OK=.001434
      BETA(1)=.00515
      BETA(2)=.00356
      BETA(3)=.00379
      ICE(1)=0
      ICE(2)=0
      ICE(3)=0
      IZM(1)=1
      IZM(2)=1
      IZM(3)=1
      TKELEFT(1)=0.
      TKELEFT(2)=0.
      TKELEFT(3)=0.
      QTMX(1)=0.
      QTMX(2)=0.
      QTMX(3)=0.
      DO 2 I=1,328
  2   AHEAT(I)=0.
      REWIND 14
      CALL VOLUME(VS,42,VO(1),BD(1))
      CALL VOLUME(VC,216,VO(2),BD(2))
      CALL VOLUME(VN,70,VO(3),BD(3))
      REWIND 12
      READ (12) ATEMP,ABOT
      REWIND 13
      READ (13) AYEAR
C
C  READ JULIAN DAY ON WHICH MET DATA STARTS
C  IF JO GE 500 THE MODEL GOES THROUGH A MEAN YEARLY CYCLE
      REWIND 11
```

```
      JD=107
      READ (5,101) JO
  101 FORMAT(I5)
C
C
C****DAILY LOOP****
      REWIND 5
    1 JD=JD+1
C  GET ATMOSPHERIC FLUXES
      CALL INPUT(JO)
      IF (JD.EQ.474) STOP
C  GET BOTTOM HEAT FLUXES
      CALL SED
C  GET INTERBASIN HEAT EXCHANGE
      CALL EX
C  LET MOLECULAR DIFFUSION ACT ON THE WATER COLUMN
      CALL MOL
C  SOLVE THE MIXED LAYER EQUATION
      CALL STRAT
C  ENSURE THAT THE HYPOLIMNION IS STABLE
      CALL MIX
C  OUTPUT RESULTS
      WRITE (11) AFLUX,ICE,IZM,ISHEAR,ATEMP
C
C  CHECK FOR ICE COVER
      IF (TS(1).LE.0.) ICE(1)=1
      IF (TC(1).LE.0.)ICE(2)=1
      IF (TN(1).LE.0.) ICE(3)=1
C
C
C979  IF(JD.GE.146) STOP
C****LOOP END
      IF (JD.LT.473) GO TO 1
      REWIND 12
      WRITE (12) ATEMP,ABOT
      STOP
      END
C
C
C
C////////////////////////////////////////////////////////////////////////////
C\\\\\\\\\\\\\\\\\\\\\\\\\\\\\\\\\\\\\\\\\\\\\\\\\\\\\\\\\\\\\\\\\\\\\\\\\\\\
C
C
      SUBROUTINE INPUT(JO)
C
C        THIS SUBROUTINE GETS DAILY METEOROLOGICAL VARIABLES AND COMPUTES
C     ATMOSPHERIC HEAT AND MOMENTUM FLUXES.
C
      COMMON /GEN/DZ,CE,CQ,QLAT,F7TO10,CA,CD,ROAIR,TKSED,ROSED,CSED,
     %DAY,XV,BINT(2,30),RO,G,C,ETA,CK,CL,CT,CS,JD,H2OK
C
      COMMON /BASIN/BD(3),VO(3),BETA(3),ICE(3),IZM(3),TKELEFT(3),QTMX(3)
     % ,ISHEAR(3)
C
      COMMON /VOL/VS(42),VC(216),VN(70)
C
      COMMON /TEMP/TS(42),TC(216),TN(70)
C
      COMMON /BOT/SS(10,42),SC(10,216),SN(10,70)
C
      COMMON /FLUX/TAU(3),PHILW(3),PHISW(3),PHILAT(3),PHISEN(3),
     %PHISED(3),PHIEX(3)
```

```
C
      COMMON /HEAT/QS,QC,QN
C
      COMMON /YEAR/ASTRO(3,366),TAM(12),TIM(12),RAM(12),RIM(12),
     %WM(12),HM(12)
C
C
C****TOTAL STORAGE****
      REAL AGEN(81),ABASIN(15),AVOL(328),ATEMP(328),ABOT(10,328),
     %AFLUX(21),AHEAT(3),AYEAR(1170)
      EQUIVALENCE (AGEN,DZ),(ABASIN,BD),(AVOL,VS),(ATEMP,TS),(ABOT,SS)
     %,(AFLUX,TAU),(AHEAT,QS),(AYEAR,ASTRO)
C
C
C      MOST VARIABLES ARE AS DESCRIBED IN THE MAIN PROGRAM
C     ADDITIONAL VARIABLES ARE :
C        TI,TA - MINIMUM AND MAXIMUM DAILY TEMPERATURE
C        RI,RA - MINIMUM AND MAXIMUM DAILY RELATIVE HUMIDITY.
C            U - DAILY MEAN WIND SPEED
C            H - DAILY NUMBER OF SUNNY HOURS
C          QSW - DAILY SHORTWAVE INCIDENT RADIATION
C            T - MEAN TEMPERATURE AT SHEBROOKE
C        VA,EA - MEAN VAPOR PRESSURE AND SPECIFIC HUMIDITY AT SHERBROOKE
C        VO,EO - VAPOR PRESSURE AND SPECIFIC HUMIDITY AT WATER SURFACE
C            S - RELATIVE INSOLATION
C           ST - TIME OF YEAR IN RADIANS FROM THE SUMMER SOLSTICE
C
C   COMPUTE SIDERAL TIME OF THE YEAR
C      AND THE TRUE JULIAN DAY.
      ST=JD*.017202424+3.3189927
      JDD=MOD(JD-1,365)+1
C   GET THE INPUT DATA
      IF (JD.LT.JO) CALL MEAN(TA,TI,RA,RI,U,H,QSW)
      IF (JD.GE.JO) READ(5,10) ID,IM,TA,TI,RA,RI,U,H,QSW
   10 FORMAT (2I2,1X,7F5.1)
      IF(EOF(5).NE.0.) GO TO 999
C  TRANSFORM WIND FROM KM/HR TO CGS UNITS
      U=U/.036
C   TRANSFORM S.W. RADIATION FROM LANGLEYS TO CGS UNITS
      QSW=QSW/DAY
C  COMPUTE RELATIVE INSOLATION
      S=H/ASTRO(2,JDD)
C  COMPUTE SHORT WAVE RADIATION FLUX IF NOT MEASURED (GENERAL FORMULA BY GREY)
C   TWO FIRST COEFFICIENT OBTAINED BY LEAST SQUARES FIT OF LAKE DATA
      IF (QSW.EQ.0.)QSW=(.246+.734*S)*(515.-23.*SIN(ST)+309.*COS(ST)
     %-4.*SIN(ST*2.)-5.*COS(ST*2.))/DAY
C  COMPUTE TOTAL ABSORBED SHORTWAVE RADIATION USING THE DAILY ALBEDO FUNCTION
C SEE THESIS SECTION 4.3
      RO=QSW*(.934+S*(ASTRO(3,JDD)-.057))
C  COMPUTE THE MEAN DAILY VAPOR PRESSURE (AT SHERBROOKE (MB) , ASSUMING THAT
C THE MINIMUM RELATIVE HUMIDITY OCCURS AT THE TIME OF MAXIMUM TEMPERATURE
C AND VICE VERSA.
      VA=(RA*(6.1747+.36254*TI+.025058*TI*TI)+RI*(6.1747+.36254*TA+
     %.025058*TA*TA))/200.
C    NOW CHANGE VAPOR PRESSURE (MB) TO SPECIFIC HUMIDITY (G/CM**3)
      EA=VA*7.522E-7
C  COMPUTE MEAN DAILY TEMPERATURE AT SHERBROOKE (INCLUDING CORRECTION FOR
C  LAPSE RATE FOR HEIGHT DIFFERENCE BETWEEN THE LAKE AND THE AIRPORT.
      T=(TA+TI)/2+.27
C
C***LOOP FOR EACH BASIN
      DO 5 I=1,3
      IMIN=1
```

```
      IF (I.EQ.2) IMIN=43
      IF (I.EQ.3) IMIN=259
      IMAX=IMIN+BD(I)/DZ
      TO=ATEMP(IMIN)
C  COMPUTE VAPOR PRESSURE (MB) AT THE WATER SURFACE
      VO=6.1747+.36254*ATEMP(IMIN)+.025058*ATEMP(IMIN)*ATEMP(IMIN)
C  COMPUTE SPECIFIC HUMIDITY (G/CM**3) AT THE WATER SURFACE
      EO=VO*7.522E-7
C   CHECK FOR ICE
      IF (ICE(I).EQ.0) GO TO 2
      PHISW(I)=0.1*RO
      PHILAT(I)=0.
      PHISEN(I)=0.
      PHILW(I)=0.
      TAU(I)=0.
      GO TO 3
C  COMPUTE THE FLUXES PROPER
C   EXCEPT FOR LONG WAVE RADIATION THE NUMERIC CONSTANTS IN THE FOLLOWING
C  LINES, ARE COEFFICIENT DETERMINED BY L.S. FIT TO COMPUTE FLUXES USING
C  SHERBROOKE WEATHER OBSERVATION.
   2  PHISW(I)=RO
      PHILAT(I)=-((EO-EA)*U*1.6)*CE*QLAT*F7TO10
      PHISEN(I)=-((TO-TA)*U*1.9-410.)*CQ*ROAIR*CA*F7TO10
      TAU(I)=CD*ROAIR*(76000.+U*U*2.3)*F7TO10**2
C   TKA AND TKO ARE THE ABSOLUTE TEMPERATURES OF THE LAKE SURFACE AND THE
C  AIR ABOVE IT.
      TKA=TO+1.5-.93*(TO-TA)+273.16
      TKO=TO+273.16
      PHILW(I)=1.35E-12*(TKA**4*(1-.261*EXP(-.777E-3*(TKA-273.16)**2))
     %*(1.+.18*(1-S))-.98*TKO**4)
C
C  SPREAD THE HEAT TO EACH SLICE OF H2O(45% OF THE SHORT WAVE FLUX PENETRATES
C THE WATER, THE REST IS ABSORBED IN THE FIRST LAYER).
  3   DZBETA=DZ*BETA(I)
      Q1=PHISW(I)*.45
      DO 11 J=IMIN,IMAX
      Q2=Q1-.45*PHISW(I)*EXP(-(J-IMIN+1)*DZBETA)
      Q1=Q1-Q2
  11  ATEMP(J)=ATEMP(J)+Q2/DZ*DAY
      IF (ICE(I).EQ.1) GO TO 5
      AHEAT(I)=(PHILAT(I)+PHISEN(I)+PHILW(I)
     %+.55*PHISW(I))
      ATEMP(IMIN)=ATEMP(IMIN)+AHEAT(I)*DAY/DZ
C***LOOP END
C
   5  CONTINUE
C
      RETURN
C
C  END OF DATA
 999  JD=474
      RETURN
      END
C
C
C/////////////////////////////////////////////////////////////////////////
C\\\\\\\\\\\\\\\\\\\\\\\\\\\\\\\\\\\\\\\\\\\\\\\\\\\\\\\\\\\\\\\\\\\\\\\\\
C
C
C
C
C
C
```

```
      SUBROUTINE MEAN(TI,TA,RI,RA,W,H,QSW)
C
C           THIS SUBROUTINE SUPPLIES SEASONAL VALUES OF WEATHER VARIABLES
C     FOR SHERBROOKE.
C
      COMMON /GEN/DZ,CE,CQ,QLAT,F7TO10,CA,CD,ROAIR,TKSED,ROSED,CSED,
     %DAY,XV,BINT(2,30),RO,G,C,ETA,CK,CL,CT,CS,JD,H2OK
C
      COMMON /BASIN/BD(3),VO(3),BETA(3),ICE(3),IZM(3),TKELEFT(3),QTMX(3)
     % ,ISHEAR(3)
C
      COMMON /VOL/VS(42),VC(216),VN(70)
C
      COMMON /TEMP/TS(42),TC(216),TN(70)
C
      COMMON /BOT/SS(10,42),SC(10,216),SN(10,70)
C
      COMMON /FLUX/TAU(3),PHILW(3),PHISW(3),PHILAT(3),PHISEN(3),
     %PHISED(3),PHIEX(3)
C
      COMMON /HEAT/QS,QC,QN
C
      COMMON /YEAR/ASTRO(3,366),TAM(12),TIM(12),RAM(12),RIM(12),
     %WM(12),HM(12)
C
C
C****TOTAL STORAGE****
      REAL AGEN(81),ABASIN(15),AVOL(328),ATEMP(328),ABOT(10,328),
     %AFLUX(21),AHEAT(3),AYEAR(1170)
      EQUIVALENCE (AGEN,DZ),(ABASIN,BD),(AVOL,VS),(ATEMP,TS),(ABOT,SS)
     %,(AFLUX,TAU),(AHEAT,QS),(AYEAR,ASTRO)
      I1=JD/30.5+1
      I1=MOD(I1+11,12)+1
      I2=MOD(I1,12)+1
      DIF=JD/30.5+1.-I1
      TA=TAM(I1)+(TAM(I2)-TAM(I1))*DIF
      TI=TIM(I1)+(TIM(I2)-TIM(I1))*DIF
      RA=RAM(I1)+(RAM(I2)-RAM(I1))*DIF
      RI=RIM(I1)+(RIM(I2)-RIM(I1))*DIF
      W=WM(I1)+(WM(I2)-WM(I1))*DIF
      H=HM(I1)+(HM(I2)-HM(I1))*DIF
      QSW=0.
      RETURN
      END
C
C
C//////////////////////////////////////////////////////////////////////////////
C\\\\\\\\\\\\\\\\\\\\\\\\\\\\\\\\\\\\\\\\\\\\\\\\\\\\\\\\\\\\\\\\\\\\\\\\\\\\\\\\\\\\
C
C
      SUBROUTINE SED
C
C      THIS SUBROUTINE COMPUTES THE HEAT EXCHANGE WITH THE SEDIMENTS
C
C     THE VARIABLES ARE AS DISCRIBED IN THE MAIN PROGRAM
C
      COMMON /GEN/DZ,CE,CQ,QLAT,F7TO10,CA,CD,ROAIR,TKSED,ROSED,CSED,
     %DAY,XV,BINT(2,30),RO,G,C,ETA,CK,CL,CT,CS,JD,H2OK
C
      COMMON /BASIN/BD(3),VO(3),BETA(3),ICE(3),IZM(3),TKELEFT(3),QTMX(3)
     % ,ISHEAR(3)
C
      COMMON /VOL/VS(42),VC(216),VN(70)
```

```
C
      COMMON /TEMP/TS(42),TC(216),TN(70)
C
      COMMON /BOT/SS(10,42),SC(10,216),SN(10,70)
C
      COMMON /FLUX/TAU(3),PHILW(3),PHISW(3),PHILAT(3),PHISEN(3),
     %PHISED(3),PHIEX(3)
C
      COMMON /HEAT/QS,QC,QN
C
      COMMON /YEAR/ASTRO(3,366),TAM(12),TIM(12),RAM(12),RIM(12),
     %WM(12),HM(12)
C
C
C****TOTAL STORAGE****
      REAL AGEN(81),ABASIN(15),AVOL(328),ATEMP(328),ABOT(10,328),
     %AFLUX(21),AHEAT(3),AYEAR(1170)
      EQUIVALENCE (AGEN,DZ),(ABASIN,BD),(AVOL,VS),(ATEMP,TS),(ABOT,SS)
     %,(AFLUX,TAU),(AHEAT,QS),(AYEAR,ASTRO)
C
C
C   COMPUTE FACTORS TO USED REPEATEDLY
      TKDZ=TKSED/DZ
      DAYDZRC=DAY/(DZ*ROSED*CSED)
C
C**LOOP ON BASINS
      DO 1 IB=1,3
      BETADZ=BETA(IB)*DZ
      IMIN=1
      IF (IB.EQ.2) IMIN=43
      IF (IB.EQ.3) IMIN=259
      IMAX=IMIN+BD(IB)/DZ
      QT=0.
C
C***********LOOP ON WATER SLABS
      DO 2 ISLAB=IMIN,IMAX
C  FLUX INTO THE WATER
      Q1=(ABOT(1,ISLAB)-ATEMP(ISLAB))*TKDZ*2
C  DONT FORGET TO ADD THE SOLAR RADIATION INCIDENT ON THE SEDIMENT
      Q0=Q1*(AVOL(ISLAB)-AVOL(ISLAB+1))/DZ
      ATEMP(ISLAB)=ATEMP(ISLAB)+Q0/AVOL(ISLAB)*DAY
      Q1=Q1-.45*PHISW(IB)*EXP((-ISLAB+IMIN-1)*BETADZ)
      QT=QT+Q1*(AVOL(ISLAB)-AVOL(ISLAB+1))/DZ
C  FLUX WITHIN THE SEDIMENTS
      DO 3 ISLICE=1,9
      Q2=-(ABOT(ISLICE,ISLAB)-ABOT(ISLICE+1,ISLAB))*TKDZ
      ABOT(ISLICE,ISLAB)=ABOT(ISLICE,ISLAB)+(Q2-Q1)*DAYDZRC
    3 Q1=Q2
    2 ABOT(10,ISLAB)=ABOT(10,ISLAB)-Q1*DAYDZRC
C**********LOOP END
C
C  COMPUTE EQUIVALENT SURFACE FLUX
      PHISED(IB)=QT/AVOL(IMIN)*DZ
C**LOOP END
    1 CONTINUE
      RETURN
      END
C
C
C
C//////////////////////////////////////////////////////////////////////
C\\\\\\\\\\\\\\\\\\\\\\\\\\\\\\\\\\\\\\\\\\\\\\\\\\\\\\\\\\\\\\\\\\\\\\\
C
```

```
C
C
      SUBROUTINE MOL
C
C
C   THIS SUBROUTINE SIMULATES MOLECULAR DIFFUSION IN THE WATER COLUMN
C
C   IF ONE DESIRED TO INCLUDE A FORM OF TURBULENT DIFFUSION BELOW THE
C MIXED LAYER , IT WOULD SUFFICE TO CHANGE THE VALUE USED HERE FOR THERMAL
C CONDUCTIVITY OF THE WATER COLUMN, TO AN APPROPRIATE EDDY DIFFUSION
C COEFFICIENT.
C
      COMMON /GEN/DZ,CE,CQ,QLAT,F7TO10,CA,CD,ROAIR,TKSED,ROSED,CSED,
     %DAY,XV,BINT(2,30),RO,G,C,ETA,CK,CL,CT,CS,JD,H2OK
C
      COMMON /BASIN/BD(3),VO(3),BETA(3),ICE(3),IZM(3),TKELEFT(3),QTMX(3)
     % ,ISHEAR(3)
C
      COMMON /VOL/VS(42),VC(216),VN(70)
C
      COMMON /TEMP/TS(42),TC(216),TN(70)
C
      COMMON /BOT/SS(10,42),SC(10,216),SN(10,70)
C
      COMMON /FLUX/TAU(3),PHILW(3),PHISW(3),PHILAT(3),PHISEN(3),
     %PHISED(3),PHIEX(3)
C
      COMMON /HEAT/QS,QC,QN
C
      COMMON /YEAR/ASTRO(3,366),TAM(12),TIM(12),RAM(12),RIM(12),
     %WM(12),HM(12)
C
C
C****TOTAL STORAGE****
      REAL AGEN(81),ABASIN(15),AVOL(328),ATEMP(328),ABOT(10,328),
     %AFLUX(21),AHEAT(3),AYEAR(1170)
      EQUIVALENCE (AGEN,DZ),(ABASIN,BD),(AVOL,VS),(ATEMP,TS),(ABOT,SS)
     %,(AFLUX,TAU),(AHEAT,QS),(AYEAR,ASTRO)
C
      H2OKDZ=H2OK/DZ
C***LOOP ON THE THREE BASINS
      DO 1 I=1,3
C  SET THE BOUNDING INDEXES
      IMIN=1
      IF (I.EQ.2) IMIN=43
      IF (I.EQ.3) IMIN=259
      IMAX=IMIN+BD(I)/DZ
      Q1=0.
      IF (ICE(I).EQ.1) Q1=-ATEMP(IMIN)*H2OKDZ*2.
C*******LOOP ON EACH SLAB
      DO 2 J=IMIN,IMAX
      Q2=H2OKDZ*(ATEMP(J)-ATEMP(J+1))
      ATEMP(J)=ATEMP(J)+(Q1-Q2*AVOL(J+1)/AVOL(J))/DZ*DAY
    2 Q1=Q2
C*******LOOP END
    1 CONTINUE
C***LOOP END
      RETURN
      END
C
C
C//////////////////////////////////////////////////////////////////////
C\\\\\\\\\\\\\\\\\\\\\\\\\\\\\\\\\\\\\\\\\\\\\\\\\\\\\\\\\\\\\\\\\\\\\\
```

```
C
C
      SUBROUTINE EX
C
C
C      THIS SUBROUTINE COMPUTES THE INTER BASIN HEAT EXCHANGE
C
C
C    ALL VARIABLES ARE AS DESCRIBED IN THE MAIN PROGRAM
C
C
C
      COMMON /GEN/DZ,CE,CQ,QLAT,F7TO10,CA,CD,ROAIR,TKSED,ROSED,CSED,
     %DAY,XV,BINT(2,30),RO,G,C,ETA,CK,CL,CT,CS,JD,H2OK
C
      COMMON /BASIN/BD(3),VO(3),BETA(3),ICE(3),IZM(3),TKELEFT(3),QTMX(3)
     % ,ISHEAR(3)
C
      COMMON /VOL/VS(42),VC(216),VN(70)
C
      COMMON /TEMP/TS(42),TC(216),TN(70)
C
      COMMON /BOT/SS(10,42),SC(10,216),SN(10,70)
C
      COMMON /FLUX/TAU(3),PHILW(3),PHISW(3),PHILAT(3),PHISEN(3),
     %PHISED(3),PHIEX(3)
C
      COMMON /HEAT/QS,QC,QN
C
      COMMON /YEAR/ASTRO(3,366),TAM(12),TIM(12),RAM(12),RIM(12),
     %WM(12),HM(12)
C
C
C****TOTAL STORAGE****
      REAL AGEN(81),ABASIN(15),AVOL(328),ATEMP(328),ABOT(10,328),
     %AFLUX(21),AHEAT(3),AYEAR(1170)
      EQUIVALENCE (AGEN,DZ),(ABASIN,BD),(AVOL,VS),(ATEMP,TS),(ABOT,SS)
     %,(AFLUX,TAU),(AHEAT,QS),(AYEAR,ASTRO)
C
C
C
      QS1=0.
      QS2=0.
      Q1=0
      Q2=0
C***LOOP ON INTERCONNECTING SLABS
      DO 1 I=1,30
C     CHECK IF THE BASIN IS ICE COVERED
      IF(ICE(1)*ICE(2).EQ.0)Q1=(TS(I)-TC(I))*XV*DZ*BINT(1,I)
      IF (ICE(2)*ICE(3).EQ.0)Q2=(TC(I)-TN(I))*XV*DZ*BINT(2,I)
      IF (VS(I).NE.0.)TS(I)=TS(I)-Q1/VS(I)*DAY
      TC(I)=TC(I)+(Q1-Q2)/VC(I)*DAY
      TN(I)=TN(I)+Q2/VN(I)*DAY
      QS1=QS1+Q1
    1 QS2=QS2+Q2
C   COMPUTE EQUIVALENT SURFACE FLUX
      PHIEX(1)=-QS1/VS(1)*DZ
      PHIEX(2)=(QS1-QS2)/VC(1)*DZ
      PHIEX(3)=QS2/VN(1)*DZ
      RETURN
      END
C
C
```

```
C////////////////////////////////////////////////////////////////////////
C\\\\\\\\\\\\\\\\\\\\\\\\\\\\\\\\\\\\\\\\\\\\\\\\\\\\\\\\\\\\\\\\\\\\\\\\
C
C
      SUBROUTINE MIXLAY(IHM,E,QTX,TMX,ETA3U3,IMIN,IMAX,IB)
C
C  THIS SUBROUTINE COMPUTE THE AVAILABLE TKE AND THE POTENTIAL ENERGY
C OF A MIXED LAYER OF DEPTH IHM*DZ.
C
C
      COMMON /GEN/DZ,CE,CQ,QLAT,F7T010,CA,CD,ROAIR,TKSED,ROSED,CSED,
     %DAY,XV,BINT(2,30),RO,G,C,ETA,CK,CL,CT,CS,JD,H20K
C
      COMMON /BASIN/BD(3),VO(3),BETA(3),ICE(3),IZM(3),TKELEFT(3),QTMX(3)
     % ,ISHEAR(3)
C
      COMMON /VOL/VS(42),VC(216),VN(70)
C
      COMMON /TEMP/TS(42),TC(216),TN(70)
C
      COMMON /BOT/SS(10,42),SC(10,216),SN(10,70)
C
      COMMON /FLUX/TAU(3),PHILW(3),PHISW(3),PHILAT(3),PHISEN(3),
     %PHISED(3),PHIEX(3)
C
      COMMON /HEAT/QS,QC,QN
C
      COMMON /YEAR/ASTRO(3,366),TAM(12),TIM(12),RAM(12),RIM(12),
     %WM(12)
C
C
C****TOTAL STORAGE****
      REAL AGEN(81),ABASIN(15),AVOL(328),ATEMP(328),ABOT(10,328),
     %AFLUX(21),AHEAT(3),AYEAR(1170)
      EQUIVALENCE (AGEN,DZ),(ABASIN,BD),(AVOL,VS),(ATEMP,TS),(ABOT,SS)
     %,(AFLUX,TAU),(AHEAT,QS),(AYEAR,ASTRO)
C
C  DETERMINE THE TEMPERATURE AND THE VOLUME OF THE MIXED LAYER
      VMX=0.
      QMX=0.
C***LOOP ON EACH SLAB WITHIN THE MIXED LAYER
      DO 1 I=IMIN,IHM
      QMX=ATEMP(I)*AVOL(I)+QMX
    1 VMX=AVOL(I)+VMX
C***LOOP END
      TMX=QMX/VMX
C
C  DETERMINE DENSITY AND DENSITY GRADIENTS
      ALFMX=ALPHA(TMX)
      ROMX=RHO(TMX)
      ROH=ROMX
      ROHH=0.
      IF (IHM+2.GT.IMAX) GO TO 2
      ROH=RHO(ATEMP(IHM+1))
      ROHH=RHO(ATEMP(IHM+2))
    2 DRO=ROH-ROMX
      DRODZ=(ROHH-ROH)/DZ
C
C
C  COMPUTE POTENTIAL ENERGY
      EPOT=0.
      FACTOR=ALFMX*G*DZ*DZ
      DO 3 I=IMIN,IHM
```

```
      ID=I-IMIN+1
    3 EPOT=EPOT+FACTOR*(ATEMP(I)-TMX)*(ID-.5)
C
C  COMPUTE THE CONVECTIVE VELOCITY SCALE
      HM=(IHM-IMIN+1)*DZ
      UF3=ALFMX*HM*G/(RO*C)*AHEAT(IB)
      IF (UF3.LT.0.) UF3=0.
C
C  COMPUTE TOTAL TURBULENT VELOCITY SCALE
      QTX=(ETA3U3+UF3)**.33333333
      RS=0.
      RI=0.
      COEF=0.
      IF (DRO.LE.0.) GO TO 5
      IF (QTX.EQ.0.) GO TO 5
      RI=DRO*G*HM/(QTX*QTX)
      IF (DRODZ.GT.0.)RS=HM/QTX*SQRT(G*DRODZ/ROMX)
C
C      COMPUTE AVAILABLE TKE
      IF (RS.NE.0.)COEF=RS**3/(RS+RI)**2
    5 EKIN=QTX**3*DAY*.5*(CK-CL*COEF)
C
C     COMPUTE ENERGY DIFFERENCE
      E=EPOT-EKIN
      RETURN
      END
C
C
C
C///////////////////////////////////////////////////////////////////////
C\\\\\\\\\\\\\\\\\\\\\\\\\\\\\\\\\\\\\\\\\\\\\\\\\\\\\\\\\\\\\\\\\\\\\\\
C
C
      FUNCTION ALPHA(T)
C    COMPUTE COEFFICIENT OF THERMAL EXPANSION
      ALPHA=6.793952E-5-1.819058E-5*T+3.005055E-7*T*T-4.480332E-9*
     %T**3+3.28166E-11*T**3
      RETURN
      END
C
C
C
C///////////////////////////////////////////////////////////////////////
C\\\\\\\\\\\\\\\\\\\\\\\\\\\\\\\\\\\\\\\\\\\\\\\\\\\\\\\\\\\\\\\\\\\\\\\
C
      FUNCTION RHO(T)
C    COMPUTE WATER DENSITY
      RHO=.9998426+6.793952E-5*T-9.09529E-6*T*T+1.001685E-7*T**3
     %-1.120083E-9*T**4+6.536332E-12*T**5
      RETURN
      END
C
C
C
C///////////////////////////////////////////////////////////////////////
C\\\\\\\\\\\\\\\\\\\\\\\\\\\\\\\\\\\\\\\\\\\\\\\\\\\\\\\\\\\\\\\\\\\\\\\
C
C
      SUBROUTINE STRAT
C
C        THIS SUBROUTINE SOLVES THE MIXED LAYER THE EQUATION.
C
C
```

```
C
      COMMON /GEN/DZ,CE,CQ,OLAT,F7T010,CA,CD,ROAIR,TKSED,ROSED,CSED,
     %DAY,XV,BINT(2,30),RO,G,C,ETA,CK,CL,CT,CS,JD,H2OK
C
      COMMON /BASIN/BD(3),VO(3),BETA(3),ICE(3),IZM(3),TKELEFT(3),QTMX(3)
     % ,ISHEAR(3)
C
      COMMON /VOL/VS(42),VC(216),VN(70)
C
      COMMON /TEMP/TS(42),TC(216),TN(70)
C
      COMMON /BOT/SS(10,42),SC(10,216),SN(10,70)
C
      COMMON /FLUX/TAU(3),PHILW(3),PHISW(3),PHILAT(3),PHISEN(3),
     %PHISED(3),PHIEX(3)
C
      COMMON /HEAT/QS,QC,QN
C
      COMMON /YEAR/ASTRO(3,366),TAM(12),TIM(12),RAM(12),RIM(12),
     %WM(12),HM(12)
C
C
C****TOTAL STORAGE****
      REAL AGEN(81),ABASIN(15),AVOL(328),ATEMP(328),ABOT(10,328),
     %AFLUX(21),AHEAT(3),AYEAR(1170)
      EQUIVALENCE (AGEN,DZ),(ABASIN,BD),(AVOL,VS),(ATEMP,TS),(ABOT,SS)
     %,(AFLUX,TAU),(AHEAT,QS),(AYEAR,ASTRO)
C      MOST VARIABLES ARE AS DESCRIBED IN THE MAIN PROGRAM
C
C
C****LOOP ON THE THREE BASIN
      DO 1 I=1,3
      IB=I
C  COMPUTE WIND MIXING VELOCITY SCALE CUBED
      ETA3U3=(SQRT(TAU(I)/RO)*ETA)**3
      TAUMX=TAU(I) /RO
C  DETERMINE THE BOUNDING INDEXES FOR THIS BASIN
      IMIN=1
      IF (I.EQ.2) IMIN=43
      IF (I.EQ.3) IMIN=259
      IMAX=IMIN+BD(I)/DZ
      IHM=IZM(I)+IMIN-1
      CALL MIXLAY(IHM,E,QTX1,TMX1,ETA3U3,IMIN,IMAX,I)
      ELEFT1=TKELEFT(I)-E
      IF(ELEFT1.GT.0.) GO TO 10
   21 QTX=QTX1
      TMX=TMX1
      ELEFT=ELEFT1
      IF(IHM.EQ.IMIN) GO TO 30
      IHM=IHM-1
      CALL MIXLAY(IHM,E,QTX1,TMX1,ETA3U3,IMIN,IMAX,I)
      ELEFT1=TKELEFT(I)-E
      IF (ELEFT1.LT.0.) GO TO 21
      GO TO 30
   10 QTX=QTX1
      TMX=TMX1
      ELEFT=ELEFT1
   11 IF(IHM+1.EQ.IMAX) GO TO 30
      IHM=IHM+1
      CALL MIXLAY(IHM,E,QTX,TMX,ETA3U3,IMIN,IMAX,I)
      ELEFT=TKELEFT(I)-E+(QTMX(I)**2*IZM(I)-QTX**2*(IHM-IMIN+1))*DZ
      IF (ELEFT.GT.0.) GO TO 11
   30 IZM(I)=IHM-IMIN+1
```

```
      TKELEFT(I)=ELEFT
      QTMX(I)=QTX
      DO 31 K=IMIN,IHM
   31 ATEMP(K)=TMX
      IF (ICE(I).EQ.1) GO TO 1
      RIMX=G*(RHO(ATEMP(IHM+1))-RHO(TMX))/TAUMX*IZM(I)*DZ
      XL=1300000.
      IF (I.EQ.1) GO TO 5
      IF(IZM(I).LT.30) XL=2600000.
    5 IF(IZM(I).LT.18) XL=3900000.
      SHEARC=XL/(2*IHM*DZ)*(BD(I)/(BD(I)-IZM(I)*DZ))**.5
      ISHEAR(I)=0.
      IF (RIMX.LT.SHEARC) ISHEAR(I)=1
    1  CONTINUE
      RETURN
      END
C
C
C
C
C//////////////////////////////////////////////////////////////////////
C\\\\\\\\\\\\\\\\\\\\\\\\\\\\\\\\\\\\\\\\\\\\\\\\\\\\\\\\\\\\\\\\\\\\\\
C
C
C
      SUBROUTINE MIX
C
C           THIS SUBROUTINE CHECKS FOR STATIC STABILITY OF THE STRATIFICATION
C   IF AN UNSTABLE LAYER IS FOUND IT IS MIXED WITH ADJACENT LAYERS UNTILL
C   STABILITY IS REGAINED.
C
      COMMON /GEN/DZ,CE,CQ,QLAT,F7TO10,CA,CD,ROAIR,TKSED,ROSED,CSED,
     %DAY,XV,BINT(2,30),RO,G,C,ETA,CK,CL,CT,CS,JD,H2OK
C
      COMMON /BASIN/BD(3),V0(3),BETA(3),ICE(3),IZM(3),TKELEFT(3),QTMX(3)
     % ,ISHEAR(3)
C
      COMMON /VOL/VS(42),VC(216),VN(70)
C
      COMMON /TEMP/TS(42),TC(216),TN(70)
C
      COMMON /BOT/SS(10,42),SC(10,216),SN(10,70)
C
      COMMON /FLUX/TAU(3),PHILW(3),PHISW(3),PHILAT(3),PHISEN(3),
     %PHISED(3),PHIEX(3)
C
      COMMON /HEAT/QS,QC,QN
C
      COMMON /YEAR/ASTRO(3,366),TAM(12),TIM(12),RAM(12),RIM(12),
     %WM(12),HM(12)
C
C
C****TOTAL STORAGE****
      REAL AGEN(81),ABASIN(15),AVOL(328),ATEMP(328),ABOT(10,328),
     %AFLUX(21),AHEAT(3),AYEAR(1170)
      EQUIVALENCE (AGEN,DZ),(ABASIN,BD),(AVOL,VS),(ATEMP,TS),(ABOT,SS)
     %,(AFLUX,TAU),(AHEAT,QS),(AYEAR,ASTRO)
C
C
C***LOOP ON THE BASINS
      DO 1 I=1,3
C  COMPUTE INDEXES
      IMIN=1
```

```
      IF (I.EQ.2) IMIN=43
      IF (I.EQ.3) IMIN=259
      IMAX=IMIN+BD(I)/DZ
C********LOOP ON LAYERS
      DO 2 JJ=IMIN,IMAX
      J=JJ
    3 IF((ATEMP(J+1).GT.3.98).AND.(ATEMP(J).GE.ATEMP(J+1))) GO TO 2
      IF((ATEMP(J+1).LE.3.98).AND.(ATEMP(J).LE.ATEMP(J+1))) GO TO 2
      VLM=AVOL(J+1)
      Q=ATEMP(J+1)*VLM
    5 VLM=VLM+AVOL(J)
      Q=Q+ATEMP(J)*AVOL(J)
      TMP=Q/VLM
      J=J-1
      IF(J.EQ.IMIN-1) GO TO 4
      IF((TMP.GT.3.98).AND.(TMP.LE.ATEMP(J))) GO TO 4
      IF((TMP.LE.3.98).AND.(TMP.GE.ATEMP(J))) GO TO 4
      GO TO 5
    4 IK=J+1
      IKK=JJ+1
      DO 6 K=IK,IKK
    6 ATEMP(K)=TMP
    2 CONTINUE
C********LOOP END
    1 CONTINUE
C***LOOPEND
      RETURN
      END
      SUBROUTINE VOLUME(V,MA,VO,HMX)
C
C          THIS SUBROUTINE COMPUTES THE VOLUME OF EACH 50CM SLAB
C     FROM THE MORPHOMETRIIC INFORMATION ON TAPE14.
C
C        V(IZ)= THE VOLUME OF H2O BETWEEN (IZ-1)DZ AND IZ*DZ
C        VO   = THE TOTAL VOLUME
C
      REAL V(MA),VOL(120)
    1 READ(14,2) VOL
    2 FORMAT(" ",6E13.7)
      DO 5 I=1,MA
    5 V(I)=0.
      V(1)=(VOL(1)+VOL(2))*250000.
      VO=V(1)
      K=MA/2
      DO 3 I=1,K
      KK=I*2
      V(KK)=(VOL(I+1)*.75+VOL(I+2)*.25)*500000.
      VO=VO+V(KK)
      IF (V(KK).LE.0.) GO TO 4
      KK=KK+1
      V(KK)=(VOL(I+1)*.25+VOL(I+2)*.75)*500000.
      VO=VO+V(KK)
      IF (V(KK).LE.0.) GO TO 4
    3 CONTINUE
    4 HMX=(KK-1)*50.-1.
      V(KK)=0.
      RETURN
      END
EOI ENCOUNTERED.
```